NOVEL FLUOROELASTOMERS COMPOSED of TETRAFLUOROETHYLENE and VINYLIDENE FLUORIDE OLIGOMERS SYNTHESIZED in CARBON DIOXIDE for USE in SOFT LITHOGRAPHY to ENABLE a PLATFORM for the FABRICATION of SHAPE- and SIZE-SPECIFIC, MONODISPERSE BIOMATERIALS

Jennifer Yvonne Kelly

A dissertation submitted to the faculty of the University of North Carolina at Chapel Hill in partial fulfillment of the requirements for the degree of Doctor of Philosophy in the Department of Chemistry

Chapel Hill
2008

Approved By

Advisor: Joseph M. DeSimone

Reader: Maurice Brookhart

Reader: Ed Samulski

Reader: Jeffrey Johnson

Reader: Paul Resnick

ABSTRACT

JENNIFER YVONNE KELLY: Novel Fluoroelastomers Composed of Tetrafluoroethylene and Vinylidene Fluoride Oligomers Synthesized in Carbon Dioxide for Use in Soft Lithography to Enable a Platform for the Fabrication of Shape- and Size-Specific, Monodisperse Biomaterials (Under the direction of Dr. Joseph M. DeSimone)

Fluorinated elastomers are materials with tremendous utility that have found use as minimally adhesive mold materials in soft lithography. The first objective of this research involved the synthesis of novel functional, fluorinated oligomers in supercritical carbon dioxide ($scCO_2$) and the fabrication of the resulting fluorooligomers into solid elastomers using free radical crosslinking chemistry. Commercially available fluoroelastomers are typically synthesized in aqueous media using fluorinated surfactants or in non-aqueous conditions using fluorinated solvents. This research effort focused on the synthesis of low molecular weight oligomers consisting of tetrafluoroethylene (TFE) and vinylidene fluoride (VF_2) with a cure site comonomer in $scCO_2$ at low temperatures. Using CO_2 as a polymerization medium allows for safe handling of TFE, is environmentally responsible by mitigating the typical generation of halogenated, organic, or aqueous waste, and circumvents the use of fluorinated surfactants as these copolymers are soluble in CO_2. Investigations included characterizing the fluorinated oligomers and the solid elastomeric materials using NMR, DSC, TGA, GPC, IR, and via surface and mechanical property analysis.

The second objective of this research included the use of fluoroelastomers as minimally adhesive mold materials in soft lithography applications using the Particle

Replication In Non-wetting Templates (PRINT™) technology for the fabrication of protein particles of discrete size and shape. Lyophilized protein particles are generally highly disperse in particle size, tend toward aggregation, and are often made through complicated processes. In attempts to engineer mono-disperse protein particles, the use of wet-milling, spray-freeze-drying, micro-emulsion, or super critical fluid methods have been reported. The PRINT process enables a gentle, facile route to mono-disperse particles composed of protein with and without cargo. This research objective included fabricating protein PRINT particles of varying sizes, shapes, and compositions (e.g., Abraxane, albumin, tranferrin, insulin, interferon-beta, hemoglobin, trypsin, horseradish peroxidase, and IgG). Several biophysical characterizations were performed to verify the protein structure was not significantly altered during the PRINT process, including SEM, FTIR, fluorescence microscopy, and CD. Furthermore, ELISA and enzymatic activity assays were performed to investigate biological integrity and function of all proteins. The PRINT technology was found to be a gentle method to create nanoparticles of biologically relevant proteins.

DEDICATION

To my mother, Roswitha E. Kelly, and my late father, William L. Kelly,

for their love and support

ACKNOWLEDGEMENTS

I would like to express my utmost appreciation to my research advisor, Prof. Joseph M. DeSimone for his support and guidance throughout the years. Words cannot articulate how much it has meant to me for his continued support. My sincerest thanks extend to Prof. DeSimone for countless opportunities in such a unique research laboratory where I have learned a tremendous amount both in science and in life. I would like to thank my graduate committee and my department for their support, guidance and time. I would like to extend my gratitude to Prof. George Roberts and Dr. Paul Resnick for invaluable discussions.

I would like to express my appreciation to all of the members of DeSimone group, past and present. Dr. Mary Napier has been an invaluable member to the DeSimone group. Many thanks for all of your time, help, and the meeting you attended. I would like to thank Dr. Christine Conwell, Dr. Patricia Ropp, Prof. Gary Pielak, and Dr. Ashutosh Tripathy for their help and teachings in protein chemistry. Dr. Udo Michel and Dr. Colin Wood were a tremendous help working with high pressure equipment. I would also like to thank the Middle Lab crew and occupants in Caudill 230-234, 251, and 255 for making this experience so fun and great over the years. My appreciation needs to extend to the Ashby group for their friendship and discussions on fundamental polymer science.

I would like to express my appreciation to a terrific few ladies whose friendship will always be with me. Dr. Mary Robert Garrett, Dr. Ginger Rothrock, Dr. Candice Brannen, and bringing back solid gold, Meredith Hampton; thank you.

Finally, I would like to thank my family for their ongoing love and support, especially my late father, for instilling his beliefs, my mother, for always being there for me, and my brother and his family, for always being so generous.

TABLE OF CONTENTS

Page

LIST OF TABLES

LIST OF FIGURES

LIST OF SCHEMES

LIST OF ABBREVIATIONS AND SYMBOLS

AIBN	2,2-azobis(2-methypropionitrile)
BCA	bicinchoninic acid
BPO	benzoyl peroxide
C-8	perfluorooctonoic acid
CD	circular dichroism
CDE	1,4-cyclohexane dimethanol divinyl ether
CFC	chloro fluoro carbon
Cl_2H_2	chloroform
CO_2	carbon dioxide
CSM	cure site monomer
CTFE	chlorotrifluoroethylene
DAP	di(acryloyl) piperazine
DEAP	diethoxyacetophenone
DLS	dynamic light scattering
DMPA	2,2-dimethoxy-2-phenylacetophenone
DSC	differential scanning calorimetry
EHPDC	di-(2-ethylhexyl)peroxydicarbonate
ELISA	enzyme linked immuno sorbent assay
EPA	environmental protection agency
EVEBr	perfluoro(2-bromoethyl vinyl ether)
FTIR	fourrier transform infrared spectroscopy

γ_l	surface tension
GPC	gel permeation chromatography
γ_s	surface energy
${}^{d}\gamma s$	dispersion component
${}^{p}\gamma s$	polar component
H_2O	water
HCPK	hydroxycyclohexyl phenyl ketone
HF	hydrogen fluoride
HFP	hexafluoropropylene
HFPO dimer peroxide	bis(perfluoro-2-*N*-propoxypropionyl) peroxide
HMP	2-hydroxy-2-methyl propiophenone
HPFP	1-hydropentafluoropropylene
HRP	horseradish peroxidase
IR	infrared spectroscopy
$MeCl_2$	methylene chloride
MEK	methylethylketone
MgO	magnesium oxide
NaCl	sodium chloride
NMR	nuclear magnetic resonance
OD	optical density
PBS	phosphate buffer system
PDMS	polydimethyl siloxane

PEG	polyethylene glycol
PET	positron emission topography
PFPE	perfluoropolyether
PI	photoinitiator
PMVE	prefluoro methyl vinyl ether
PP	poly(propylene)
PPVE	perfluoropropyl venyl ether
PRINT	Particle Replication In Nonwetting Templates
PTFE	poly(tetrafluoroethylene)
PVP	poly(vinyl pyrrolidone)
R_fVE	perfluoro alkyl vinyl ether
$scCO_2$	supercritical carbon dioxide
SEM	scanning electron miscrscopy
Si	silicone
SPARC	secreted protein acidic and rich in cysteine
TAIC	triallyl isocyan
TFE	tetrafluoro ethylene
TFT	α,α,α-trifluorotoluene
T_g	glass transition temperature
TGA	thermogravimetric analysis
THF	tetrahydrofuran
UV	ultra violet
VF_2	vinylidene fluoride

wt-%	weight percent
θ	contact angle

CHAPTER 1

FLUOROELASTOMERS

1.0 Introduction.

1.1 Fluoropolymers. Fluoropolymers are a special class of macromolecules, the most notable is poly(tetrafluoroethylene) (PTFE). Also known by DuPont's trade name, Teflon® contains impeccable non-wetting and thermal stability characteristics most well-known for its use in cook-ware applications.[1-3] The commercial production of fluoropolymers is relatively small compared to their hydrocarbon analogues such as poly(ethylene) of poly(vinyl chloride).[1] Fluoropolymer production with high resistance to deformation and high modulus includes fibers and polymers; plastics, flexible or rigid plastics having mechanical properties between fibers and elastomers; elastomers, having a completely amorphous morphology and some degree of crosslinking, can undergo very large, reversible elongations at relatively low stress; thermosets, chemically crosslinked polymers that do not flow when heated; thermoplastics, physically crosslinked polymers that do soften and flow when heated; and thermoplastic elastomers, elastomeric block copolymers containing a phase separated morphology and physical crosslinks.[1, 3-5] The manufacturing of fluoropolymers for special applications is limited by their relatively high cost.[1-3]

Fluorinated materials are relatively new and their development and use in a variety of applications remains largely unexplored. High performance polymers used in traditional industries, such as fabric coatings, fire retardant foams, wire coatings, o-rings, membranes, and coatings require exceptional properties.[1, 3, 5] In many cases fluorinated materials outperform even the best hydrocarbon macromolecules. Fluorinated materials encompass unique applications and are particularly attractive compounds due to their versatility and broad range of properties. These properties include a wide range of

molecular weights, high thermal and mechanical stability, low temperature sustainability, chemical-, ageing-, and weather-resistance, solvent inertness, and oxidative stability, making them suitable for use in aggressive environments.[1-3, 5] Furthermore, these compounds possess semi-crystalline or completely amorphous morphologies.[5] The unique combination of these attributes with low indices of refraction, extremely low surface energies, nonflammable nature, and low dielectric constants is a result of the low polarizability and the strong electronegativity of the fluorine atom, its small Van der Waals radius and the strong C–F bond.[6]

The fluorine content within a material greatly influences its properties. Polymers containing no aliphatic hydrogen bonds and only strong C–F and C–C bonds are termed "perfluorinated" and typically demonstrate the most resilient properties of fluorinated materials.[3, 5, 7] For example, PTFE not only offers non-wetting properties, but also unsurpassed high temperature tolerances as a result of its high degree of crystallinity, high melting temperature, and high melt viscosity; compared to its aliphatic counterpart, poly(ethylene), which exhibits far less temperature stability.[2, 3] The remarkable properties of high molecular weight PTFE were immediately evident with its accidental discovery, as were the difficulties of converting the materials into shape-specific objects since traditional solution and melt processing techniques were impossible to implement.[2, 3, 8] The need for a more easily processed form of PTFE led to discoveries of perfluorinated and eventually fluorinated copolymers. The degree of fluorine content within copolymers gives tunable structure-property relationships leading to novel materials as reported extensively in the literature.[9-16]

Among fluorinated materials, fluorinated and perfluorinated elastomers, have been extensively used in many common industries,[5] but have found their place more recently in current scientific research.[17-23] Advancing research and technologies in imprint lithography,[23] soft, solvent-resistant microfluidic devices,[21, 22] high surface area proton exchange membranes,[20, 24, 25] and drug delivery[17] are a few examples utilizing fluoroelastomers. Nano- and biotechnologies are exploiting perfluoroelastomers by enabling a novel drug delivery platform, PRINT,[17] that may offer viable solutions in personalized medicine. Traditional elastomer synthesis suffers from processing and environmental challenges. The PRINT technology offers an alternative to overcome some of these hurdles. The synthetic aims described in Chapter 2 combine traditional methods of fluoroelastomer synthesis with an unconventional technique to develop new fluoroelastomers overcoming the effects of the environmental impacts previously endured. Similar materials are employed to scale-up the fabrication of novel shape- and size-specific synthetic and biological drug delivery vehicles for cancer treatment (Chapter 3). The methodology developing the PRINT technology creating the platform and the first accounts of nano-molding of monodisperse, shape and size- specific protein particles is presented in Chapter 4.[26]

1.2 Fluorinated Elastomers. Fluoroelastomers are a special class of fluorinated polymers that exhibit a unique combination of high chemical, thermal and electric stabilities, non-flammability, inertness to solvents, hydrocarbons, acids and alkalis, low refractivity index, low surface energy, gas permeability, and oxidation and ageing

resistance.[5] Fluoroelastomers are remarkable materials, suitable for use in particularly aggressive and demanding applications.

Fluoroelastomers exhibit unsurpassed thermal and chemical stability due to the abundance of fluorine atoms in the carbon backbone. The excellent oxidative resistance in perfluorinated elastomers exists in part due to the lack of weaker C-H bonds on the polymer backbone.[5] Their stability is attributed to steric hindrance due to the presence of fluorine and stronger van der Waals forces between hydrogen and fluorine atoms present within the macromolecules (when applicable).[27] The elasticity is derived from low crystallinity, low glass transition temperatures (T_gs), and an amorphous morphology. Fluorinated elastomers have realized great strides in improving soft lab-on-a-chip microfluidic devices[21, 22] that are solvent resistant and could be utilized in analytical separations, biowarefare detections, and fast synthesis of positron emission tomography imaging agent. However, the advantages in morphology and solvent resistance are overshadowed by the synthetic challenges and difficulty in traditional curing and crosslinking.

Currently, the most relevant and commercially available fluoroelastomers are either comprised mostly of vinylidene fluoride (VF_2) or tetrafluoroethylene (TFE).[28] Homopolymers of VF_2 or TFE are semicrystalline rendering them insoluble in many organic solvents and unable to be melt processed. However, the introduction of a comonomer disrupts the polymer crystallinity and systematically alters the polymer properties. The copolymerization changes the symmetry of the polymer backbone, affecting both intramolecular and intermolecular forces. Properties such as melting point, glass transition temperature, crystallinity, stability, permeability, elasticity, and chemical

reactivity may be regulated within wide limits by introducing comonomers. The systematic variation of polymer composition allows for structure-property relationship investigations.

Common comonomers for VF_2 systems include hexaflouropropylene (HFP), 1-hydropentafluoropropylene (HPFP), and chlorotrifluoroethylene (CTFE).[2, 3, 5, 15, 29] For special applications monomers such as perfluoroalkyl vinyl ethers are also incorporated. These are typically used in TFE-based elastomer systems.[2, 3, 5, 15, 29] As noted, properties of the elastomers are directly related to the fluorine content; elastomers containing between 62-70 wt% fluorine have remarkable resistance to solvents, chemicals, flames, and against oxidative attack.[1-3, 7, 27] Compositions with higher fluorine content are achievable depending on monomer selection, which in turn is chosen for its suitability to a given application. Less traditional materials have emerged in recent years containing fluoro-phosphazenes[7] and fluoro- silicones[4, 7, 30] presenting even more complex topologies.[7] The research discussed in Chapter 2 relies primarily on traditionally based materials, but applies those chemistries to a novel synthetic methodology.

1.2.1 Fluoroelastomers from Tetrafluoroethylene. Due to the crystalline nature of the (PTFE) homopolymer, comonomers are employed to aid in its processibility.[2, 3, 28, 31-37] It has been shown in the literature that propylene and TFE can be readily copolymerized in a nearly alternating manner to give a fluoroelastomer.[33-35, 37-46] Fluorinated alkenes (such as TFE) are electron withdrawing olefins and react easily with electron donating monomers like propylene. This donor-acceptor copolymerization can also be achieved using TFE with ethylene or vinyl ether monomers.[47, 48]

Copoylmerization with ethylene leads to a highly crystalline material rendering itself less useful for elastomeric applications without the incorporation of additional comomers such as a fluorinated vinyl ether or a cure site monomer (CSM). Tetrafluoroethylene-containing polymers are typically prepared by emulsion polymerization[34, 35] using salts of perfluorooctanoic or perfluorononanoic acids as the surfactant to enable thermodynamically stable emulsions. A modified persulfate redox system[39] (typically an ammonium persulfate) initiates polymerization.[2, 3] With a stable emulsion polymerization system, high molecular weight copolymers are synthesized at or close to room temperature. At higher temperatures, the risk of chain transfer to monomers can occur.[49-55] Copolymerizations of TFE often contain unwanted side reactions such as hydrogen abstraction from monomer or initiator due to its extreme reactivity. With significant chain transfer reactions, the yielded product is limited to low molecular weight. Asahi Glass developed a preferred polymerization system containing TFE and propylene resulting in high molecular weight polymers, but not without the need for additional co-reagents in their redox systems.[5] It should be noted that handling TFE and conducting polymerizations thereof demands special care, as TFE can react extremely violently, and the utmost caution should be exercised with TFE especially in avoiding auto-acceleration effects during polymerization.

Elastomers of p(TFE/PP) are cured based on the presence of hydrogen atoms in the backbone of these copolymers stemming from the propylene moiety. It was found that under high temperatures unsaturated sites in the backbone will form, leading to facile curing using peroxides and radical traps.[27] Radical traps are compounds with a high avidity for free radical species and in this context contain vinyl groups and functions as a

crosslinker. In addition to high temperature curing, these copolymers can also p(VF_2/PP) be crosslinked by high-energy radiation at room temperature, accompanied by the release of hydrofluoric acid (HF).[2, 3, 38, 44, 45] Safer cure systems have been employed offering similar tensile strength compared to VF_2 based systems (further discussion to follow in VF_2-based elastomer sections). Subsequent to curing, the materials showed superior resistance to acids and bases. Nevertheless, these elastomers were outperformed in compression set resistance, low-temperature properties, and resistance to aromatic solvents by materials containing less hydrogen. Studies of TFE copolymers and their properties provide significant contributions to fluoroelastomer technologies, but the abundant presence of hydrogen in the polymer undoubtedly leaves these materials vulnerable to chemical or thermal degradation.[5] A significant contribution to the field of perfluorinated elastomers[56] came from copolymers of TFE and prefluoro methyl vinyl ether (PMVE). The discovery at DuPont lead to an "elastomeric Teflon" that is resistant to the most hostile environments, and is referred to by the trade name, Kalrez®. Such materials will be discussed in greater depth in Chapter 3.

1.2.2 Fluoroelastomers from Vinylidene Fluoride. For investigating materials synthesized under better control with respect to reaction kinetics and better processing properties, VF_2-based systems are the preferred materials. Poly(vinylidene fluoride) materials exhibit very interesting piezo-, pyro-, and ferro-electrical properties.[57-61] These homopolymers are inert to many solvents, oils, and acids and hence provide desirable base materials within the field of fluoroelastomers. Similar to PTFE, homopolymers of VF_2 are semicrystalline and require a comonomer in order to reduce the crystallinity and

form an amorphous elastomer. Fluoroelastomers containing VF_2 traditionally use hexafluoro propylene (HFP) as a comonomer to make the copolymer amorphous. The copolymerization proceeds essentially in an alternating manner when both monomers are charged in similar ratios. Steric effects are likely to prevent homopropagation of HFP. The cure site in VF_2/HFP copolymers are the hydrogen atoms of VF_2 that are flanked on either side by HFP units.[28] These hydrogen atoms in such an environment are acidic and thus susceptible to abstraction. Scheme 1-1 illustrates the general reaction of base attack on the $-CH_2-$ creating an unsaturated site. Later generations of the VF_2-based elastomers incorporated TFE as an additional comonomer. More recent efforts to improve solvent resistance by increasing the fluorine content was achieved by modifying the charge ratio of the monomers and including the addition of a CSM such as bromotrifluoroethylene. Further advances in this area integrated perfluoroalkyl vinyl ethers to afford better low temperature properties. These VF_2-based elastomers possess outstanding resistance to flames, chemicals, solvents, heat, and oxidation.[5] Bisnucleophiles such as bisphenols or diamines facilitate curing of these materials but afford poor retention of physical properties while peroxide-assisted crosslinking leads to enhanced properties in the presence of a CSM.

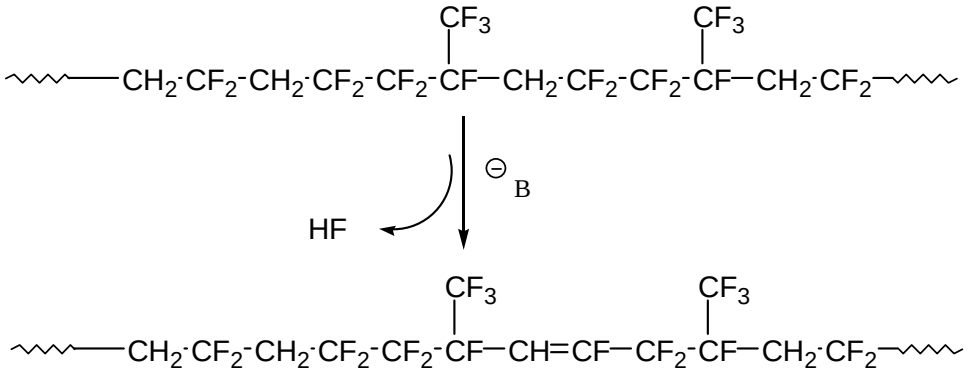

Scheme 1-1. Base Attack on Vinylidene Fluoride/Hexafluoropropylene Copolymers Leading to Unsaturation.

A crosslinking mechanism utilizing peroxides is facilitated by the incorporation of a CSM such as brominated vinyl ethers into the backbone in the presence of a radical trap. For terpolymer systems composed of VF_2, HFP, and perfluoro alkyl vinyl ether (R_fVE) reactivity challenges may present themselves as R_fVE monomers do not readily homopolymerize similarly to HFP, and slow relative reactivity ratios to TFE may dampen these systems depending on the amount of R_fVE charged to the system. In the case of R_fVE especially, increased reaction temperatures may lead to better reaction kinetics and faster polymerization rates, but also produce undesired carboxylic acid or acid fluoride endgroups.[62] The addition of TFE in VF_2-based systems increases the thermal stability at higher temperatures, but at the cost of poor low temperature properties.

Vinylidene fluoride-based polymers are also traditionally synthesized in aqueous emulsions.[63] Similar to TFE emulsions, perfluorooctonic acid analogues serve as surfactants to produce a stable emulsion. As describe previously, ammonium persulfate salts typically act as initiators in these systems resulting in ionic end groups. Though ionic end groups are predominant in this case, non-ionic end groups are achievable with chain transfer reactions,[2, 3, 5] or by disproportionation reactions terminating the

polymerization. Often, buffers need to be added to the reaction to improve the stability of the emulsion. The resulting emulsions are coagulated by the addition of electrolytes, which are specifically selected depending on the desired product and the stability of the emulsion. The least stable emulsions may coagulate by shear as well. Subsequent to coagulation, the precipitated polymer is washed numerous times with water and dried in an oven, resulting in the generation of an aqueous waste stream and an energy intensive drying step.[27]

Special elastomer applications may require compositions that include fluorinated vinyl ethers that may or may not act as a CSM. As previously eluded to, it is ordinarily very difficult to homopolymerize R_fVE to high conversion due to their low reactivity to homopropagation and steric hindrance. Co- and terpolymerization on the other hand, is generally very attainable. Copolymers of VF_2 and R_fVE have been successfully synthesized in molar ratios between 19:1 and 1:1. Terpolymers of VF_2/TFE/R_fVE have also been synthesized in molar ratios ranging from 1:1:1 to 2:1:2.[27]

As previously discussed, TFE and VF_2- based elastomers traditionally are created by radical polymerization to high molecular weight and subsequent curing, resulting in a flexible network. Some copolymers contain elastomeric properties having a linear topology without any additional curing steps. Fluorelastomeric behavior is enhanced, or in some cases can only be attained as a crosslinked network. (By definition, elastomer properties are achieved by creating an amorphous material, having a low glass transition temperature (typically below room temperature), and optimally contains a crosslinked network.[1-3]) A network is attained with reversible, physical crosslinks (thermoplastic), with microstructure phase separation creating anchoring islands such as with A-B-A

triblock copolymers with glassy A and amorphous B blocks. A more robust, irreversible network can be achieved through chemical crosslinks (i.e. thermoset- covalent bonds forming the three-dimensional network). In either case, only certain monomer compositions will produce crosslinked systems, as described for TFE and VF_2 containing elastomers.

1.3 Curing Fluoroelastomers. Most chemically and mechanically robust fluoroelastomers are thermosets, and as such the implementation of chemical crosslinks should ideally enhance mechanical strength, result in the ability for complete strain recovery, avoid occurrence of a large permanent sets when under stress, endure large stresses and strains, and should not introduce any sites for potential oxidative stress or degradation[6]. In traditional systems, two general classes of fluoroelastomers exist: those from ionic curing and those from radical curing. Within ionic cure systems,[64] the most commonly used are amino systems or bisphenol crosslinkers. In either case, the hydrogen atoms of the VF_2 monomers are sites of interest as their electronic properties can be exploited due to the two $-CF_2-$ groups on either side making the hydrogen atoms acidic and prone to extraction. The polymer structure and the strength of the crosslinks are very important in establishing the physical properties of the elastomer.[5]

Radical curing is carried out typically under radiation or with the thermal degradation of a peroxide free radical initiator. Though abstraction of hydrogen atoms from the polymer backbone can lead to successful crosslinking, this type of cure chemistry excels with a cure site monomer or a radically labile functional group incorporated into the polymer backbone in order to assist in constructing a three

dimensional network and is better facilitated in the presence of a radical trap (crosslinker) in the cure step.

1.3.1 Ionic Curing: Amines, Diamines and Diaminecarbamates. Elastomers were originally cured using diamine[65] and polyamine nucleophiles.[5] The mechanism of crosslinking involves the initial removal of hydrogen fluoride (HF) from the VF_2 segments, generating highly polarized -CH=CF- units. These are susceptible to Michael addition by diamines (or polyamines) forming a highly crosslinked network.[66] An accelerator or phase transfer catalyst, typically MgO, helps diffusion of the base into the material. Prior to addition to the double bond, the bonds are shifted with an allylic fluorine ion shift, producing a new double bond. Scheme 1-1 illustrates the ionic reaction mechanism described herein. Aliphatic amines and polyamines were the first in use for this type of curing, but due to intense reactivity associated with these compounds, less reactive Schiff bases were substituted. However they, too, were soon replaced by bisphenol curing agents, due to processing difficulties and poor retention of physical properties at high temperatures from the chemically weaker crosslinks.[28] Volatiles, including HF, were emitted during the crosslinking reaction resulting in undesirable porous products.

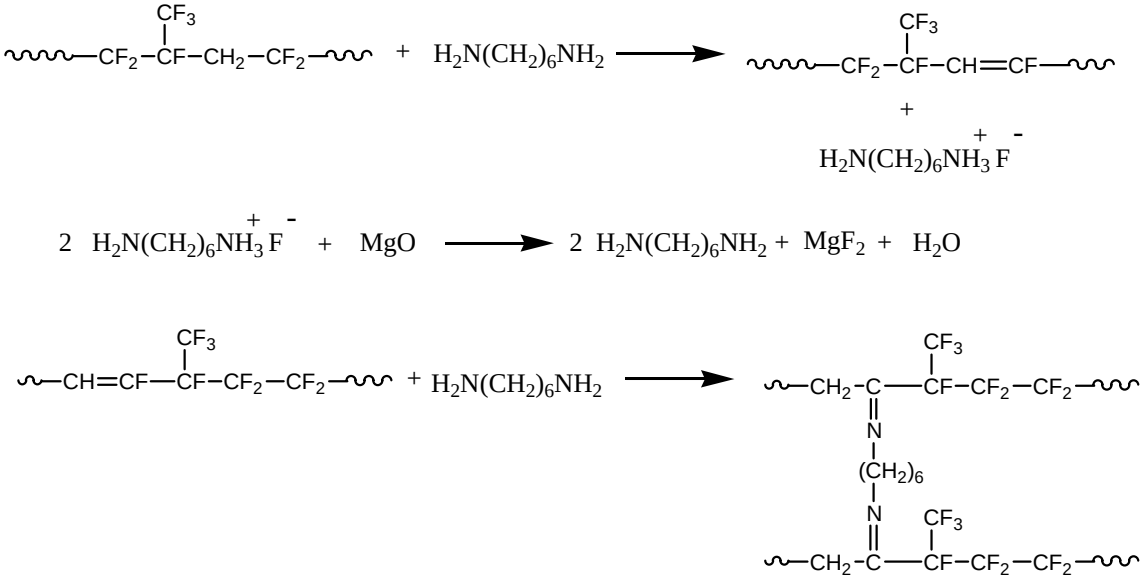

Scheme 1-2. Curing Vinylidene Fluoride-Based Elastomers Using Diamines.

1.3.2 Ionic Curing with Bisphenol Systems. Bisphenol nucleophiles are still largely utilized in curing VF_2 based elastomers.[5] The overall mechanism is quite similar to the diamine mechanism. These crosslinkers react only in the presence of a phosphonium or ammonium salt in combination with a metal compound, acting as an accelerator. The metal salt reacts with the bisphenol to produce a strong base intermediate, which can abstract hydrogen fluoride from the polymer backbone. In special structural sequences the double bond formed from HF abstraction can shift, which allows for another molecule of HF to be abstracted, resulting in a diene. Establishing unsaturated sites in the polymer backbone is the rate determining step in these ionic cure reactions. Substitution of fluorine atoms at the double bonds with the strong base phenolate compounds results in crosslinking. Due to its ensuing properties, 2,2'-bis(hydroxyphenyl) hexafluoropropane, bisphenol AF, is commonly used as the bis-nucleophile. Copolymers containing fluorinated alkyl vinyl ethers are typically not cured using this system as the substitution reaction would yield a loss of trifluoromethoxide which further degrades to HF and carbon dioxide.[5] Consequently, the elastomer is left with excessive porosity due to the released volatiles and sharply decreased physical and mechanical properties. Even without the presence of R_fVEs in the polymer backbone, the bisphenol cure systems introduce weak junctions in the material which are susceptible to further nucleophilic attack by basic compounds as the crosslinking mechanism produces more unsaturated sites than are needed for complete curing. These undesirable weak points illustrate one of the major drawbacks for these cure systems.

Radical cure systems serve as a great alternative to help mitigate some of the weaknesses seen in the ionic bisphenol cure systems. These radical cure systems are able

to improve the processability resulting in faster and more facile conversion of the polymer into a stable, chemically crosslinked elastomeric material.

1.3.3 Radical Curing.

1.3.3.1 Radical Curing: Peroxides. Current industrial processes rely on the curing of functionalized fluoroelastomers using peroxides[66]. Unlike the ionic cure mechanism, this chemistry utilizes a radical mechanism, the first step consisting of the thermal decomposition of a peroxide. The peroxide decomposition provides a free radical that can abstract a hydrogen or methylene group on the polymer backbone, creating a polymeric radical. The polymeric radical can then react directly or through an intermediate using a radical trap to form crosslinks. Another approach involves incorporating a functionalized branchpoint into the polymer by copolymerizing in the presence of a cure site monomer (CSM). The CSM contains a highly reactive group (such as bromine or iodine) susceptible to radical attack, and thus facilitating the crosslinking process.[5] Scheme 1-3 illustrates a summary of the free radical crosslinking mechanism via a peroxide and radical trap.[27]

A radical trap such as triallyl isocyanurate (TAIC) provides stable properties. Other radical traps may be more suitable for a given application. Typical compositions include zero to five weight percent of the radical trap to the polymer, while the peroxide is utilized in a range at or under six weight percent.[5] A basic metal oxide (acid acceptor) and filler may be added to the cure mixture to enhance physical and thermal properties of the fluoroelastomer.[5] As previously mentioned a bromine or iodine containing CSM can be incorporated into the polymer backbone during polymerization and is susceptible to

free-radical attack during the curing steps. (Though the polymerization of these materials undergoes a radical mechanism, the propensity for chain propagation is far greater than halogen abstraction; hence most halogenated monomer remains intact during polymerization.) Some common brominated CSMs include bromotrifluoroethylene, 1-bromo-2,2'-difluoroethylene, and perfluoro(2-bromoethyl vinyl ether), the latter also improving low temperature properties. The introduction of iodine-containing fluoroelastomers, though synthetically more challenging, facilitates injection molding considerably. In either case, the radical produced from the thermal decomposition of the initiator may abstract a halogen from the polymer or add to the radical trap. This latter reaction is favored as it generates a more stable radical. In turn, the radical intermediate likely abstracts a halogen from the polymer, producing a polymeric radical. The driving force for such a reaction is in the transfer of the halogen from the electron poor fluoropolymer to the electron rich hydrocarbon of the radical trap. As these steps are repeated, they afford a three dimensional network.

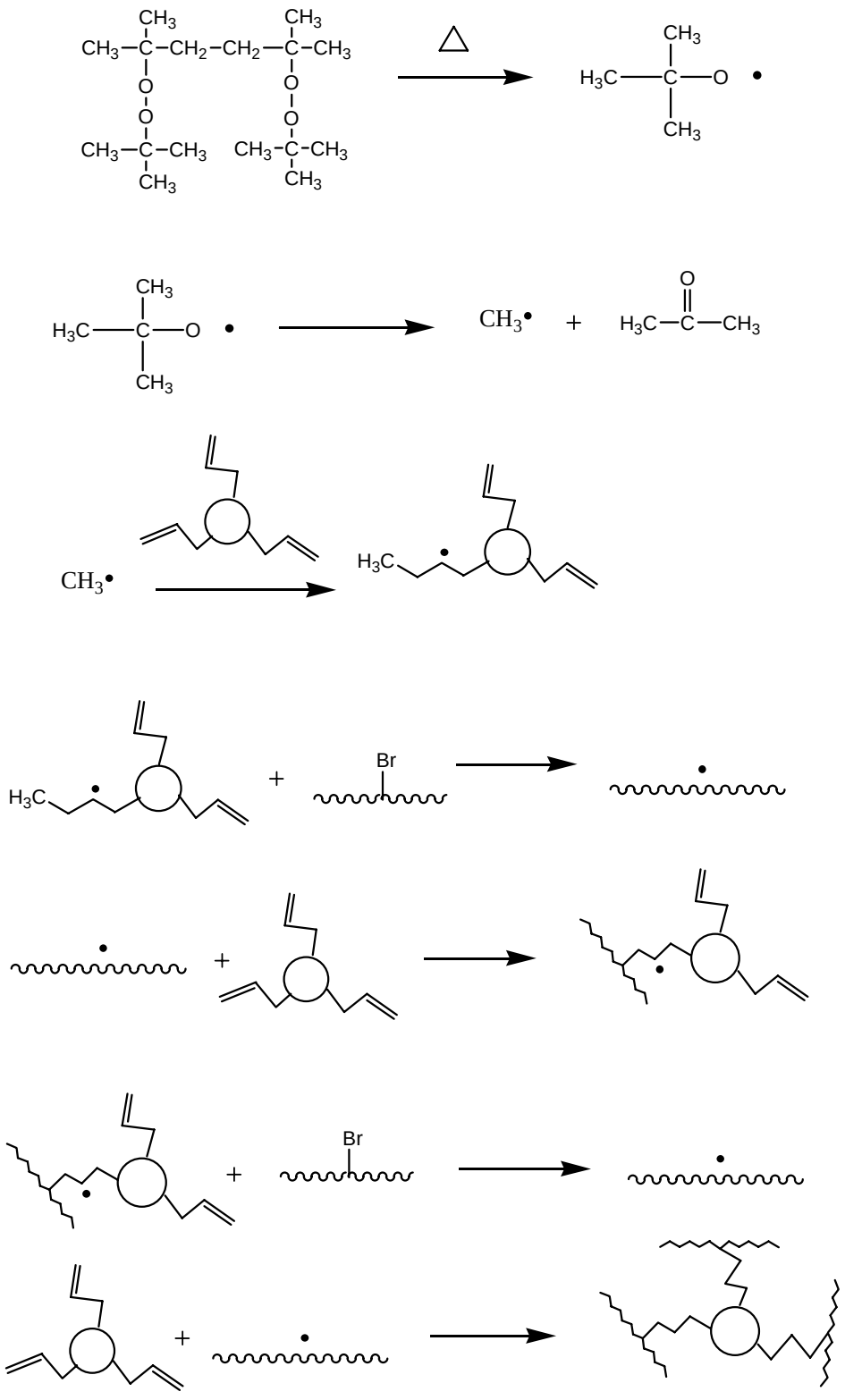

Scheme 1-3. Proposed Radical Crosslinking Mechanism Using a Bromine-Containing CSM and a Peroxide/ TAIC System.

1.3.3.2 Radical Curing: Radiation. High energy gamma radiation is another means of crosslinking VF_2 containing fluoropolymers or poly(TFE/propylene) systems.[5, 62, 67-69] The mechanism emulates that of peroxide curing. Upon irradiation, hydrogen containing polymers produce polymeric radicals. The presence of a radical trap improves curing efficiency. In the absence of a radical trap polymeric radicals tend to combine, creating a relatively inert material to chemical and oxidative attack with good resistance to heat aging.[5] To accelerate the radiation process, sensitizers such as vinyl ethynyl phenylol resins are added, though they are not crucial for property attainment. The lack of impurities from added fillers and chemicals comprises the main advantage of radiation curing.

1.3.3.3 Radical Curing: Photoinitiators. More recently, progress has been made in the curing of functionalized fluoroelastomers using photoinitiators and ultraviolet (UV) light.[70, 71] In this system, rather than the reaction being initiated thermally, as with peroxide initiators, free radicals are produced by photo-irradiation using UV light. Though conventional fluoropolymer technology does not readily utilize UV processes, more attention is being given to this field in academic research laboratories. The use of UV irradiation mitigates large shrinkage effects that are typically present in thermally cured systems. In a radical crosslinking mechanism, the efficiency of crosslinking is dependent on the reactivity of the cure site monomer in the functionalized polymer chain. The initial source of the radicals is not of much concern as long as the reactivity is such that it will abstract an atom either from the polymer backbone or from a radical trap when present.

1.3.4 Current State-of-the-Art Elastomer Processing. Currently, commercially available fluorinated elastomers still face major challenges in synthesis and processing. The manufacturing costs are high due to multiple step synthesis, high monomer costs, high number of coreagents needed, and relatively high reaction temperatures and times. Poor reactivity of reagents and processing difficulties due to very high molecular weights of the polymers[5] present additional difficulties.

1.3.4.1 Mixing, Milling, and Molding: Challenges. Since most conventional fluoroelastomers are high molecular weight polymers prior to crosslinking, processing these materials by mixing and molding prior to curing can prove challenging owning to their high viscosity at room temperature. The flow characteristics are paramount in determining what type of processing methods will be chosen and whether the addition of facilitating reagents is needed. Mixing techniques focus on avoiding contamination, minimizing exposure to water, and maximizing energy input. Use of open milling requires skilled operators, results in limited productivity, and incurs environmental contamination. Though the process is simple, long standing times are needed to ensure an even distribution of fillers and coreagents. Even under the most optimal circumstances open milling does not offer much control.

An internal mixer can shorten mixing times. However, these systems, also referred to as Banbury mixing,[5, 72] require intensive cooling units and low starting temperatures due to the massive heat buildup that results from the viscous shearing and low elongation at break of the fluoropolymer. Molding, however, is the most common

processing procedure implemented in the elastomer industry. Standard technologies in compression, transfer, injection molding, extrusion, and calendaring are applicable for fluoroelastomers. Mold designs need to take potential shrinkage into account as some materials can have up to three percent size reduction in size. Even modest capital investments in presses and instrumentation are not always sufficient. Due to their inherent viscosity some procedures (i.e. injection molding) are difficult at best and often require the addition of low molecular weight polyethylene and mold release agents for successful processing.

1.3.4.2 Post-Cure. The best properties are obtained in a two step vulcanizing process.[5, 73] In the first step, referred to as compression molding, both heat, typically between 150 to 180 °C, and pressure, around 10 to 30 psi, are utilized to mold a sample in a press. The second step is often referred to as the post-cure step and consists of heat (200 – 250 °C) in air at atmospheric pressure for 12-24 hours. This approach ensures optimal physical properties. The specific mechanism that affords these improved properties is not well understood but it is known that an increased degree of crosslinking is observed.[5] It has been suggested that bonds are formed from a Diels-Alder type reaction between neighboring unsaturated, dehydrofluorinated units. The post-cure step also allows volatile side products such as HF and water to escape. Though from a materials composition perspective, isolating the elastomer from unsafe biproducts such as HF is advantageous, but also increases the shrinkage of the final product. The increased crosslinking resulting from the post cure contributes to additional shrinkage introducing a serious problem for fluoropolymers.

1.3.4.3 Liquid Precursor Approach. As previously discussed, the primary objective in elastomer research is to obtain an amorphous material with a low Tg and desirable mechanical properties. Present benchmark materials are high in molecular weight and undergo chemical crosslinking to increase performance. High molecular weight fluorinated and perfluorinated polymers face processing and molding challenges due to their thermal stabilities and solvent resistance already present in the un-cured state, especially for those of TFE analogues. The next generation of fluoroelastomers faces some challenges such as reactivity of the reagents, cost, overall reaction kinetics, environmental impacts, and functionality to enable the exploitation of their properties that are already technologically advanced.

Though the level of chemical inertness of perfluoroelastomers surpasses VF_2-based elastomers, progress is being made to improve the crosslinking conditions through the incorporation of co-reagents and creating facile post-cure methods for the fabrication of stable elastomer materials.[5] As outlined in the previous sections above, ionic curing involves using co-reagents to facilitate nucleophilic attack on the polymer backbone with loss of hydrofluoric acid. This method faces many processing difficulties and creates relatively poor retention of physical properties. High molecular weight polymers that are crosslinked using a free radical approach in conjunction with a CSM integrated into the backbone endure processing challenges as well but are an easier approach to curing than ionic systems. A more cost effective, facile approach in developing new fluorinated elastomers in a few simple steps that are environmentally friendly has yet to be met.

The approach developed for the next generation materials is simple and obtainable by modifying certain key parameters from some already well established methods. A VF2 based platform with a CSM incorporated into its backbone for radical curing was chosen due to the challenges and disadvantages of the other systems mentioned above. A brominated vinyl ether CSM was chosen for its low temperature properties. Perfluoro(2-bromoethyl vinyl ether) (EVEBr), as do other fluorinated vinyl ethers, readily polymerize with VF_2. The incorporation of functional comonomers to enable facile crosslinking and to break up the crystallinity is essential for fluoroelastomer technology. Additional comonomers were investigated for studying structure-property relationships.

One way to make the curing steps and processing easier is to synthesize low molecular weight oligmers in exchange for current high molecular weight fluoropolymers. The synthesis of fluorinated oligomers has recently been emerging in the literature. Research in polymerizing telomers[74-94] and oligomers,[4, 95-97] iodine transfer reactions,[98-101] and fluorotelechelic macrodiols[102-111] with subsequent crosslinking has been studied. Low viscosity oligomers will not present processing challenges and upon curing into mechanically and chemically robust materials circumvents the need for fillers, accelerators, sensitzers, phase transfer catalysts, and other coreagents. In contrast to high molecular weight polymers, low molecular weight functional oligomers are liquids at room temperature and present immense utility. Such liquids can take on any shape and when containing a cure site monomer (CSM) or other functionality, can subsequently be crosslinked to form a chemically and mechanically robust, solid material. Liquid macromolecular precursors have recently drawn much attention for novel applications

such as soft microfluidic devices,[22] soft lithographic capabilities[19, 23] and particle replication,[17] which will be further discussed in Chapters 3 and 4. Thermal or photochemical crosslinking of liquid precursors into solids has created new pathways to facilitate quick production of devices and other soft materials.

Additionally, most fluorinated elastomers are prepared by free radical emulsion polymerization using fluorinated surfactants and modified persulfate initiator systems.[27] However, the use of fluorinated surfactants is becoming obsolete. A class of fluorinated surfactants commonly identified as C-8's, stemming from fluorinated octanoic acid has been widely used to form stable emulsion polymerizations of PTFE in aqueous media. Octanoic acid was recently discovered to be a biopersistant compound, thus forcing the EPA into an investigation and subsequently banning this class of fluorinated surfactants[112]. A solution polymerization process for synthesizing fluoropolymers is not encouraged nor well accepted as fluorinated solvents are even less environmentally friendly than traditional organic solvents. This creates challenges to design materials with outstanding properties without harming the environment.

In attempts to overcome the many challenges in developing new and improved fluorinated elastomers, the research described herein focuses on developing a facile, environmentally friendly synthesis of a fluorinated oligomeric precursor in supercritical carbon dioxide is proposed. As a green solvent, carbon dioxide enables the safe handling of even the reactive monomer, TFE. These perpolymers could be subsequently cured into a stable fluoroelastomer utilizing free radical crosslink chemistry that is well established in this industry. By starting with an oligomeric, liquid precursor, one improves processability and can mold the elastomers to any size and shape for customized

application realization. The utilization of crosslinking low molecular weight, liquid macromolecules will exploit facile fabrication of fluorinatated elastomers in efforts to improve physical properties.

The polymerization of oligomers composed of VF_2 and/or TFE, along with a cure site monomer will be focused upon. Photochemical crosslinking facilitates fast and easy processing into solid elastomers and circumvents the shrinkage often resulting from thermal cure steps. This strategy can be employed to pattern or mold a substrate upon curing, and henceforth various applications can be realized, including microfluidics, high-surface area proton exchange membranes, and specialty coatings. By optimizing reaction conditions of the polymer synthesis and of the cure chemistry, efforts to tailor the physical and chemical properties of these materials for improved performance are investigated.

1. Odian, G., *Principles of Polymerization*. 3rd ed.; John Wiley & Sons, INC.: New York, 1991; p 313-314.

2. Scheirs, J., *Modern Fluoropolymers*. John Wiley & Sons, Ltd: New York, 1997; p 435-485.

3. Banks, R. E. S., B.E.; Tatlow, J. C., *Organofluorine Chemistry Principles and Commercial Applications*. Plenum Press: New York, 1994.

4. Ameduri, B.; Boutevin, B.; Guida-Pietrasanta, F.; Rousseau, A., Fluorinated oligomers, telomers and (co)polymers: synthesis and applications. *Journal of Fluorine Chemistry* **2001,** 107, (2), 397-409.

5. Ameduri, B.; Boutevin, B.; Kostov, G., Fluoroelastomers: synthesis, properties and applications. *Progress in Polymer Science* **2001,** 26, (1), 105-187.

6. Wall, L. A., Fluoropolymers. **1972**, (New York: Wiley).

7. Ameduri, B.; Boutevin, B., Update on fluoroelastomers: from perfluoroelastomers to fluorosilicones and fluorophosphazenes. *Journal of Fluorine Chemistry* **2005,** 126, (2), 221-229.

8. Chu, B.; Wu, C.; Buck, W., Light-Scattering Characterization of Poly(Tetrafluoroethylene) .2. Ptfe in Perfluorotetracosane - Molecular-Weight Distribution and Solution Properties. *Macromolecules* **1989,** 22, (2), 831-837.

9. Erhard, D. P.; Giesa, R.; Altstadt, V.; Schmidt, H. W., Synthesis and structure-property relationships of fluorinated poly(ether imide)s as electret materials. *Macromolecular Chemistry and Physics* **2007,** 208, (14), 1522-1529.

10. Kang, J. W.; Kim, J. P.; Lee, J. S.; Kim, J. J., Structure-property relationship of fluorinated co-poly(arylene ether sulfide)s and co-poly(arylene ether sulfone)s for low-loss and low-birefringence waveguide devices. *Journal of Lightwave Technology* **2005,** 23, (1), 364-373.

11. Goto, K.; Akiike, T.; Inoue, Y.; Matsubara, M., Polymer design for thermally stable polyimides with low dielectric constant. *Macromolecular Symposia* **2003,** 199, 321-331.

12. Delucchi, M.; Turri, S.; Barbucci, A.; Bassi, M.; Novelli, S.; Cerisola, G., Fluoropolyether coatings: Relationships of electrochemical impedance spectroscopy measurements, barrier properties, and polymer structure. *Journal of Polymer Science Part B-Polymer Physics* **2002,** 40, (1), 52-64.

13. Hu, H. S. W.; Griffith, J. R.; Buckley, L. J.; Snow, A. W., Fluoropolymers with low dielectric constants: Triallyl ether-hydrosiloxane resins. *Microelectronics Technology* **1995,** 614, 369-378.

14. Ameduri, B.; Boutevin, B., Copolymerization of fluorinated monomers: recent developments and future trends. *Journal of Fluorine Chemistry* **2000,** 104, (1), 53-62.

15. Gelin, M. P.; Ameduri, B., Fluorinated block copolymers containing poly(vinylidene fluoride) or poly(vinylidene fluoride-co-hexafluoropropylene) blocks from perfluoropolyethers: Synthesis and thermal properties. *Journal of Polymer Science Part a-Polymer Chemistry* **2003,** 41, (1), 160-171.

16. Kostov, G.; Ameduri, B.; Boutevin, B.; Bauduin, G.; Stankova, M., Synthesis and characterization of original functional polymers of tetrafluoroethylene and 4,5,5-trifluoro-4-ene pentyl acetate. *Journal of Polymer Science Part a-Polymer Chemistry* **2004,** 42, (7), 1693-1706.

17. Rolland, J. P.; Maynor, B. W.; Euliss, L. E.; Exner, A. E.; Denison, G. M.; DeSimone, J. M., Direct fabrication and harvesting of monodisperse, shape-specific nanobiomaterials. *Journal of the American Chemical Society* **2005,** 127, (28), 10096-10100.

18. Liu, B.; Rolland, J. P.; DeSimone, J. M.; Bard, A. J., Fabrication of ultramicroelectrodes using a "Teflon-like" coating material. *Analytical Chemistry* **2005,** 77, (9), 3013-3017.

19. Rolland, J. P.; Hagberg, E. C.; Denison, G. M.; Carter, K. R.; De Simone, J. M., High-resolution soft lithography: Enabling materials for nanotechnologies. *Angewandte Chemie-International Edition* **2004,** 43, (43), 5796-5799.

20. Zhou, Z. L.; Dominey, R. N.; Rolland, J. P.; Maynor, B. W.; Pandya, A. A.; DeSimone, J. M., Molded, high surface area polymer electrolyte membranes from cured liquid precursors (vol 128, pg 12963, 2006). *Journal of the American Chemical Society* **2006,** 128, (48), 15547-15547.

21. Wood, C. D.; Michel, U.; Rolland, J. P.; DeSimone, J. A., New fluoropolymer materials. *Journal of Fluorine Chemistry* **2004,** 125, (11), 1671-1676.

22. Rolland, J. P.; Van Dam, R. M.; Schorzman, D. A.; Quake, S. R.; DeSimone, J. M., Solvent-resistant photocurable "liquid teflon" for microfluidic device fabrication. *Journal of the American Chemical Society* **2004,** 126, (8), 2322-2323.

23. Maynor, B. W.; Larue, I.; Hu, Z.; Rolland, J. P.; Pandya, A.; Fu, Q.; Liu, J.; Spontak, R. J.; Sheiko, S. S.; Samulski, R. J.; Samulski, E. T.; DeSimone, J. M., Supramolecular nanomimetics: Replication of micelles, viruses, and other naturally occurring nanoscale objects. *Small* **2007,** 3, (5), 845-849.

24. Souzy, R.; Ameduri, B.; Boutevin, B.; Gebel, G.; Capron, P., Functional fluoropolymers for fuel cell membranes. *Solid State Ionics* **2005,** 176, (39-40), 2839-2848.

25. Souzy, R.; Ameduri, B.; Boutevin, B.; Capron, P.; Marsacq, D.; Gebel, G., Proton-conducting polymer electrolyte membranes based on fluoropolymers incorporating perfluorovinyl ether sulfonic acids and fluoroalkenes: Synthesis and characterization. *Fuel Cells* **2005,** 5, (3), 383-397.

26. Kelly, J. Y.; DeSimone, J. M., Shape-Specific, Monodisperse Nano-Molding of Protein Particles. *J. Am. Chem. Soc.* **2008,** *130,* 5438-5439.

27. Logothetis, A. L., Chemistry of Fluorocarbon Elastomers. *Progress in Polymer Science* **1989,** 14, (2), 251-296.

28. Uschold, R. E., Fluoroelastomers - Todays Technology and Tomorrows Polymers. *Polymer Journal* **1985,** 17, (1), 253-263.

29. Taguet, A.; Ameduri, B.; Dufresne, A., Crosslinking and characterization of commercially available poly(VDF-co-HFP) copolymers with 2,4,4-trimethyl-1,6-hexanediamine. *European Polymer Journal* **2006,** 42, (10), 2549-2561.

30. Ameduri, B.; Boutevin, B.; GuidaPietrasanta, F.; Manseri, A.; Ratsimihety, A.; Caporiccio, G., Synthesis of hybrid fluorinated silicones .1. Influence of the spacer between the silicon atom and the fluorinated chain in the preparation and the thermal properties of hybrid homopolymers. *Journal of Polymer Science Part a-Polymer Chemistry* **1996,** 34, (15), 3077-3090.

31. Ameduri, B.; Bauduin, G.; Kostov, G. K.; Petrova, P.; Rousseau, A., Synthesis and polymerization of fluorinated monomers bearing a reactive lateral group - Part 7. Copolymerization of tetrafluoroethylene with omega-hydroxy trifluorovinyl monomers. *Journal of Applied Polymer Science* **1999,** 73, (2), 189-202.

32. Ameduri, B.; Boutevin, B.; Kostov, G.; Petrov, P.; Petrova, P., Synthesis and polymerization of fluorinated monomers bearing a reactive lateral group - Part 8 - Study of the tetrafluoroethylene-propylene rubber modification by 4,5,5-trifluoro-4-penten-1-ol as a comonomer. *Journal of Polymer Science Part a-Polymer Chemistry* **1999,** 37, (21), 3991-3999.

33. Kostov, G. K. P., P. Chr., Study of Synthesis of Properties of Tetrafluoroethylene-Propylene Copolymers. *Journal of Polymer Science Part A: Polymer Chemistry* **1992,** 30, 1083-1088.

34. Kostov, G. K. P., P. Chr., Emusion Copolymerization of Tetrafluoroethylene and Propylene with Redox System Containing tert-Butylperbenzoate. I. Polymerization

Conditions and Components. *Journal of Polymer Science: Part A: Polymer Chemistry* **1994,** 32, 2229-2234.

35. Petrov, P. C. K., G. K., Emusion Copolymerization of Tetrafluoroethylene and Propylene with Redox System Containing tert-Butylperbenzoate. II. Polymerization Mechanism. *Journal of Polymer Science: Part A: Polymer Chemistry* **1994,** 32, 2235-2239.

36. Kostov, G. K.; Petrov, P. C., Stress-relaxation study of tetrafluoroethylene-propylene rubbers. *Polymer* **1995,** 36, (19), 3683-3686.

37. Kostov, G. B., J. M.; Guida-pietrasants, F.; Bauduin, G.; Petrov, P., Study of the microstructure and thermal properties of tetrafluoroethylene-propylene elastomers. *European Polymer Journal* **1999,** 35, 743-749.

38. Tabata, Y.; Ishigure, K.; Sobue, H., Radiation-Induced Copolymerization of Tetrafluoroethylene with Propylene at Low Temperature. *Journal of Polymer Science Part a-General Papers* **1964,** 2, (5pa), 2235.

39. Kojima, G.; Tabata, Y., Radiation-Induced Cross-Linking of a Tetrafluoroethylene-Propylene Copolymer. *Journal of Macromolecular Science-Chemistry* **1971,** A 5, (6), 1087.

40. Tabata, Y.; Fujikawa, J., Electron Spin Resonance Study on Grafting of Tetrafluoroethylene onto Polyethylene. *Journal of Macromolecular Science-Chemistry* **1971,** A 5, (5), 821-&.

41. Tabata, Y.; Fujikawa, J.; Oshima, K., Grafting of Monochlorotrifluoroethylene onto Polyethylene by Pre-Irradiation Method. *Journal of Macromolecular Science-Chemistry* **1971,** A 5, (5), 831-&.

42. Kostov, G. K.; Petrov, P. C., Emulsion Copolymerization of Tetrafluoroethylene and Propylene with Redox System Containing Tert-Butylperbenzoate .1. Polymerization Conditions and Components. *Journal of Polymer Science Part a-Polymer Chemistry* **1994,** 32, (12), 2229-2234.

43. Petrov, P. C.; Kostov, G. K., Emulsion Copolymerization of Tetrafluoroethylene and Propylene with Redox System Containing Tert-Butylperbenzoate .2. Polymerization Mechanism. *Journal of Polymer Science Part a-Polymer Chemistry* **1994,** 32, (12), 2235-2239.

44. Yamaguchi, K.; Hayakawa, N.; Okamoto, J., Molecular-Weight Characteristics of Tetrafluoroethylene-Propylene Copolymer Produced by Radiation-Induced Emulsion Co-Polymerization. *Journal of Applied Polymer Science* **1978,** 22, (9), 2653-2660.

45. Suzuki, N.; Matsuda, O.; Okamoto, J., Radiation-Induced Emulsion Copolymerization of Tetrafluoroethylene with Propylene .3. Polymerization Mechanism. *Journal of Polymer Science Part a-Polymer Chemistry* **1974,** 12, (9), 2045-2052.

46. Kostov, G.; Bessiere, J. M.; Guida-Pietrasanta, F.; Bauduin, G.; Petrov, P., Study of the microstructure and thermal properties of tetrafluoroethylene-propylene elastomers. *European Polymer Journal* **1999,** 35, (4), 743-749.

47. Tabata, Y.; Shibano, H.; Sobue, H., Copolymerization of Tetrafluoroethylene with Ethylene Induced by Ionizing Radiation. *Journal of Polymer Science Part a-General Papers* **1964,** 2, (4pa), 1977.

48. Tabata, Y.; Sobue, H.; Oshima, K.; Ishigure, K., Copolymerization of Tetrafluoroethylene with Isobutene Induced by Ionizing Radiation. *Journal of Polymer Science Part a-General Papers* **1964,** 2, (5pa), 2445.

49. Tuminello, W. H.; Buck, W. H.; Kerbow, D. L., Rheological Molecular-Weight Distribution Determinations of Ethylene Tetrafluoroethylene Copolymers - Implications for Long-Chain Branching. *Macromolecules* **1993,** 26, (3), 499-503.

50. Mori, T.; Tsuchiya, Y.; Okahata, Y., Polymerizations of tetrafluoroethylene in homogeneous supercritical fluoroform and in detergent-free heterogeneous emulsion of supercritical fluoroform/water. *Macromolecules* **2006,** 39, (2), 604-608.

51. Okaniwa, M.; Okaniwa, M., Synthesis of poly (tetrafluoroethylene)/poly(butadiene) core-shell particles and their graft copolymerization. *Journal of Applied Polymer Science* **1998,** 68, (2), 185-190.

52. Tanaka, T.; Honda, Y.; Ishitobi, M., Highly Anisotropic Molecular Thin Films Prepared by Oriented Growth on Poly(tetrafluoroethylene) Surfaces. *Langmuir* **2001,** 17, (7), 2192-2198.

53. Yu, W. H.; Kang, E. T.; Neoh, K. G., Controlled Grafting of Comb Copolymer Brushes on Poly(tetrafluoroethylene) Films by Surface-Initiated Living Radical Polymerizations. *Langmuir* **2005,** 21, (1), 450-456.

54. Breiby, D. W.; Solling, T. I.; Bunk, O.; Nyberg, R. B.; Norrman, K.; Nielsen, M. M., Structural Surprises in Friction-Deposited Films of Poly(tetrafluoroethylene). *Macromolecules* **2005,** 38, (6), 2383-2390.

55. Zhang, Y.; Katoh, T.; Endo, A., Changing Molecular Orientation in Fluorocarbon Thin Films Deposited by Different Photo-Processing: Synchrotron Radiation Etching vs Laser Ablation. *J. Phys. Chem. B* **2000,** 104, (26), 6212-6217.

56. Barney, A. L. K., W. J.; van Gulick, N. M., A High-Performance Fluorocarbon Elastomer. *Journal of Polymer Science: Part A-1* **1970,** 8, 1091-1098.

57. Higashihata, Y. S., J.; Yagi, T., *Ferroelectrics* **1981,** 32, 85-92.

58. Marcus, M. A., *Ferroelectrics* **1982,** 40, 29-35.

59. Lovinger, A. J., *Science* **1983,** 220, 1115-1121.

60. Lovinger, A. J.; Davis, D. D.; Cais, R. E.; Kometani, J. M., On the Curie-Temperature of Poly(Vinylidene Fluoride). *Macromolecules* **1986,** 19, (5), 1491-1494.

61. Betz, R., *Ferroelectrics* **1987,** 75, 397-409.

62. Forsythe, J. S. H., D. J. T.; Logothetis, A. L.; Seguchi, T.; Whittaker, A. K., NMR Study of the Radiation-Induced Cross-Linking of Poly(tetrafluoroethylene-co-perfluoromethyl vinyl ether). *Macromolecules* **1997,** 30, 8101-8108.

63. Apostolo, M. A., V.; Storti, G.; Morbidelli, M,, Kinetics of the Emulsion Polymerization of Vinylidene Fluoride and Hexafluoropropylene. *Macromolecules* **199,** 32, 989-1003.

64. Schmiegel, W. W., Crosslinking of Elastomeric Vinylidene Fluoride Copolymers with Nucleophiles. *Die Angewandte Makromolekulare Chemie* **1979,** 76/77, 39-65.

65. Paciorek, K. L.; Lajiness, W. G.; Lenk, C. T., Differential Thermal Analysis of Fluoroelastomer Systems. *Journal of Polymer Science* **1962,** 60, (169), 141.

66. Taguet, A.; Ameduri, B.; Boutevin, B., Crosslinking of vinylidene fluoride-containing fluoropolymers. *Crosslinking in Materials Science* **2005,** 184, 127-211.

67. Forsythe, J. S. H., D. J. T., The Radiation Chemistry of Fluoropolymers. *Progress in Polymer Science* **2000,** 25, 101-136.

68. Yoshida, T. F., R. E.; Wall, L. A., Stress Relaxation of gamma-Irradiated Fluorocarbon Elastomers. *Journal of Polymer Science: Part A* **1965,** 3, 1685-1712.

69. Lyons, B. J., Radiation Crosslinking of Fluoropolymers - A Review. *Radiation Physics and Chemistry* **1995,** 45, (2), 159-174.

70. Lalevee, J.; Allonas, X.; Jradi, S.; Fouassier, J. P., Role of the medium on the reactivity of cleavable photoinitiators in photopolymerization reactions. *Macromolecules* **2006,** 39, (5), 1872-1879.

71. Bongiovanni, R.; Malucelli, G.; Sangermano, M.; Priola, A., Fluorinated networks through photopolymerisation processes: synthesis, characterisation and properties. *Journal of Fluorine Chemistry* **2004,** 125, (2), 345-351.

72. Allan T. Worm, W. G., Flourocarbon Elastomers. In *Encyclopedia of Polymer Science and Technology*, John Wiley & Sons, INC: New York, 2002.

73. Smith, J. F. P., G. T., The Mechanism of Post Cure of Viton A* Fluorocarbon Elastomer. *Journal of Applied Polymer Science* **1961,** V, (16), 460-46.

74. Romack, T. J.; Combes, J. R.; Desimone, J. M., Free-Radical Telomerization of Tetrafluoroethylene in Supercritical Carbon-Dioxide. *Abstracts of Papers of the American Chemical Society* **1995,** 209, 127.

75. Duc, M.; Ameduri, B.; Boutevin, B.; Kharroubi, M.; Sage, J. M., Telomerization of vinylidene fluoride with methanol. Elucidation of the reaction process and mechanism by a structural analysis of the telomers. *Macromolecular Chemistry and Physics* **1998,** 199, (7), 1271-1289.

76. Duc, M.; Ameduri, B.; David, G.; Boutevin, B., Kinetics of radical telomerization of vinylidene fluoride in the presence of CCl(3)Z chain transfer agents. *Journal of Fluorine Chemistry* **2007,** 128, (2), 144-149.

77. Duc, M.; Boutevin, B.; Ameduri, B., Radical telomerisation of vinylidene fluoride with diethyl hydrogenphosphonate - Characterisation of the first telomeric adducts and assessment of the transfer constants. *Journal of Fluorine Chemistry* **2001,** 112, (1), 3-12.

78. Destarac, M.; Matyjaszewski, K.; Silverman, E.; Ameduri, B.; Boutevin, B., Atom transfer radical polymerization initiated with vinylidene fluoride telomers. *Macromolecules* **2000,** 33, (13), 4613-4615.

79. Marie, A.; Fournier, F.; Tabet, J. C.; Ameduri, B.; Walker, J., Collision-induced dissociation studies of poly(vinylidene) fluoride telomers in an electrospray-ion trap mass spectrometer. *Analytical Chemistry* **2002,** 74, (13), 3213-3220.

80. Balague, J.; Ameduri, B.; Boutevin, B.; Caporiccio, G., Controlled step-wise telomerization of vinylidene fluoride, hexafluoropropene and trifluoroethylene with iodofluorinated transfer agents. *Journal of Fluorine Chemistry* **2000,** 102, (1-2), 253-268.

81. Taguet, A.; Sauguet, L.; Ameduri, B.; Boutevin, B., Fluorinated cotelomers based on vinylidene fluoride (VDF) and hexafluoropropene (HFP): Synthesis, dehydrofluorination and grafting by amine containing an aromatic ring. *Journal of Fluorine Chemistry* **2007,** 128, (6), 619-630.

82. Ameduri, B.; Duc, M.; Kharroubi, M.; Boutevin, B., Radical telomerization of 1,1-difluoroethylene with trichloromethyled telogens. *Abstracts of Papers of the American Chemical Society* **1998,** 216, U133-U133.

83. Lebreton, P.; Ameduri, B.; Boutevin, B.; Corpart, J. M.; Juhue, D., Radical telomerization of 1,3-butadiene with perfluoroalkyl iodides. *Macromolecular Chemistry and Physics* **2000,** 201, (10), 1016-1024.

84. Lebreton, P.; Ameduri, B.; Boutevin, B.; Cot, D.; Corpart, J. M., Radical telomerization of 1,3-butadiene with perfluoroalkyl iodides in the presence of potassium carbonate. *Journal of Polymer Science Part a-Polymer Chemistry* **2002,** 40, (21), 3743-3756.

85. Kostov, G.; Ameduri, B.; Brandstadter, S. M., Radical telomerization of 3,3,3-trifluoropropene with diethyl hydrogen phosphonate: Characterization of the first telomeric adducts and assessment of the transfer constants. *Journal of Fluorine Chemistry* **2007,** 128, (8), 910-918.

86. Balague, J.; Ameduri, B.; Boutevin, B.; Caporiccio, G., Synthesis of Fluorinated Telomers .1. Telomerization of Vinylidene Fluoride with Perfluoroalkyl Iodides. *Journal of Fluorine Chemistry* **1995,** 70, (2), 215-223.

87. Balague, J.; Ameduri, B.; Boutevin, B.; Caporiccio, G., Synthesis of Fluorinated Telomers .2. Telomerization of Trifluoroethylene with Perfluoroalkyl Iodides. *Journal of Fluorine Chemistry* **1995,** 73, (2), 237-245.

88. Balague, J.; Ameduri, B.; Boutevin, B.; Caporiccio, G., Synthesis of Fluorinated Telomers .3. Telomerization of Hexafluoropropene with Perfluoroalkyl Iodides. *Journal of Fluorine Chemistry* **1995,** 74, (1), 49-58.

89. Manseri, A.; Ameduri, B.; Boutevin, B.; Chambers, R. D.; Caporiccio, G.; Wright, A. P., Synthesis of Fluorinated Telomers .4. Telomerization of Vinylidene Fluoride with Commercially Available Alpha,Omega-Diiodoperfluoroalkanes. *Journal of Fluorine Chemistry* **1995,** 74, (1), 59-67.

90. Guiot, J.; Alric, J.; Ameduri, B.; Rousseau, A.; Boutevin, B., Synthesis of fluorinated telomers. Part 6. Telomerisation of chlorotrifluoroethylene with methanol. *New Journal of Chemistry* **2001,** 25, (9), 1185-1190.

91. Ameduri, B.; Boutevin, B., Telomerisation reactions of fluorinated alkenes. *Organofluorine Chemistry* **1997,** 192, 165-233.

92. Ameduri, B.; Duc, M.; Kharroubi, M.; Boutevin, B., Telomerization of 1,1-difluoroethylene with methanol. *Abstracts of Papers of the American Chemical Society* **1998,** 216, U90-U90.

93. Ameduri, B.; Billard, T.; Langlois, B., Telomerization of vinylidene fluoride with alkyl (or aryl) trifluoromethanethiosulfonates. *Journal of Polymer Science Part a-Polymer Chemistry* **2002,** 40, (24), 4538-4549.

94. Manseri, A.; Ameduri, B.; Boutevin, B.; Chambers, R. D.; Caporiccio, G.; Wright, A. P., Unexpected telomerization of hexafluoropropene with dissymetrical halogenated telechelic telogens. *Journal of Fluorine Chemistry* **1996,** 78, (2), 145-150.

95. Ameduri, B.; Boutevin, B., Synthesis of Chlorinated Telechelic Oligomers .1. Telomerization of Nonconjugated Dienes with Functional Telogens. *Macromolecules* **1990,** 23, (9), 2433-2439.

96. Ameduri, B.; Boutevin, B., Synthesis of Chlorinated Telechelic Oligomers .2. Telomerization of Allyl Acetate with Functional Telogens. *Macromolecules* **1991,** 24, (9), 2475-2484.

97. Ameduri, B.; Boutevin, B.; Lecrom, C.; Garnier, L., Synthesis of Halogenated Monodispersed Telechelic Oligomers .3. Bistelomerization of Allyl Acetate with Telogens Which Exhibit Alpha,Omega-Di(Trichloromethyled) End Groups. *Journal of Polymer Science Part a-Polymer Chemistry* **1992,** 30, (1), 49-62.

98. Boyer, C.; Valade, D.; Sauguet, L.; Ameduri, B.; Boutevin, B., Iodine transfer polymerization (ITP) of vinylidene fluoride (VDF). Influence of the defect of VDF chaining on the control of ITP. *Macromolecules* **2005,** 38, (25), 10353-10362.

99. Boyer, C.; Valade, D.; Lacroix-Desmazes, P.; Ameduri, B.; Boutevin, B., Kinetics of the iodine transfer polymerization of vinylidene fluoride. *Journal of Polymer Science Part a-Polymer Chemistry* **2006,** 44, (19), 5763-5777.

100. David, G.; Boyer, C.; Tonnar, J.; Ameduri, B.; Lacroix-Desmazes, P.; Boutevin, B., Use of iodocompounds in radical polymerization. *Chemical Reviews* **2006,** 106, (9), 3936-3962.

101. Ameduri, B.; Boutevin, B., Use of telechelic fluorinated diiodides to obtain well-defined fluoropolymers. *Journal of Fluorine Chemistry* **1999,** 100, (1-2), 97-116.

102. Saint-Loup, R.; Ameduri, B., Photochemical induced polymerization of vinylidene fluoride (VDF) with hydrogen peroxide to obtain original telechelic PVDF. *Journal of Fluorine Chemistry* **2002,** 116, (1), 27-34.

103. Saint-Loup, R.; Manseri, A.; Ameduri, B.; Lebret, B.; Vignane, P., Synthesis and properties of novel fluorotelechelic macrodiols containing vinylidene fluoride, hexafluoropropene and chlorotrifluoroethylene. *Macromolecules* **2002,** 35, (5), 1524-1536.

104. Ameduri, B.; Berrada, K.; Boutevin, B.; Bowden, R. D., Synthesis of Novel Telechelic Monodispersed Nonconjugated Dienes. *Polymer Bulletin* **1992,** 28, (5), 531-537.

105. Manseri, A.; Boulahia, D.; Ameduri, B.; Boutevin, B.; Caporiccio, G., Synthesis of telechelic dienes from fluorinated alpha,omega-diiodo alkanes .2. Divinyls and diallyls containing tetrafluoroethylene, vinylidene fluoride and hexafluoropropene. *Journal of Fluorine Chemistry* **1997,** 81, (2), 103-113.

106. Manseri, A.; Ameduri, B.; Boutevin, B.; Kotora, M.; Hajek, M.; Caporiccio, G., Synthesis of Telechelic Dienes from Fluorinated Alpha,Omega-Diiodoalkanes .1. Divinyl and Diallyl Derivatives from Model I(C2f4)Ni Compounds. *Journal of Fluorine Chemistry* **1995,** 73, (2), 151-158.

107. Ameduri, B.; Berrada, K.; Boutevin, B.; Bowden, R. D., Synthesis of Telechelic Monodispersed Diols .1. Telomerization of Undecylenol with Poly(Methylene)Dithiols. *Polymer Bulletin* **1992,** 28, (4), 389-394.

108. Ameduri, B.; Berrada, K.; Boutevin, B.; Bowden, R. D., Synthesis of Telechelic Monodispersed Diols .2. Telomerization of Undecylenol with Bis(2-Mercapto Ethyl) Ether and Bis(2-Mercapto Ethyl) Sulfide and Physical-Properties. *Polymer Bulletin* **1992,** 28, (5), 497-503.

109. Ameduri, B.; Berrada, K.; Boutevin, B.; Bowden, R. D., Synthesis of Telechelic Monodispersed Diols .3. Telomerization of Nonconjugated Dienes with Commercially Available or Synthesized Mercapto-Alcohols. *Phosphorus Sulfur and Silicon and the Related Elements* **1993,** 83, (1-4), 39-47.

110. Ameduri, B.; Berrada, K.; Boutevin, B.; Bowden, R. D.; Pereira, L., Synthesis of Telechelic Monodispersed Dithiols. *Polymer Bulletin* **1991,** 26, (4), 377-382.

111. Lahiouhel, D.; Ameduri, B.; Boutevin, B., A telechelic fluorinated diol from 1,6-diiodoperfluorohexane. *Journal of Fluorine Chemistry* **2001,** 107, (1), 81-88.

112. Exner, M. F., H., Perfluorinated Surfactants in Surface and Drinking Waters. *Environmental Science and Pollution Research* **2006,** 13, (5), 299-307.

CHAPTER 2

NEW FLUORINATED LIQUID OLIGOMERS SYNTHESIZED IN SUPERCRITICAL CARBON DIOXIDE AND THEIR USE AS ELASTOMERS

2.0 Introduction.

2.1 Synthesis of Fluorinated Polymers in Supercritical Carbon Dioxide.

2.1.1 Background on Carbon Dioxide as a Reaction Medium. Carbon dioxide (CO_2) as a reaction medium is a sustainable platform for the polymerization of many organic monomers and particularly for fluorinated monomers. Interest in the use of supercritical $scCO_2$ as a reaction medium and a green solvent has become ever increasing. DeSimone and coworkers have pioneered much of the work using $scCO_2$ as a continuous phase in the synthesis of multiple traditional hydrocarbon based polymers including poly(methyl methacylate),[1-5] polystyrene,[6, 7] and poly(acrylic acid)[8-10] to name a few. Fluorinated monomers are readily soluble in CO_2 and the exploitation as a green solvent for the polymerization of fluoropolymers started in the early 1990's.[11] As a reaction medium, $scCO_2$ brings many benefits to the table. Using CO_2 for fluoropolymer synthesis instead of traditional fluorinated or organic solvents or even aqueous based systems affords an environmentally friendly approach that mitigates the use of fluorinated surfactants and the generation of large quantities of halogenated, organic, or aqueous waste. Additionally, aqueous suspension or dispersion methods result in increased occurrence of carboxylic acid endgroups that are deleterious to the products' function. Other advantages include its tunability as a solvent in the supercritical range, having gas-like densities and liquid-like viscosities. For many polymers carbon dioxide can also act as a plasticizing or foaming agent. Along with its environmental advantages, energy intensive drying steps are mitigated when using CO_2 as it has a low heat of vaporization thus reducing cost, and in most cases resulting in ready to use, dry products upon venting.

The first report of CO_2 utilized in the synthesis of fluoropolymers was by DeSimone and coworkers[11]. Since then a number of different systems have been investigated including the synthesis of tetrafluoroethylene-based copolymers[12-14] with monomers such as perfluoropropyl vinyl ether (PPVE),[14] hexafluoropropylene (HFP),[13] and 2,2-bis(trifluoromethyl)-4,5-difluoro-1,3-dioxole (PDD)[15, 16] as well as vinylidene fluoride-based fluoropolymers.[17-21] The teleromerization of tetrafluoroethylene (TFE) was also described by Romack and coworkers.[22] Much work has been invested in studying vinylidene fluoride (VF_2) and HFP copolymerizations as batch reactions[23] and continuous polymerization processes.[24, 25] Ahmed and coworkers found that VF_2/HFP copolymers synthesized in CO_2 possess similar properties to analogous materials synthesized using more conventional systems.[18, 23, 24]

Fluorinated elastomer synthesis in CO_2 is of particular interest due to the solubility of fluorinated monomers in $scCO_2$. The synthesis of materials ranging from thermally resistant, high molecular weight fluoropolymers to solvent resistant fluoroelastomers in $scCO_2$ has created an opportunity for cleaner processes and cost reduction, not to mention safety risk reduction.[13, 18, 23, 24, 26] Handling TFE as a 50 wt.-% mixture in CO_2 enables safer management of this most reactive monomer, that is very exothermic when polymerized. Additionally, chain transfer reactions to solvent are not of concern when using CO_2 as a polymerization medium. Furthermore, low temperature polymerizations are possible in CO_2 which affords the ability to minimize unwanted side reactions that could lead to early termination or acid chain end groups that are thought to be involved in the material's degradation.[27, 28] Increased polymerization temperatures ranging between 70 and 95 °C result in a β-scission side reaction in the presence of alkyl

vinyl ethers, which can lead to undesired acid fluoride and carboxylic acid end groups (Scheme 2-1).[27, 28] The synthesis of fluorinated, liquid prepolymers, their characterization, and conversion into solid, solvent resistant elastomers are discussed. Crosslinked elastomers and their properties were investigated using a facile ultra violet (UV) curing approach with a well-established radical cure site monomer (CSM)/ radical trap initiator.

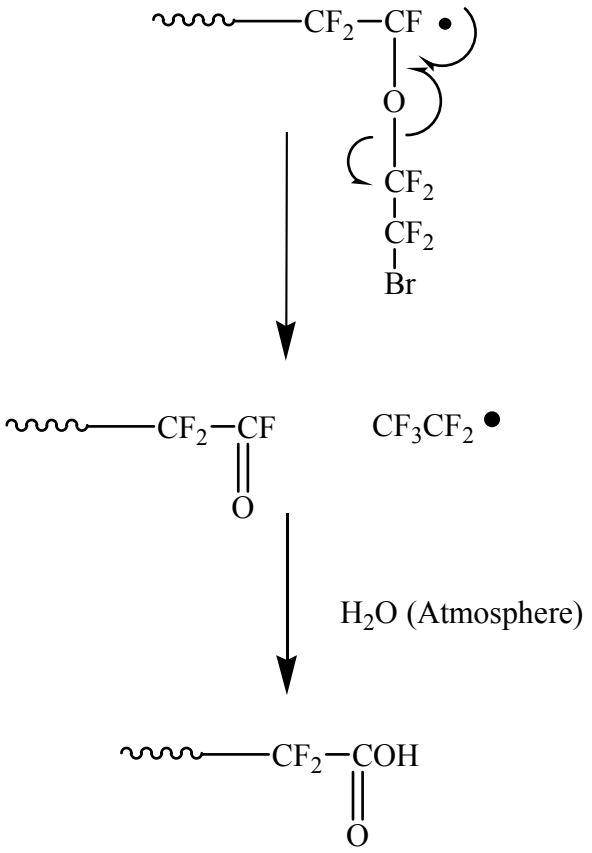

Scheme 2-1. Beta-scission reaction of fluorinated vinyl ethers during polymerization.

2.2 Synthesis of Novel Fluorinated, Liquid Macromolecules in Supercritical Carbon Dioxide.

2.2.1 Materials. TFE was obtained by DuPont as a 50 wt-% mixture in CO_2 and used as received. 2-Bromotetrafluoroethyl trifluorovinyl ether (EVEBr) was obtained from Matrix Scientific and was used as received. α,α,α-Trifluorotoluene, sodium chloride (NaCl), potassium hydroxide (KOH), and hydrogen peroxide, 30wt% (H_2O_2) was obtained from Aldrich and used as received. Vinylidene fluoride was obtained from Synquest and used as received. SFC purity CO_2 was obtained from Air Products. Di-(2-ethylhexyl)peroxydicarbonate (EHPDC) was obtained from Arkema Inc. and used as received. Bis(perfluoro-2-*N*-propoxypropionyl) peroxide (HFPO dimmer peroxide) was prepared in 1,1,2-trichloro-1,2,2-trifluoroethane (Freon® 113), according to a published procedure.[29]

2.2.2 Instrumentation. Infrared spectra were collected using a BIO-RAD FTS-7 spectrometer. Proton and fluorine NMR spectra were acquired in deuterated acetone using a Varian Unity Inova 600 NMR spectrometer. Thermogravimetric analysis was carried out using Perkin Pyris 1 TGA with a heating rate of 10 °C/min in a constant nitrogen purge. Glass transitions and melting points were measured with a Seiko 220C differential scanning calorimeter, using heating rates of 10 °C/min and 20 °C/min for the first and second heat respectively, and 100 °C/min as the cooling rate. Glass transitions were determined at the inflection point of the endotherm and melting points were determined at the peak of the endotherm. Molecular weights, relative to narrow polystyrene standards, were measured using a Waters GPC system with a Wyatt Optilab

DSP interferometric refractometer and a Wyatt Dawn EOS as the detectors. The measurements were taken at 25 °C with tetrahydrofuran as the mobile phase on three columns (Waters Stygel HR0.5, HR2, HR4, HR5). Elemental Analysis was performed by Atlantic Microlab, Inc. Photochemical crosslinking was conducted in an ELC-500 Light Exposure System equipped with an ultra-violet light source (UVA 365 nm). Mechanical property measurements were conducted using an Instron 5566 at a crosshead speed of 20 mm/min at 25 °C. The Young's modulus was calculated using the initial linear portion of the stress/strain curve (0 – 5 % strain). Static contact angles on cured polymer samples were measured using a KSV Instrument LTD CAM 200 Optical Contact Angle Meter. A screw-top syringe (Fisher) was used to deposit a liquid drop onto the flat polymer surface. Distilled water and diiodomethane were used as testing liquids and their surface tension properties are summarized in Table 2-8. The angles reported herein are the averages of at least four measurements. Scanning electron microscopy was performed on a Hitachi S-4700 SEM.

2.2.3 Synthesis of HFPO Dimer Peroxide. The HFPO dimer peroxide was synthesized in Freon 113 as previously reported.[29] Briefly, the reaction was conducted in a round bottom flask in a NaCl/ ice bath, not allowing the reaction temperature to go above 5 ºC. The perfluorinated acid fluoride reacted with H_2O_2 and KOH at the organic-(Freon 113) water interphase to for the perfluoro acyl peroxide. The final product was stored in a Frein 113 solution under dry ice. The iodine titration technique, ASTM Method E 298-91, was utilized to determine the initiator concentration in solution. The overall reaction is summarized in Scheme 2-2.

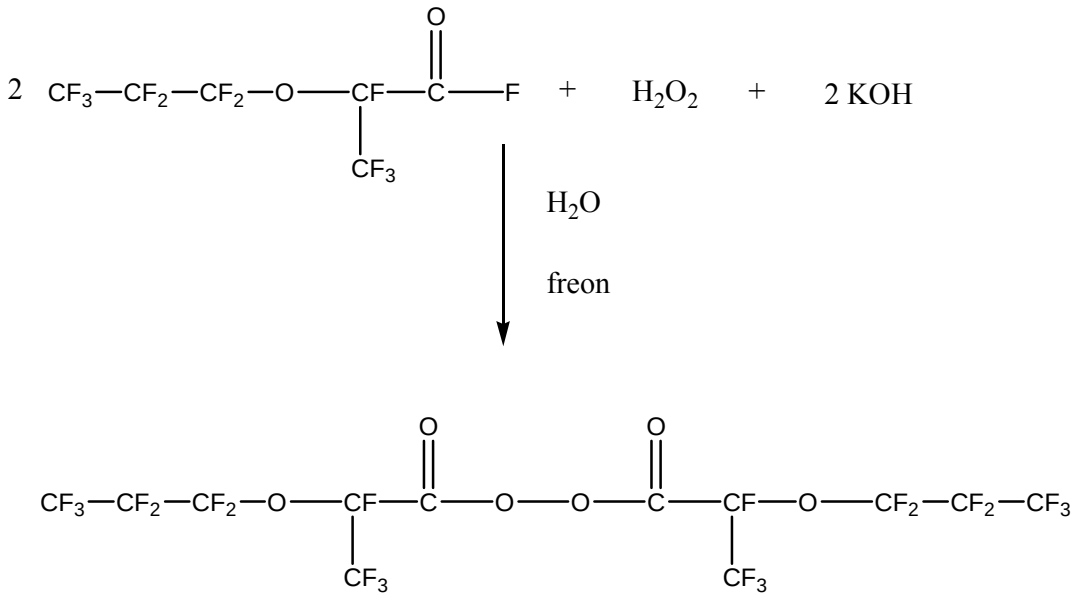

Scheme 2-2. Synthesis of HFPO dimer peroxide.

2.2.4 Synthesis of Copolymers. The experimental set-up is shown in Figure 2-1. Polymerizations were carried out in a 25 mL high-pressure reaction vessel equipped with a stir bar, thermocouple, rupture disk and a sapphire window which permits visual observation of the reaction mixture with an endoscope. In a typical reaction the high pressure reaction vessel was pressurized with CO_2 at least three times to remove oxygen and leak test the vessel after which the reaction cell was purged with argon in order to avoid introducing air into the reaction vessel and cooled to 15 °C. Under a constant blanket of argon EVEBr was charged via syringe directly into the reactor. After sealing the cell and stopping argon purge, VF_2 was introduced via a manual high pressure syringe pump (HIP, Model 62-6-10) under stirring. To add the desired amount of VF_2 the pump was pressurized to 48 bar (696 psig) and the volume of the VF_2 added was calculated from the density at 48 bar. By repeated opening and closing of the valve between the pump and the reaction vessel and repressurizing to 48 bar the desired volume was

introduced. When applicable, TFE/CO_2 mixture (50 wt.-%) was subsequently added. To add the desired amount of TFE, a manual high pressure syringe pump was again used. The pump was pressurized to 103 bar (1494 psig) with the TFE/CO_2 mixture and the volume of the TFE/CO_2 mixture added was calculated from the density at 103 bar. By repeated opening of the valve between the pump and the reaction vessel and repressurizing to 103 bar the desired volume was introduced. The reaction vessel was then heated to the desired reaction temperature, typically 50 °C. Initiator solution was transferred via syringe to a small addition tube in-line with CO_2 lines under argon purge. The reaction view cell was then filled with CO_2 using an automatic syringe pump (ISCO, Model 260 D) while simultaneously introducing the initiator. After the polymerization, the reaction vessel was cooled with a dry ice bath, and the CO_2 was slowly vented. The reaction was visually monitored through the sapphire window using an endoscope.

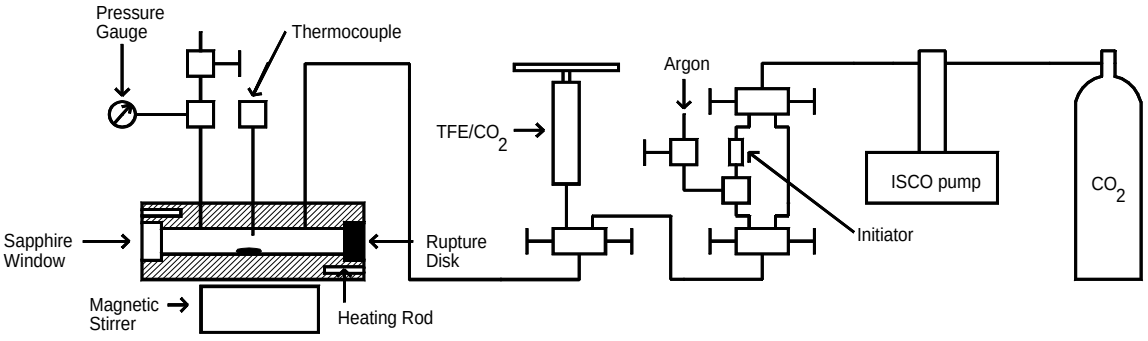

Figure 2-1. High pressure reaction set-up.

2.2.4.1 Results and Discussion of the Synthesis of p(VF_2/EVEBr) and p(VF_2/TFE/EVEBr) Elastomer Copolymers. The synthesis of new fluorinated

elastomers was conducted in supercritical carbon dioxide under varying reaction conditions. The reaction conditions strongly influence the structure-property relationship of the resulting products as well as their overall stability. This systematic study investigated the effects of initiator composition and concentration, reaction temperature, reaction pressure, and monomer concentration. Copolymers of VF_2 and EVEBr were initially investigated. The incorporation of TFE was later pursued in efforts to enhance the thermal and chemical stability.

All monomers discussed are soluble in $scCO_2$. The reaction mixture was homogenous throughout the polymerization for copolymers of VF_2 and EVEBr under certain conditions. With no TFE present, the polymerizations were initially homogeneous but become heterogenous as the polymerization proceeded. With increasing TFE incorporation though, visual observations indicated a dense liquid settling on the bottom of the reactor. With TFE feed ratios above 50 mole % precipitation polymerization was observed with white solid particulates coming out of solution within the first few minutes after initiation. Vinylidene fluoride and EVEBr copolymers were typically isolated as viscous, colorless, transparent liquids; while VF_2/EVEBr/TFE terpolymers were obtained as colorless, wax-like materials that increased in stiffness with increasing TFE content. When greater than 50 % of TFE was incorporated in the tepolymer, a semi-crystalline solid was obtained. These semi-crystalline TFE terpolymers were insoluble in conventional and fluorinated solvents while the amorphous VF_2/EVEBr and VF_2/EVEBr/TFE polymers were soluble in acetone, methylethylketone (MEK), α,α,α-trifluorotoluene (TFT), and tetrahydrofuran (THF). The mole ratio of initiator charged ranged between five and ten percent. Fluorine and proton NMR confirmed all monomers

were incorporated and no residual monomer was present after isolation and drying of the product. A number of different variables for the $scCO_2$ polymerization were investigated, including choice of thermal initiator, reaction pressure, and the feed ratio of the monomer components.

2.2.4.1.1 Initiator Investigation for CO_2 Polymerization. When choosing a thermal peroxide initiator for the synthesis of fluorinated oligomer, there are many variables to consider such as the initiator reactivity, solubility, decomposition temperature, and physical state at room temperature were some of the characteristics pertinent for this study. Table 2-1 summarizes the initiators investigated.

Table 2-1. Thermal initiator investigation used for fluorinated oligomer synthesis.

Initiator	**T ($t^1/_2$ = 10hrs) [°C]**
HFPO dimer peroxide	35[30]
Benzoyl peroxide and dimethyl analine redox system	25[31]
Di-tert-butyl-peroxide	110[32]
Ethyl Hexyl Peroxy Dicarbonate	50[33]

The ten hour half life of thermal initiators was investigated (in CO_2 or benzene depending on availability). The polymerization reaction time was desired to last at least two half-lives and thus chosen to be around 24 hours at the temperature of the ten hour half life. Di-tertbutylperoxide (tBP) has been commonly employed with VF_2

polymerizations,[34-36] however tBP has a 10 hour half life at 110 °C and it has been shown that when copolymerizing fluorinated vinyl ethers above 70 ºC, unwanted side reactions result[27, 28] thus, low reaction temperatures are preferable for these polymerization systems. Previous studies in our lab investigated polymerizations employing a solution of bis(perfluoro-2-N-propoxypropionyl) peroxide in 1,1,2-trichloro-1,2,2-trifluoroethane (Freon® 113). The 10 hour half-life in CO_2 of this HFPO dimer peroxide is 35 °C but this initiator proved problematic due to the high initiator volume needed to obtain low molecular weight oligomers. Since this initiator cannot safely be synthesized neat, the amount of co-solvent introduced into the reactor created a complicated co-solvent polymerization system that veered from a green process with the substantial addition of a chloro-fluoro carbon (CFC). Two reaction pressures were investigated, 138, 172, and 345 bar. A redox system with benzoyl peroxide and dimethylanaline was attempted a number of times with little success but ethyl hexyl peroxy dicarbonate (EHPDC) was found to be a suitable thermal initiator for the successful synthesis of functional fluorinated oligomers at low temperatures.

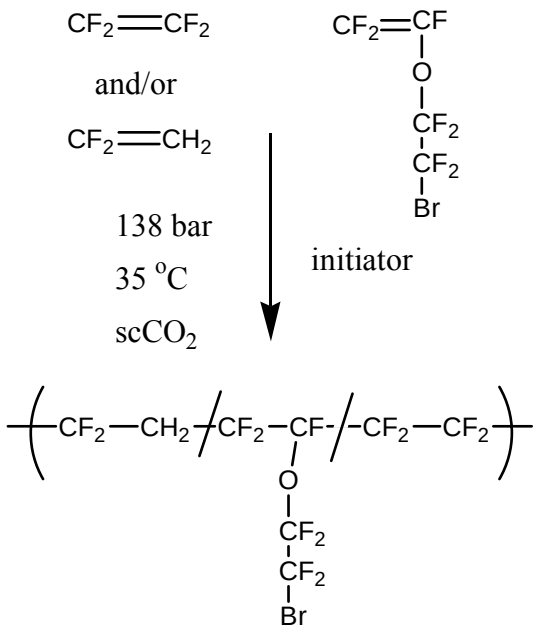

Scheme 2-3. Synthesis of functional fluorinated oligomers in carbon dioxide.

2.2.4.1.2 Monomer Feed Ratios. Investigations of percent solids, pressure, and initiator concentration were conducted. Polymerization conditions are summarized in Tables 2-2 and 2-3. Reaction conditions were carefully varied especially in cases of polymerizations that included TFE due to the highly exothermic nature of its homopolymerization and chance of autoexcelleration. Most polymerizations reported herein were conducted at 20 percent solids at 345 bar and with an initiator concentration of 0.25 mol%. The feed ratios of the three monomers were varied. To maintain a proximity to conventional fluoroelastomers with respect to the amount of CSM, the feed ratio of EVEBr for most experiments was held constant at 15 mole %. The charged ratio of VF_2 and TFE was varied from 0 – 85 mol%. The best results were observed for feed ratios close to 50/35/15 mol% of VF_2/TFE/EVEBr resulting in products with good yields (generally above 65%) and good processability. As the feed of TFE was increased above

50 mole% the materials became semi-crystalline, leading to processing challenges. These semi-crystalline waxes were difficult to get to flow and mix with the cure components and hence were difficult to crosslink.

Copolymerizations of VF_2 with EVEBr resulted in precipitation polymerizations where the precipitated polymer was swollen in CO_2. At times the product became so viscous stirring was halted. As shown in the Figure 2-2, a clear liquid settles out and is viscous enough to arrest the stir bar (white object). The physical properties of the fluorinated oligomers synthesized are summarized in Tables 2-5 and 2-6. The physical properties show no obvious correlation between the average molecular weights and their thermal properties. In general with increasing molecular weight, increasing thermal properties are expected. The fact that no obvious trend is seen between molecular weight and thermal properties may be as a results from working within a relatively narrow range of molecular weight and due to the fact that the GPC results are calibrated from polystyrene standards, a very different type of material compared to the fluorinated oligomers. Optical images of the oligomers are illustrated in Figure 2-3.

Figure 2-2. Image of reaction vessel during vinylidene fluoride/brominated perfluoroethyl vinylether polymerization demonstrating precipitation of viscous polymer layer.

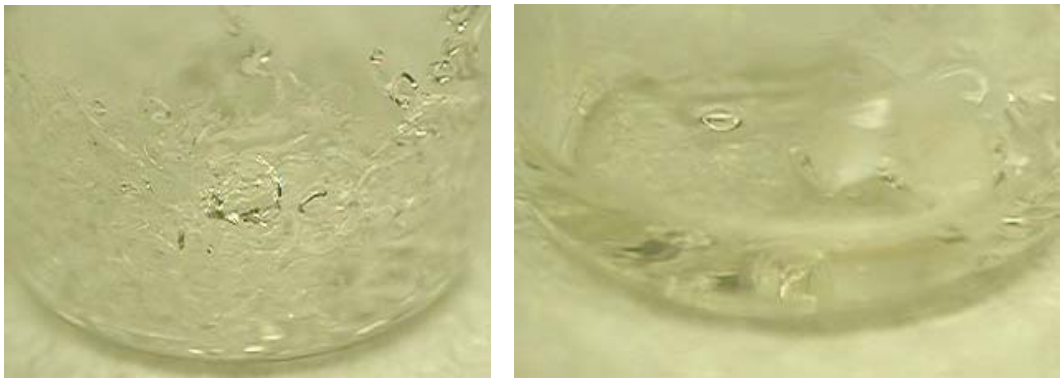

Figure 2-3. Optical images of typical viscous functional fluorinated oligomers synthesized in carbon dioxide.

Table 2-2. Reaction conditions for copolymers composed of vinyldene fluoride and brominated perfluoroethyl vinylether.

VF_2 mol% (feed)	EVEBr mol% (feed)	Pressure [bar]	Inititiator [mol %]
48 (50)	52 (50)	138	tBP [2.50]
55 (66)	45 (33)	172	HFPO [2.50]
57 (60)	43 (40)	138	EHPDC [2.00]
60 (66)	40 (33)	138	HFPO [2.50]
60 (75)	40 (25)	138	EHPDC [0.50]
61 (80)	39 (20)	345	EHPDC [0.25]
62 (68)	38 (32)	138	EHPDC [1.00]
63 (60)	37 (40)	172	HFPO [2.50]
63 (63)	37 (37)	138	HFPO [2.50]
65 (60)	35 (40)	172	HFPO [2.50]
66 (80)	34 (20)	138	EHPDC [0.25]
71 (75)	29 (25)	138	HFPO [2.50]
71 (80)	29 (20)	345	EHPDC [0.25]
73 (50)	27 (50)	138	HFPO [2.50]
73 (60)	27 (40)	172	HFPO [2.50]
79 (80)	21(20)	345	EHPDC [0.25]
80 (80)	20 (20)	138	EHPDC [0.25]
85 (50)	15 (50)	138	tBP [2.50]
88 (66)	12 (33)	138	HFPO [2.50]

Table 2-3. Reaction conditions for terpolymers composed of vinylidene fluoride, tetrafluoroethylene, and brominated perfluoroethyl vinylether using EHPDC as the initiator.

VF_2 mol% (feed)	EVEBr mol% (feed)	TFE mol% (feed)	Pressure [bar]	EHPDC[mol %]
0 (0)	10 (15)	90 (85)	345	[0.50]
6 (35)	8 (15)	86 (50)	345	[0.25]
21 (70)	34 (15)	45 (15)	345	[0.25]
24 (73)	40 (20)	36 (7)	138	[0.50]
34 (60)	18 (15)	48 (25)	345	[0.25]
52 (35)	12 (15)	36 (50)	345	[0.50]
52 (73)	38 (20)	10 (7)	345	[0.50]
64 (50)	9 (15)	27 (35)	345	[0.25]
70 (10)	7 (15)	23 (75)	345	[0.50]
72 (50)	7 (15)	21 (35)	345	[0.25]
73 (50)	7 (15)	20 (35)	345	[0.25]
76 (50)	11 (15)	13 (35)	345	[0.25]
76 (50)	17 (15)	7 (35)	345	[0.25]
79 (50)	12 (15)	9 (35)	345	[0.25]
82 (50)	10 (15)	8 (35)	345	[0.25]

2.2.4.2 Characterization.

2.2.4.2.1 Proton and Fluorine NMR of Copolymers. Fluorine NMR spectra of copolymers composed of VF_2 and EVEBr and terpolymers composed of VF_2, EVEBr, and TFE demonstrated incorporation of all the monomers charged as shown in Figures 2-4 and 2-5, respectively. Table 2-4 summarizes the assigned peaks of the spectra. The lack of unsaturated sites in the fluorine and the proton NMR spectra indicates that residual monomer was not present. The two fluorinated methylene groups of the vinyl ether side chain (-O-CF_2-CF_2-Br) integrated to the same values indicating that bromine abstraction did not occur during the polymerization. These methylene signals were used to calculate the normalized amount of EVEBr incorporated. Peaks ranging from -92 to -96 ppm and between -109 and -115 ppm were assigned to the fluorinated methylene –CF_2- groups of

VF_2. The integrals assigned to VF_2 were used to calculate the normalized amount of VF_2 incorporated into the polymer. By difference the amount of TFE incorporated into the polymer was obtained in the case of terpolymers. The incorporation of TFE was substantially larger than the feed ratio, owing to the high reactivity of the monomer. ^{1}H NMR (not shown) showed a broad peak ranging from 2.5 to 3.3 ppm corresponding to the -CH_2- unit of VF_2.

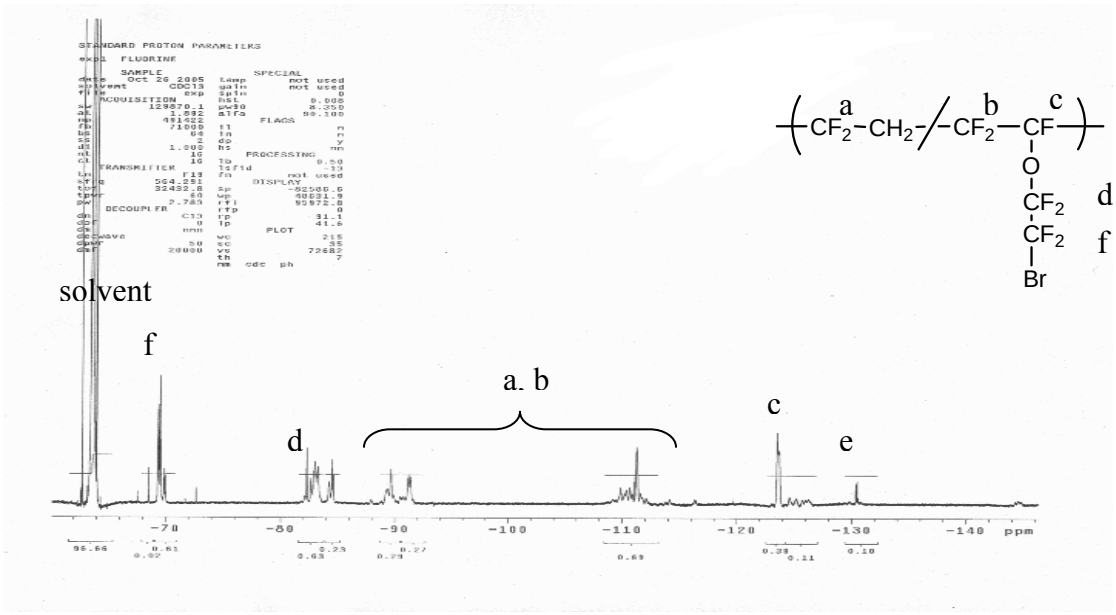

Figure 2-4. ^{19}F NMR spectrum of a typical p(73:27 VF_2-EVEBr) copolymer.

Table 2-4. Peak assignment for ^{19}F NMR spectra of synthesized co- and terpolymers.

Shift (ppm)	Designation	Structure	Assignment	Reference
-71, -72.5	Sharp intense multiplet	-CF_2-C**F**$_2$Br	(f)	37
-82, -84	Sharp intense multiplet	O-C**F**$_2$-CF_2-	(d)	38
-91.5	Broad multiplet	-C**F**$_2$-CH_2-C**F**$_2$-CF	(a,b)	38
-111.5	Broad multiplet	-C**F**$_2$-CH_2-C**F**$_2$-CF	(a,b)	37
-124	Broad multiplet	-CH_2-CF_2-C**F**-O-	(c)	37
-126	Broad multiplet	-CF-CF2-C**F**2-	(g)	38
-130	Sharp intense multiplet	-O-CF_2-C**F**$_2$-H	(e)	37
-138; -144	Sharp intense multiplet	-CF_3-C**F**H-O-CF_2-	(h)	39

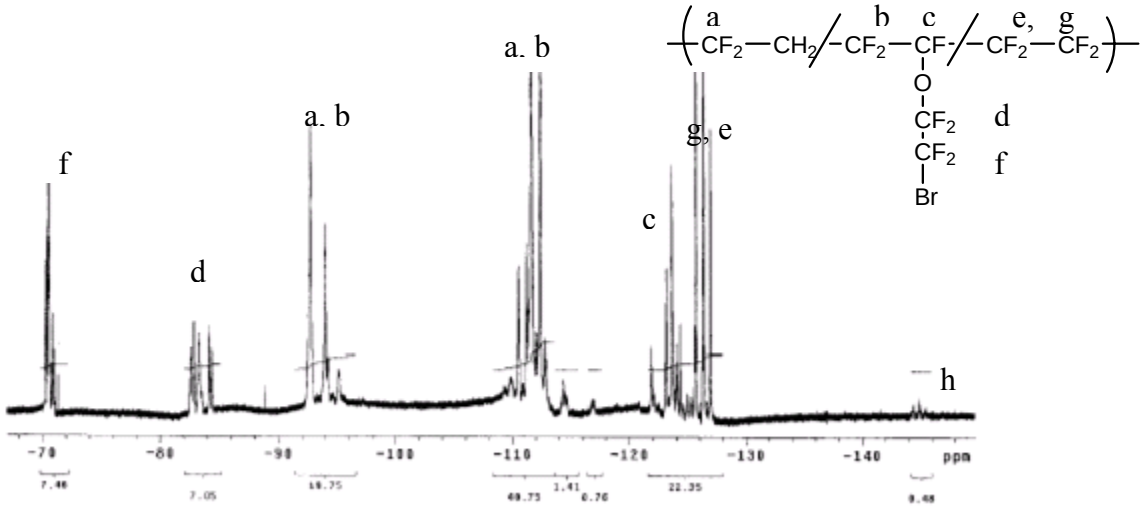

Figure 2-5. ^{19}F NMR of p(82:10:8 VF_2/TFE/EVEBr) terpolymer.

2.2.4.2.2 Thermal Property Analysis. Thermal properties of co- and terpolymers were investigated by thermogravimetric analysis (TGA) and differential scanning calorimetry (DSC). The results for both TGA and DSC are summarized in Tables 2-5 and

2-6, respectively. The thermograms of these copolymers show good thermal stability as decomposition temperatures (onset of 5 % weight loss) range from 77 to as high as 425 °C for the copolymers and from 232 to 389 °C for the terpolymers. Most of the terpolymers possess thermal stabilities above 350 °C, which is likely due to the presence of TFE in the polymer. A typical thermogram of a terpolymer composed of 52 mol% of VF_2, 12 mol% of EVEBr, and 36 mol% of TFE is illustrated in Figure 2-6. As expected, glass transition temperatures were found to increase as the molecular weights of the polymers increased or for polymers with similar molecular weights as the amount of TFE in the composition were increased. Glass transition temperatures of the copolymers range from -63 to -23 °C, while the T_g's of terpolymers range between -30 to -4 °C. As most oligomers were liquids at room temperature, all the T_g's were below room temperature. Having low T_g's (relative to room temperature) is also extremely beneficial and imperative, as these oligomers will need to retain a low T_g after crosslinking to maintain their elastomeric properties. Glass transition temperatures are influenced by molecular weight such that as the polymer molecular weight increases, so does the T_g until the critical molecular weight of entanglements for the polymer is reached at which point the T_g levels off. Glass transition temperatures are also affected by side chain mobility of the vinyl ether. As expected, with an increasing amount of EVEBr incorporated into the polymer backbone the T_g decreases. Figure 2-7 illustrates a typical thermogram of a copolymer composed of 55 mole% of VF_2 and 45 mole% of EVEBr using DSC.

Table 2-5. Physical properties of copolymers.

VF_2 [mol%][a]	EVEBr [mol%][a]	M_n [kg/mol][b]	M_w [kg/mol][b]	PDI[b]	T_g [°C][c]	5 % loss[d]
55 (60)	45 (40)	14.2	24.9	1.8	-30	369 °C
57 (60)	43 (40)	9.0	23.0	3.3	-59	77 °C
60 (66)	40 (33)	8.9	16.8	1.9	-63	174 °C
60 (75)	40 (25)	14.0	45.0	3.2	-31	375 °C
61 (80)	39 (20)	29.0	61.0	2.1	-32	NSA
62 (68)	38 (32)	13.0	35.0	2.7	-54	110 °C
63 (60)	37 (40)	7.4	14.4	2.0	-37	211 °C
63 (63)	37 (37)	6.6	12.9	1.8	-41	115 °C
63 (60)	37 (40)	7.4	14.4	2.0	-37	211 °C
66 (80)	34 (20)	15.0	53.0	3.5	-30	422 °C
71 (75)	29 (25)	7.6	11.2	1.5	-56	303 °C
71 (80)	29 (20)	31.0	112.0	3.6	-25	425 °C
73 (50)	27 (50)	3.9	8.7	2.5	-27	273 °C
73 (60)	27 (40)	6.2	14.1	2.3	-38	110 °C
80 (80)	20 (20)	15.0	53.0	3.5	-30	NSA
88 (66)	12 (33)	7.3	16.7	1.9	-37	185 °C

a: obtained using fluorine NMR; b: obtained by using GPC; c: obtained by using DSC; d: obtained by using TGA; NSA: no sample available.

Table 2-6. Physical properties of terpolymer.

VF_2 mol%[a] (feed)	EVEBr mol%[a] (feed)	TFE mol%[a] (feed)	M_n [kg/mol][b]	M_w [kg/mol][b]	PDI[b]	T_g [°C][c]	5 % loss[d]
21 (70)	34 (15)	45 (15)	41.0	129.0	3.1	-27	NSA
24 (73)	40 (20)	36 (7)	21.0	69.0	3.3	-30	345 °C
34 (60)	18 (15)	48 (25)	33.0	69.0	2.1	-23	375 °C
52 (73)	38 (20)	10 (7)	25.0	100.0	3.9	-27	NSA
52 (35)	12 (15)	36 (50)	49.0	89.0	1.8	-6	389 °C
64 (50)	9 (15)	27 (35)	83.0	145.0	1.8	-13	367 °C
70 (10)	7(15)	23 (75)	63.0	107.0	1.7	-4	NSA
72 (50)	7 (15)	21 (35)	50.0	70.0	1.4	-11	388 °C
73 (50)	7 (15)	20 (35)	78.0	137.0	1.8	-19	385 °C
76 (50)	11 (15)	13 (35)	50.0	118.0	2.4	-9	380 °C
76 (50)	17 (15)	7 (35)	74.0	129.0	1.7	-21	369 °C
79 (50)	12 (15)	9 (35)	42.0	68.0	1.6	-23	232 °C
82 (50)	10 (15)	8 (35)	63.0	120.0	1.9	-18	384 °C

a: obtained using fluorine NMR; b: obtained by using GPC; c: obtained by using DSC; d: obtained by using TGA; NSA: no sample available.

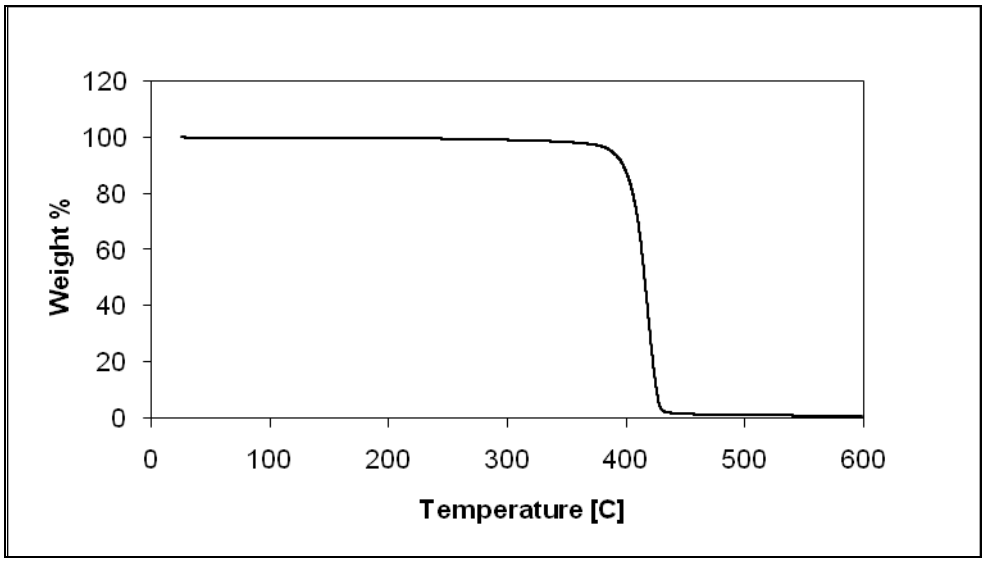

Figure 2-6. Thermogravimetric analysis of p(52:12:36 VF_2/EVEBr/TFE) terpolymer.

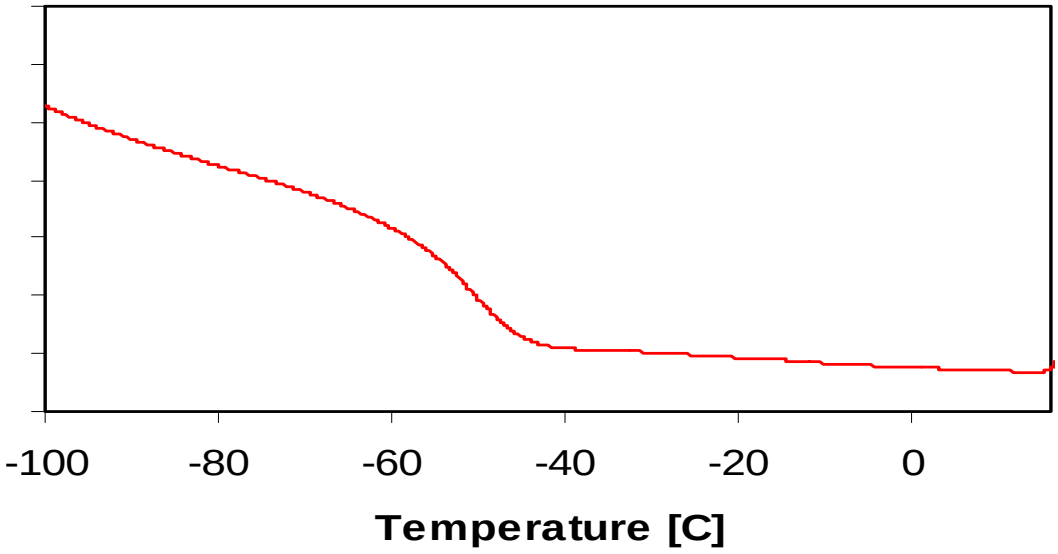

Figure 2-7. DSC thermogram of the second heat of p(55:45 VF_2/EVEBr) copolymer.

2.2.4.2.3 Gel Permeation Chromatography. The fluorinated oligomers were soluble in THF and were analyzed using GPC. Qualitative molecular weight values were obtained against polystyrene standards. Results of GPC characterization is summarized in Tables 2-4 and 2-5 for the co- and terpolymers respectively. Number average molecular weights (M_n) for the copolymer of VF_2 and EVEBr ranged from 3.9 to 31.00 Kg/mol with polydispersity indexes ranging from 1.5 to 3.5, typical for free radical polymerizations. Number average molecular weights of terpolymers composed of VF_2, EVEBr, and TFE ranged from 21.0 to 83.0 Kg/mol. Polydispersity indices of the terpolymers ranged from 1.7 to 3.3. Some terpolymer samples were insoluble in THF due to high % TFE and resulting crystallinity and thus unable to be characterized using GPC.

2.2.4.3 Conclusions: Synthesis in $scCO_2$. Co- and terpolymers of different compositions containing VF_2, EVEBr as a cure site monomer, and at times TFE, were synthesized in supercritical carbon dioxide and analyzed using NMR, IR, TGA, DSC and GPC. The synthesis in CO_2 of these fluorinated elastomers allowed for safe handling of TFE, was more environmentally responsible as it negated the typical generation of halogenated, organic, or aqueous waste, and circumvented the use of fluorinated surfactants. Upon venting, a dry product was isolated, decreasing the energy demand of the process as an energy intensive drying step is not necessary. A facile polymerization process for the synthesis of functionalized, fluorinated oligomers is realized using CO_2. These liquid, functionalized, fluorinated macromolecules allow for facile processing in the conversion to solid elastomers.

2.3 Crosslinking Liquid Oligomers.

2.3.1 Materials. A variety of radical traps were used included triallyl isocyanurate (TAIC), 1,4-cyclohexane dimethanol divinyl ether (CDE), and di(acryloyl) piperazine (DAP). These were all obtained from Aldrich and used subsequent to deinhibition by flowing through a neutral alumina column. Photoinitiator including 2,2-dimethoxy-2-phenylacetophenone (DMPA), hydroxycyclohexyl phenyl ketone (HCPK), 2-hydroxy-2-methyl propiophenone (HMP), and diethoxyacetophenone (DEAP) were obtained from Sigma Aldrich and were used as received. Thermal initiators included 2,2-azobis(2-methypropionitrile) (AIBN), benzoyl peroxide (BPO), and di(2-ethylhexyl) peroxy dicarbonate (EHPDC) and were also obtained from Sigma Aldrich and used as received unless stated otherwise. AIBN was recrystallized from methanol prior to use.

2.3.2 Conversion of Functional Liquid Oligomers to Solid Elastomers. The chemical crosslinking of fluorinated materials as discussed in Chapter 1 has been well established in the literature, especially in the patent literature. Cured elastomers are achieved by two main pathways either via an ionic or radical mechanism. The functional, liquid prepolymers synthesized in CO_2 were to be radically crosslinked with a radical trap in the presence of a brominated CSM. The concentration and choice of either thermal or photoinitiators was investigated for facile, rapid curing. Further optimization was considered by varying the radical trap and its concentration.

Liquid precursors were thoroughly cured using a radical trap and initiator. Triisocyanurate acted as the radical trap and (DMPA) was found to be the best photoinitiator based on the elastomeric mechanical properties, highest degree of

successful crosslinking and lowest % sol-fraction. All components were added with the radical trap/initiator wt-% to liquid precursor between 5:1 and 25:5. Components were dissolved in small volumes of methylethylketone (MEK) to ensure thorough, homogenous mixing. The viscous, homogenous mixture was then placed onto a glass substrate or silicon master, underneath a crystallization dish containing open MEK vials for slow evaporation overnight. The films are then placed in the vacuum oven overnight for full removal of solvent. In the case of photoinitiators, the films were purged using nitrogen for ten minutes. The films were then cured using 365 nm wavelength light in a UV oven for typically ten minutes under constant nitrogen flow. In the case of thermal initiators, films were placed in an isothermal oven at different temperatures for various time intervals. Temperature and cure times were explored for facile, rapid curing procedures. The amount of radical trap added to the copolymer was kept at 5 or 10 wt-%, while the initiator concentration was held at 1 wt-%. Three wt-% was briefly investigated to ensure the most effective and efficient crosslinking was being achieved but no change in mechanical or surface properties was found using this increased initiator concentration. Thin films or replica molds of the cured mixtures were fabricated and characterized. Thin films were also poured onto silicon masters to study pattern replication and wettability.

2.3.2.1 Initiators: Thermal. Current benchmark VF_2-based elastomers are typically crosslinked thermally using coagents and thermally degradable peroxides. The following thermal initiators were investigated: 2,2-azobis(2-methypropionitrile) (AIBN), benzoyl peroxide (BPO) and di(2-ethylhexyl) peroxy dicarbonate (EHPDC). Though attempts were made to cure our materials using thermal initiators, challenges to obtain

smooth surfaces on the solid elastomers were unable to be overcome. The main challenges that prohibited smooth film formation included cure temperatures at reasonable half lives above the boiling point of the coreagent and not having access to sophisticated molding devices that would result in smooth surfaces. In comparison to the photoinitiators, the thermal initiators had a lower success rate in curing the liquid precursors. Preliminary studies (without liquid precursors) show that cure mixes containing one weight percent initiator (except in the case of BPO), fails to initiate the crosslinking of the radical trap at a sufficient enough rate, so the end product remained uncured or only partially cured. The preliminary studies also confirmed that the crosslinker 1,4-cyclohexane dimethanol divinyl ether (CDE), is completely unsuitable for our system due to extremely low reactivity.

When using EHDPDC, a one hour reaction time was insufficient in producing fully cured, non-tacky and flexible elastomers, even though the preliminary studies without the liquid precursor in the cure mix showed some promise. A possible reason for the failure to cure is because peroxides are commonly known to undergo ß-scission at higher temperatures (more than 70 ºC in the case of EHPDC), and decompose into the methyl radical and a carboxylic acid. This is an uncontrollable side reaction, that can reduce the efficiency of the propagation step and hence the crosslinking reaction. Obtaining fully cured elastomers with smooth surfaces were unsuccessful when a thermal initiator. Investigations continued in efforts to find coreagents that would result in fully cured elastomers with desirable properties.

2.3.2.2 Initiators: Photochemical. Among the photoinitiators, 2,2-dimethoxy-2-phenylacetophenone (DMPA), hydroxycyclohexyl phenyl ketone (HCPK), 2-hydroxy-2-methyl propiophenone (HMP), and diethoxyacetophenone (DEAP) were investigated. Reactions with DMPA resulted in the most efficient and effective crosslinking, because in the free radical bromine abstraction mechanism the benzoyl radical produces a very short triplet state lifetime (0.25 ns) and a dissociation quantum yield of 0.95, the highest of all type I photoinitiators. Experiments on four different types of photoinitiators demonstrated that 2,2-dimethoxy-2-phenylacetophenone (DMPA) was the superior initiator for producing fluoroelastomers of excellent chemical and thermal stabilities. Lalevee et al. have conducted a study into the reactivities of cleavable photoinitiators in photo-polymerization reactions.[40] In the paper, they reported that the benzoyl radical has an initiation rate constant (k_i) on the order of 10^4 $M^{-1}s^{-1}$, compared to the k_i of aliphatic and aromatic ketyl radicals (rate is on the order of 10^7 $M^{-1}s^{-1}$ in methyl methacrylate and methyl acrylate). Although benzoyl radicals react with monomers at a lower rate constant, they will add to the unsaturation of vinyl monomers. The deactivation routes include reaction with oxygen and termination with another radical. This has two important consequences in determining the cure efficiency: termination side reactions with constituents of the polymerization mixture are prevented, and monomer quenching is not a competitive reaction to the α-cleaving process. Also DMPA is a photoinitiator that is designed especially for free radical vinyl polymerizations, and is the most prominent member of its class. Diethoxyacetophenone (DEAP) does have the benefit of initiating crosslinking to produce highly elastic membranes however, but sol-gel analysis proves that these are not necessarily the best crosslinked elastomers. Lower sol fractions

were obtained when DMPA was used over DEAP as a photoinitiator and thus produced better crosslinked networks. Table 2-7 summarizes elastomer stabilities when using DMPS as a photoinitiator. Elastomers cured with 2-hydroxy-2-methyl propiophenone (HMP) left in THF for 20 hours, produced one of the highest percentage weight loss of gel, at 35.6 %. This was using a cure mix of p(73:27 VF_2/EVEBr) with 25:5 wt-% TAIC/HMP.

Finally hydroxycyclohexyl phenyl ketone (HCPK) gave the poorest performance as a photoinitiator in efforts to initiate crosslinking of the functional fluorooligomers. Even using high amounts (up to 7 wt-%) of HCPK failed to initiate the crosslinking process. Greater than three wt-% of photoinitiator in the cure mixture was needed to produce successfully cured membranes. There is of course room for improvement, for example increasing the cure time and reducing its temperature according to the half-life of a thermal initiator. However the aim of the project was to alleviate reaction times, and improve processability and reactivities of the reagents. There are some difficulties with the handling of the extremely reactive, exothermic thermal initiators, and alternative methods of transferring the cure mix onto the substrate without the use of external stimuli such as a heat gun, need to be employed. There are also purification, solubility, and toxicity issues with the initiators tested. So because thermal initiators have reactivity issues and do not perform to the same consistency as photoinitiators that undergo controllable α-scission, there would be no further advantages in optimizing thermal initiator conditions.

Table 2-7. Chemical stability summary of cured elastomers.

p(VF_2/EVEBr/TFE) mole ratio[a]	TAIC (wt%)	DMPA (wt%)	Performance in THF
(21/34/45)	10	5	Stable to solvent remains intact
(24/40/36)	5	5	Unstable to solvent swells and fractures
(24/40/36)	10	5	Stable to solvent remains intact
(52/73/10)	10	5	Stable to solvent remains intact
(60/40/0)	10	5	Stable to solvent flexible, swollen
(62/38/0)	25	5	Unstable to solvent swells and fractures
	10	5	Stable to solvent remains flexible but slightly fractured
(66/34/0)	10	5	Stable to solvent remains intact
(71/29/0)	10	5	Stable to solvent flexible, swollen remains intact
(80/20/0)	10	5	Stable to solvent flexible, swollen

a: obtained using ^{19}F-NMR;

2.3.2.3 Radical Trap Crosslinkers. Radical traps are compounds with a high affinity for free radical species and in this context contain vinyl groups and functions as a crosslinker. The choice and concentration of a radical trap to crosslink the functional, liquid oligomers play an important role in the extent of crosslinking. Different compositions were investigated to discover optimal cure conditions. Allylic and vinyl radical traps were studied including triallyl isocyanurate (TAIC), 1,4-cyclohexane dimethanol divinyl ether (CDE), and di(acryloyl) piperazine (DAP). Triallyl isocyanurate

(TAIC) proved to deliver the best results in curing these flourooligomers, as it is the leading radical trap for conventional fluoroelastomers cured via a radical mechanism. The divinyl ethers would have complemented the overall polymer structure, however even with initiator feeds as high as seven weight percent of thermal or photochemical initiators, successful curing was unattainable. Vinyl ethers do not homopolymerize in the presence of radical initiators due to their electron rich double bonds and their reactivity can be challenging even to copolymerize with certain monomers. Divinyl ethers are more suitable for use in cationic systems, where the monomer being crosslinked contains at least two reactive groups (e.g. divinyl ethers and bismaleimides), unlike the fluoropolymers in this study that contain only one reactive site on the cure site monomer. Di(acryloyl) piperazine proved problematic due to onset of crystallization upon solvent removal.

With increasing concentration of the radical trap in the cure mix, the mechanical properties of the cured membrane became increasingly brittle and less flexible. If homogenous mixing is not ensured and more functional groups are present relative to CSM sites, increasing brittleness is expected as the radical trap would homopolymerize significantly decreasing the overall average molecular weight between crosslinks. With decreased molecular weight between crosslinks, chain mobility decreases and overall flexibility is compromised in exchange for a rigid material. The elastomer also became opaque as feed ratios of TAIC surpassed 25 weight percent. It should be noted that removal of the inhibitor in the radical trap was pertinent. A few experiments adding the radical trap inhibited and deinhibited at the same concentration clearly showed that successful cure states were obtained when the radical trap was deinhibited.

2.3.2.4 Mechanism. Similar to reaction Scheme 1-3 in Chapter 1, the synthesized oligomers undergo bromine abstraction and are incorporated into a crosslinked network in the presence of a radical trap. The main difference is the origin of the radical source. In Scheme 1-3, the radical source originates from the thermal decomposition of a peroxide. Here, the less conventional radical source results from the UV decomposition of a photoinitiator. The generation of polymeric radicals is attained in the abstraction of bromine on the end of the cure site chain, which in turn adds onto the electron rich allyic bonds of the radical trap. Eventually a dense 3-dimensional network of fluoropolymers covalently linked together with the radical trap, is formed. Figures 2-8 through 2-11 illustrate optical images of cured elastomers.

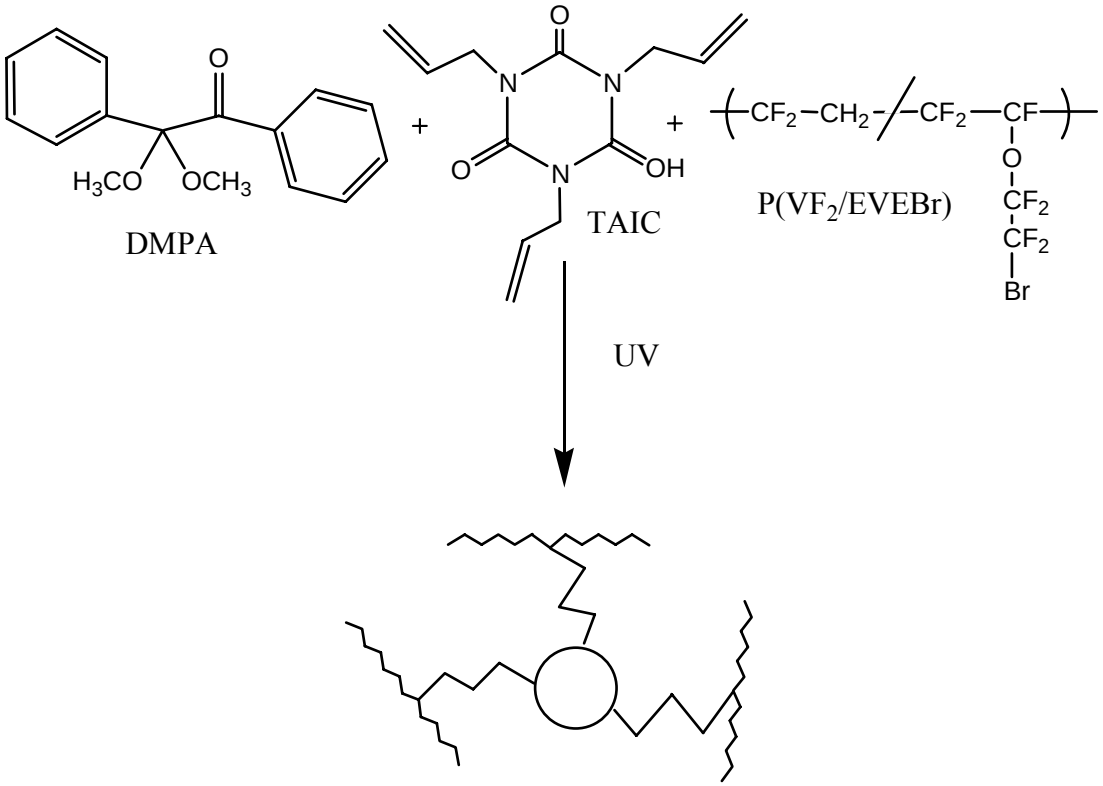

Scheme 2-4. Crosslinking functional oligomers in the presence of DMPA and TAIC.

Figure 2-8. Optical image of p(88:12 VF_2/EVEBr) cured using 25:1 wt-% of TAIC/DMPA.

Figure 2-9. Optical image of p(55:45 VF_2/EVEBr) cured using 25:5 wt-% of TAIC/DEAP.

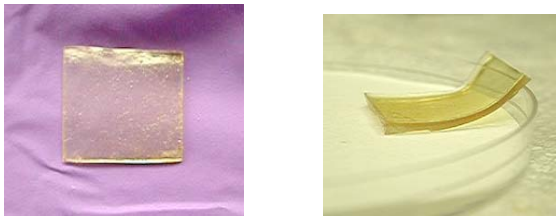

Figure 2-10. Optical Image of p(88:12 VF_2/EVEBr) Cured using 25:5 wt-% of TAIC/DEAP.

Figure 2-11. Optical image of p(63:37 VF_2/EVEBr) cured using 25:5 wt-% of TAIC/DEAP.

2.3.3 Characterization.

2.3.3.1 Thermal Analysis. Thermal stability is typically noted by the temperature at which five weight percent of a sample is lost using Thermal Gravimetric Analysis (TGA). Thermal stability analysis was conducted on cured elastomers of different compositions and compared to the original liquid prepolymer before crosslinking. Differential Scanning Calorimetry (DSC) was used to analyze thermal properties, including glass transition temperatures. The cured elastomers were characterized and compared to the respective functional prepolymer.

2.3.3.1.1 Thermogravimetric Analysis (TGA). Samples of cured elastomers were analyzed using TGA under a constant heating rate of 10 °C. The sample mass was monitored with respect to temperature. Thermal stability was measured as the temperature at which five weight percent of sample was lost. Upon crosslinking the liquid precursors, the materials became increasingly thermally stable, as expected. Table 2-7 summarizes the thermal properties of the cured elastomers. In going from an uncured oligomer to a cured elastomer, there is a significant increase in the temperature at which the material undergoes a five percent weight loss (mean temperature is 576.6^{o}C). This thermal stability is a result of the established network matrix, the lack of labile functional groups, and the triazine composition of the radical trap.

2.3.3.1.2 Differential Scanning Calorimetry (DSC) Analysis. An increase in the glass transition temperatures upon crosslinking of the fluoropolymer oligomers is evident as illustrated in Table 2-8 and Figures 2-12 and 2-13. The explanation for this behavior

again lies in the structural differences in the polymer chains between the cured and uncured states. As the crosslinking of the fluoropolymers occurs, chain mobility decreases resulting to an increase in glass transition temperature. The glass transition temperature remains relatively low however, below room temperature, ensuring elastomer properties.

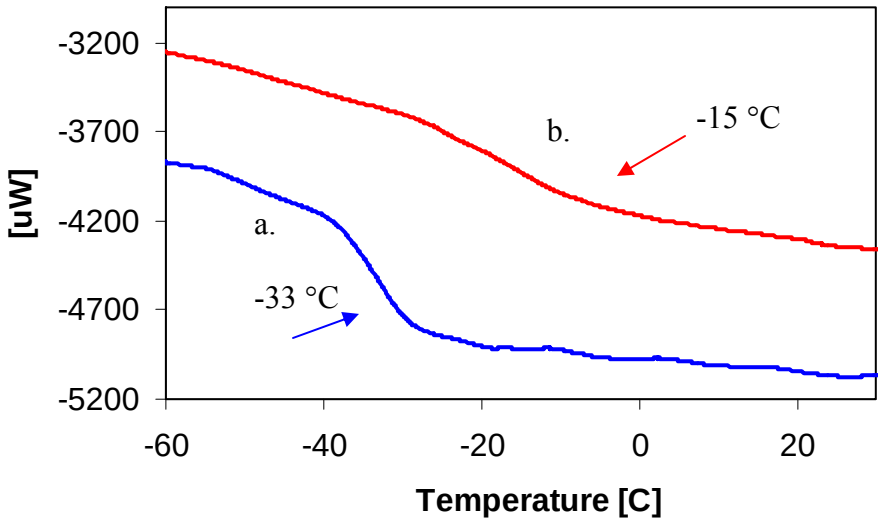

Figure 2-12. DSC thermograms illustrating glass transition temperatures of cured and uncured elastomers p(55:45 VF_2/EVEBr); a. uncured; b. cured with 25:5 wt-% of TAIC/DMPA.

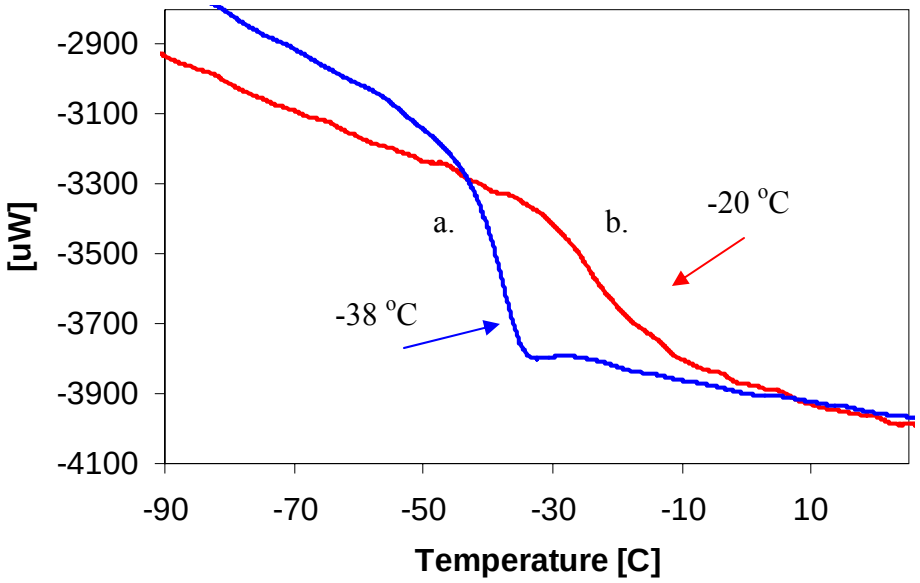

Figure 2-13. DSC thermogram illustrating glass transition temperatures of cured and uncured p(88:12 VF_2/EVEBr) (88/12); a. uncured; b. cured with 25:5 wt-% of TAIC/DMPA.

Table 2-8. Thermal properties of cured and uncured fluoroelastomers.

p(VF_2/EVEBr/TFE) mole ratio[a]	(TAIC/PI) (wt %)	5 % weight loss (^oC)[b]	T_g (uncured) (^oC)[c]	T_g (cured) (^oC)[c]
(21/34/45)	(10/5)	562	-28	-19
(24/40/36)	(10/5)	583	-30	-21
	(5/5)	582		-21
(52/73/10)	(10/5)	583	-27	-20
(57/43/0)	(25/5)	595	-59	-13
	(25/5)	556		-12
	(10/5)	587		-13
(60/40/0)	(10/5)	575	-31	-16
(62/38/0)	(25/5)	563	-54	-19
	(25/5)	591		-17
	(10/5)	558		-12
(63/37/0)	(25/5)	583	-37	-19
	(25/5)	566		-19
(66/34/0)	(10/5)	576	-25	-15
(71/29/0)	(10/5)	576	-25	-17
(73/27/0)	(25/5)	563	-38	-19
(80/20/0)	(10/5)	585	-30	-22
(88/12/0)	(25/5)	595	-37	-23

a: obtained using ^{19}F NMR; b: obtained by TGA; c: obtained by DSC

2.3.3.2 Swelling, Stability, and Sol-Gel Analysis. Swelling experiments of cured elastomers were initially conducted in methylene chloride solvent And then for a more thorough analysis the chemical stability of cured elastomers they were investigated in tetrahydrofuran (THF) as well. Experimental results are summarized in Table 2-8. Swelling experiments offer useful information regarding the efficiency of the crosslinking reaction. A covalently crosslinked elastomer by definition will not dissolve in any solvent. Polymer chains may however be extracted from the network if they were not incorporated into the cured matrix and are not extensively entangled throughout the network. Swelling data illustrates the material's propensity to a particular solvent and typically determined by dimensional changes. The dimensions of a regularly shaped piece of elastomer are first measured along with its mass and then the material is soaked in a

solvent for a given measure of time. After the given amount of time, the material is removed from the solvent, blotted dry and the dimensions and mass are determined again. The difference in mass and dimensions before and after swelling are used to calculate the swelling.

Dimensional change upon solvent exposure was challenging to record as the films were increasingly fragile in the swollen state. Elastomers cured from higher molecular weight oligomers proved to be more chemically stable and were less brittle than the materials resulting from lower molecular weight precursors. With increasing amount of TFE incorporated into the prepolymer, the chemical resistance increased as well. Elastomers exposed to acid or base remained chemically inert as evident by no or little dimensional change and the lack of dissolution.

The chemical stability of the fluorinated elastomers using swelling experiments in THF and sol-fraction analysis using Infrared (IR) Spectroscopy and Gel Permeation Chromatography (GPC) was investigated. Cured elastomer samples soaked in THF for four hours and again for at least 20 hours. After samples soaked in THF for four hours, elastomer samples were extracted and the THF solution was analyzed using GPC. The procedure was repeated for 20 hours of soak times of the fluorinated elastomer in THF.

2.3.3.2.1 Infrared Spectroscopy. The IR spectra of the cured elastomers (gel portion) differed from the spectra of the respective sol-fractions. Most notably, the difference was found in the presence of the crosslink functionality groups, the methylene and triazide groups, in the gel portion. Figure 2-7 illustrates a typical IR spectrum of a gelled elastomers and the respective sol-fraction after 20 hours. Two significant stretches associated with the elastomer gel are present between 3440 and 3370 cm^{-1} and between 3060 and 2850 cm^{-1}. The first series of peaks in the region of 3440–3370 cm^{-1} are from either the amide groups (on the radical trap) or from carboxylic acid groups, potentially generated by β-scission of the aromatic ketyl radical (Scheme 2-3). The other series of stretches in the 2960 cm^{-1} region are from the saturated C–H groups on the link between the fluoropolymer and radical trap (Figure 2-6), giving evidence that the materials have been successfully crosslinked. The lack of unsaturated stretches, typically appearing at 3095 to 3010 cm-1 for the =C–H stretch or at 1660 to 1600 cm-1 for the –C=C– bend, gives evidence that unreacted radical trap is not present.

A typical IR spectrum of the sol-fractions is illustrated in Figure 2-11. As expected, the presence of peaks at 1173 and 906 cm^{-1} confirm the presence of $–CF_2–$ and C–F groups. The absence of a bromine peak, which should appear in the region 690 – 515 cm^{-1}, suggests that the sol-fractions contained negligible amounts of CSM incorporated into the fluoropolymer chain. It is possible that CSMs incorporated into the polymer chain underwent substitution reactions with hydrogen atoms perhaps, without being incorporated into a crosslink.

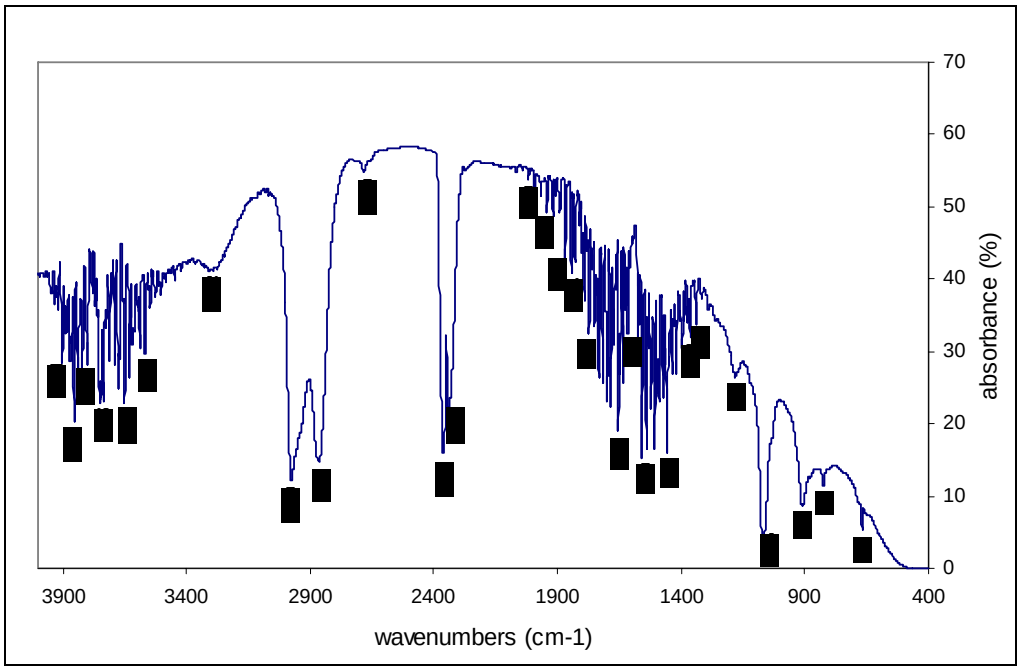

Figure 2-14. Infrared spectrum of sol-fraction from copolymer p(55:45 VF_2/EVEBr) cured with 25:5 wt % TAIC/DMPA.

2.3.3.2.2. Gel Permeation Chromatography. Molecular weight analysis of the sol-fractions was conducted using Gel Permeation Chromatography (GPC). The results are summarized in Tables 2-9 and 2-10 for co- and terpolymers, respectively. The difference in average molecular weights between the parent oligomer (M_n parent) and the sol-fractions of the elastomers becomes relatively less significant as the M_n of the parent liquid precursor increases. For example, the oligomer, p(73:27 VF_2/EVEBr) is composed of a number average molecular weight of 6.2 kg/mol and the M_n of the respective sol-fraction consisted of 4.4 Kg/mol. In examples concerning terpolymers, oligomers composed of p(21:34:45 VF_2/EVEBr/TFE) had a number average molecular weight of 41 kg/mol. This is in drastic comparison to the sol-fraction containing a number average molecular weight of 5.3 kg/mol. Curing reactions were thus more efficient and effective with terpolymer compositions in producing a more stable network. However, less

terpolymer samples were utilized, as indicated in Table 2-10, as homogenous mixing of cure components was challenging in some cases and therefore the fabrication of elastomers were unattainable.

A few elastomer samples were exposed to solvent for three hours. The sol-fraction was collected and the same sample was exposed to more solvent for at least a total of 20 hours. Results obtained from GPC indicate that the molecular weight of the sol-fraction obtained after 20 hours is slightly larger than that obtained from the sol-fraction after three hours. Both samples contain polymer chains of lower average molecular weight compared to the prepolymer before crosslinking. The trend, illustrated in Figure 2-15, can be explained by the following: during the three hour solvent soak, polymer chains that are not covalently incorporated into the matrix and are soluble in the solvent will migrate from the matrix. Smaller chains (lower molecular weight) have greater mobility and are less entangled in the network. These lower molecular weight chains diffuse out of the matrix first. Subsequent to the diffusion of the low molecular weight chains, the elastomer has void volumes where the chains used to reside. The void volumes allow for larger molecular weight chains to gain greater mobility, thus detangling themselves from the network and diffusing in the solvent continuous phase.

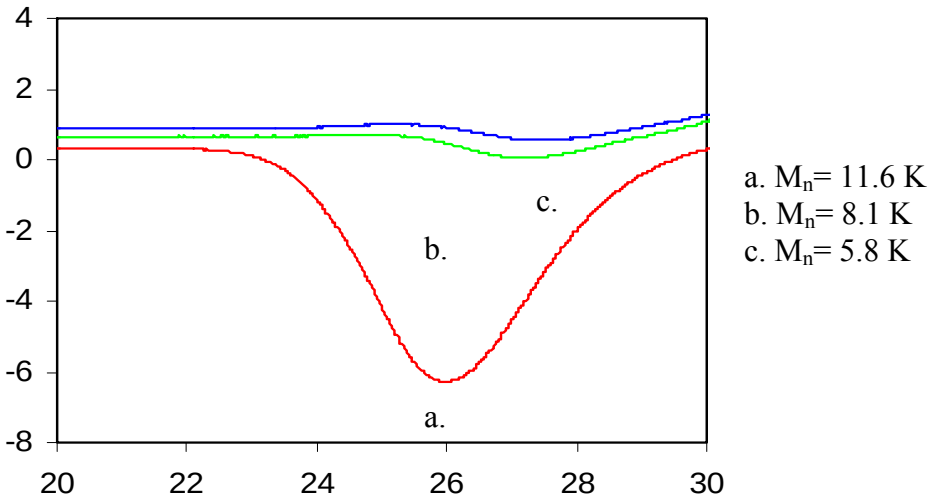

Figure 2-15. GPC traces of a. p(55:45 VF_2/EVEBr) and sol-fractions of elastomer cured with 25:5 wt % of TAIC/DMPA after b. 24 hours and c. after three hours in THF.

Table 2-9. Sol-gel analysis summary of p(VF_2/EVEBr) copolymers using GPC.

p(VF_2/EVEBr) mol%[a]	(TAIC/PI) weight%	M_n (parent) [kg/mol] [b]	M_n (sol-fraction) [kg/mol][b]	M_w (sol-fraction) [kg/mol][b]	PDI[b]	% sol fraction (20hrs in THF)[c]
55:45	(10/5)	11.6	8.0	12.2	1.52	19.9
	(25/5)		2.9	7.4	2.57	7.59
	(25/5)		2.9	6.5	2.28	5.3
	(25/5)		5.5	12.4	2.27	21.6
57:43	(10/5)	9	2.9	7.3	2.5	9.1
	(25/5)		4.3	6.4	1.5	18
	(25/5)		3.4	6.2	1.8	14.7
60:40	(10/5)	14	3.5	8.9	2.5	12
62:38	(10/5)	13	3.3	6.9	2.1	6
	(25/5)		5.5	9.2	1.7	12
	(25/5)		3.2	6.6	2.1	11.4
63:37	(25/5)	7.4	3.6	6.2	1.71	18.7
			4.5	7.8	1.75	22.9
73:27	(10/5)	6.2	4.4	7.4	1.67	22.98
	(10/5)		3.4	8.9	2.65	41.6
	(25/5)		3.3	5.6	1.68	17.4
80:20	(10/5)	15	3.6	10.4	2.9	10
88:12	(10/5)	7.3	3.9	6.8	1.77	15.9
	(25/1)		5.7	9.7	1.7	26.9
	(25/5)		2.7	5.6	2	8.9
	(25/5)		4.2	7.8	1.84	34.3
	(50/1)		4.9	9.4	1.9	19.8
	(50/5)		4.5	8.4	1.85	32.7

a: obtained by ^{19}F-NMR; b: obtained by GPC; c: obtained gravimetrically.

Table 2-10. Sol-fraction analysis summary of cured p(VF_2/EVEBr/TFE) terpolymers.

(VF_2/EVEBr/TFE) mole ratio[a]	(TAIC/DMPA) weight %	M_n (parent) [kg/mol][b]	M_n (sol-fraction) [kg/mol][b]	% weight loss (elastomer in THF for 20 hrs)[c]
(24/40/36)	(10/5)	21	3.1	1.7
(52/73/10)	(10/5)	25	3.3	9.1
(21/34/45)	(10/5)	41	5.3	23.2

a: obtained by ^{19}F-NMR; b: obtained by GPC; c: obtained gravimetrically.

2.3.3.2.3. Nuclear Magnetic Resonance Analysis. Sol fractions were analyzed using ^{19}F-NMR in order to obtain structural information of the sol-fraction and efficiency of the crosslinking method. Figure 2-16 illustrates a fluorine spectrum of the sol-fraction obtained from p(24:40:36 VF_2/EVEBr/TFE) cured with ten weight percent of TAIC and five weight percent of DMPA for 24 hours. This terpolymer under the noted conditions resulted in the most stable elastomer. After the 24 hour soak in THF only 1.7 weight percent was lost in the sol-fraction, the least of any other fabricated elastomer. Figure 2-9 also illustrates that no fluorinated methylene group adjacent to a bromine atom is present, expected at -71 and -72.5.[37] This indicated that CSMs were not present in the sol-fraction and that the crosslinking was very efficient, further illustrated by the low weight percent loss of the sol-fraction.

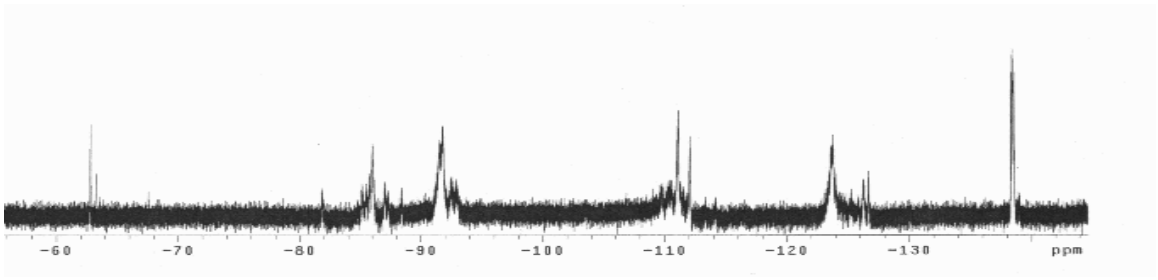

Figure 2-16. ^{19}F-NMR spectrum of sol-fraction obtained from cured p(24:40:36 VF_2/EVEBr/TFE) elastomer with 10 wt-% TAIC and 5 wt-% DMPA.

2.3.3.3 Surface Energies. Static contact angle were measured using distilled water and diiodomethane on thin films of cured elastomer. Measurements were repeated a minimum of three times on separate locations of the film, and average contact angles were calculated. The surface energies of the cured polymer films were evaluated using the Owens-Wendt-Fowkes equation. According to this approach, the surface energy of a solid (γ_s) can be resolved into dispersion and polar components ($^d\gamma s$ and $^p\gamma s$, respectively) (Equation 2-1).

$$0.5(1+0.5\theta)\bullet\frac{\gamma_l}{\sqrt{{}^d\gamma_l}}=\sqrt{{}^p\gamma_s}\bullet\sqrt{\frac{{}^p\gamma_l}{{}^d\gamma_l}}+\sqrt{{}^d\gamma_s} \qquad (2\text{-}1)$$

where θ is the contact angle. If contact angles of two liquids, for which the surface tension (γ_l) and the dispersion and polar components ($^d\gamma_l$ and $^p\gamma_l$, respectively) are known, one can calculate the surface free energy of the solid via equation 2-1. The surface tension and respective components for water and diiodomethane are summarized in Table 2-11 and were employed for the calculations of the surface free energy of our cured

polymer samples. The samples were prepared via solvent casting films of the cure mixture onto a glass slide and placing in a solvent saturated environment overnight for slow evaporation. The samples were then dried in the vacuum oven overnight or until a constant weight had been reached. The samples were then placed in the UV oven chamber with nitrogen purge for ten minutes, followed by irradiation for five to ten minutes under constant nitrogen purge. Static contact angles were measured using water and diiodomethane. Average values are summarized in Table 2-12. The calculated surface free energies and the respective components thereof are summarized in Table 2-13.

Table 2-11. Surface tension properties for test liquids for static contact angle measurements.

Test Liquid	γ_l [mN/m]	$^{d}\gamma_l$ [mN/m]	$^{p}\gamma_l$ [mN/m]
Distilled Water	73	22	51
Diiodomethane	51	50	1

Table 2-12. Static contact angle measurements.

P(VF_2/TFE/EVEBr)	Avg H_2O contact θ	Avg CI_2H_2 contact θ
34:48:18	96	39
64:27:9	91	53
66:0:34	83	59
71:0:29	74	58
73:20:7	83	56
76:13:11	102	60
76:7:17	93	46
82:8:10	97	57

Table 2-13. Owens-Wendt-Fowkes calculations.

P(VF_2/TFE/EVEBr)	γs [mN/m]	^{p}γs [mN/m]	^{d}γs [mN/m]
34:48:18	40	0	40
64:27:9	33	2	31
66:0:34	31	6	26
71:0:29	36	10	25
73:20:7	33	5	28
76:13:11	29	0	29
76:7:17	36	1	35
82:8:10	31	1	30

The average water contact angles ranged between 83 and 102 degrees. For diiodomethane, resulting average contact angles spanned between 39 and 60 degrees. It is evident from Table 2-13, that the major contribution to the solid surface energy arises from the polar components. In some cases the dispersion components barely contribute to the surface energy term. Calculated surface energies for synthesized terpolymers ranged from 29 to 40 mN/m. Though these values may be higher than typically expected for the fluoroelastomer, it is possible that the hydrocarbon content of the radical trap and methylene groups of VF_2 affect the contact angles measured. The contact angles were measured at the air/polymer interface. Molecular chain rearrangement at the air/polymer interface could bring hydrocarbon-rich groups to the surface, thus further impacting contact angle measurements.

2.3.3.4 Modulus Measurements. Solvent cast cure mixtures were prepared using a deep mold (ca width = 1 cm; length = 3 cm) using a PTFE gasket. The filled mold was placed in a solvent-saturated chamber overnight for slow solvent evaporation. The mold was then placed in a vacuum oven overnight or until a constant mass was reached,

indicative of complete removal of any residual solvent. The mold was then placed in a UV oven and purged with nitrogen for five to ten minutes. Finally, the sample was irradiated (365 nm wavelength) for typically ten minutes under constant nitrogen purge. The cured sample was then cut out of the mold and used for mechanical property measurements using an Instron. The results are summarized in Table 2-14. Figures 2-17 and 2-18 illustrate stress versus strain curves of different p(VF_2/EVEBr/TFE) terpolymers cured with 5:10 wt-% of DMPA/TAIC. Having a modulus of 3.5 MPa (p(34:18:48 VF_2/EVEBr/TFE), the material tested in Figure 2-17 could be elongated to a greater extent compared to the terpolymer analyzed in Figure 2-18. The material analyzed in Figure 2-17 was stretched seven times its length, while the terpolymer analyzed in Figure 2-18 was stretch just over twice its length before the sample broke. The latter material, however, had a higher modulus of 9.9 MPa (p(72:7:20 VF_2/EVEBr/TFE). The Young's modulus was taken from the first 5 % of the slope of the stress versus strain plot generated by the instrument. The initial indication of increasing modulus with increasing TFE content of the precursor proved to differ with some of the samples. Molecular weight seemed to have a great influence on modulus, a clear trend could not be found, however. The amount of radical trap added to the cure mixture was usually 5 wt-% in order to maintain a relative comparison to benchmark fluoroelastomers. It should be noted that the best results typically included greater than 5 wt-% of radical trap being added to the cure mixture. This may be as a result of the low molecular weight prepolymers relative to those used in commercial fluoropolymers, more CSM may need to be incorporated into the polymer backbone and more radical trap added to the cure mixture for complete chemical crosslinking and desirable mechanical properties. Table 2-

15 summarizes modulus values of common elastomer materials. Modulus values of fabricated elastomers from synthesized fluorinate p(VF_2/EVEBr/TFE) terpolymers fall within working ranges of commercially available elastomers. These results look promising and could have their place in soft elastomer applications.

Table 2-14. Mechanical properties of p(VF_2/EVEBr/TFE) copolymers.

VF_2 mol%[a]	EVEBr mol%[a]	TFE mol%[a]	M_n [kg/mol][b]	M_w [kg/mol][b]	T_g [°C][c]	Modulus [MPa][d]
34	18	48	33	69	-23	3.5
64	9	27	83	145	-13	11.4
66	34	0	15	53	-30	3.2
71	29	0	31	112	-25	1.4
73	7	20	78	137	-19	9.9
76	17	7	74	129	-21	8.4
76	11	13	50	118	-9	4.3
82	10	8	63	120	-18	12.8

a: obtained by ^{19}F-NMR; b: obtained by GPC; c: obtained by DSC; d: obtained by Instron.

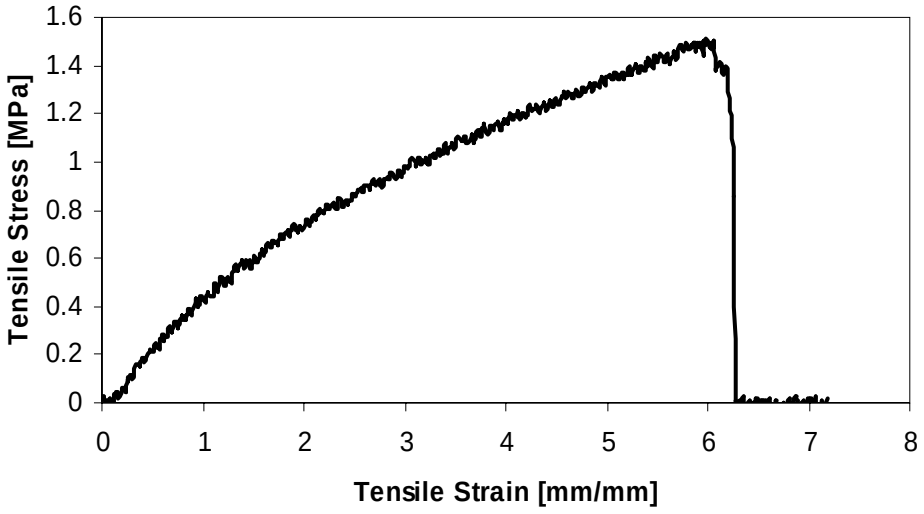

Figure 2-17. Instron testing of cured p(34:18:48 VF_2/EVEBr/TFE) elastomer with 10 wt-% TAIC and 5 wt-%DMPA.

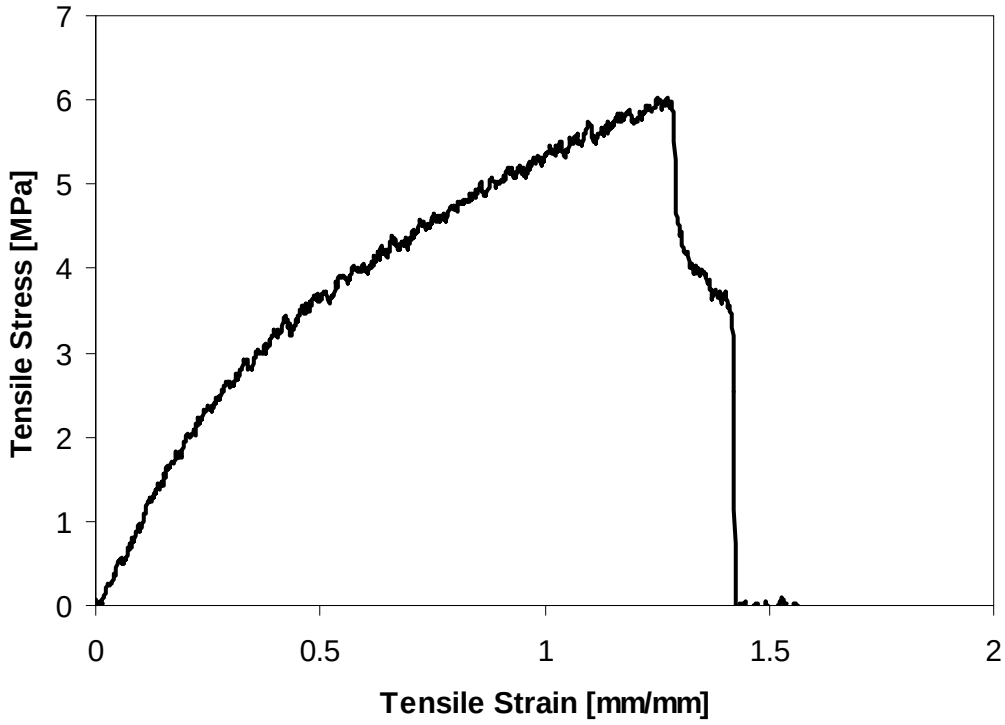

Figure 2-18. Instron testing of cured p(73:7:20 VF_2/EVEBr/TFE) elastomer with 10 wt-% TAIC and 5 wt-%DMPA.

Table 2-15. Modulus values of fluorinated materials.

Material	Modulus [MPa]
Perfluoropolyether (4K)	7.0
Perfluoropolyether (1K)	89.0
Polydimethylsiloxane (Sylgard 184)	0.8
Perfluorinated elastomers	6.0 – 13.0
Fluorinated elastomers	2.0 – 15.0
TFE/PP elastomers	2.5 – 3.5
Fluorinated silicones	1.0 – 6.0
P(VF_2/EVEBr/TFE) terpolymers	1.0 – 13.0

2.3.4 Pattern Replication. Pattern replication was accomplished by pouring the liquid cure mixture onto an etched silicon master template and photochemically crosslinking the material as described previously. The cured mold was then carefully

released from the silicon master resulting in a soft replica. These highly fluorinated VF_2 copolymer cure mixtures were found to completely wet the template surface, creating an embossed film of a true and accurate replication of the surface. Silicon masters are extremely expensive and whether they are used for imprint lithographic applications or device fabrication, utilization of a soft replicate affords a cost effective, reusable, robust alternative. Figure 2-9 illustrates SEM micrographs of the silicon master template (A) and three fluorinated elastomer replicas (B, C, D).

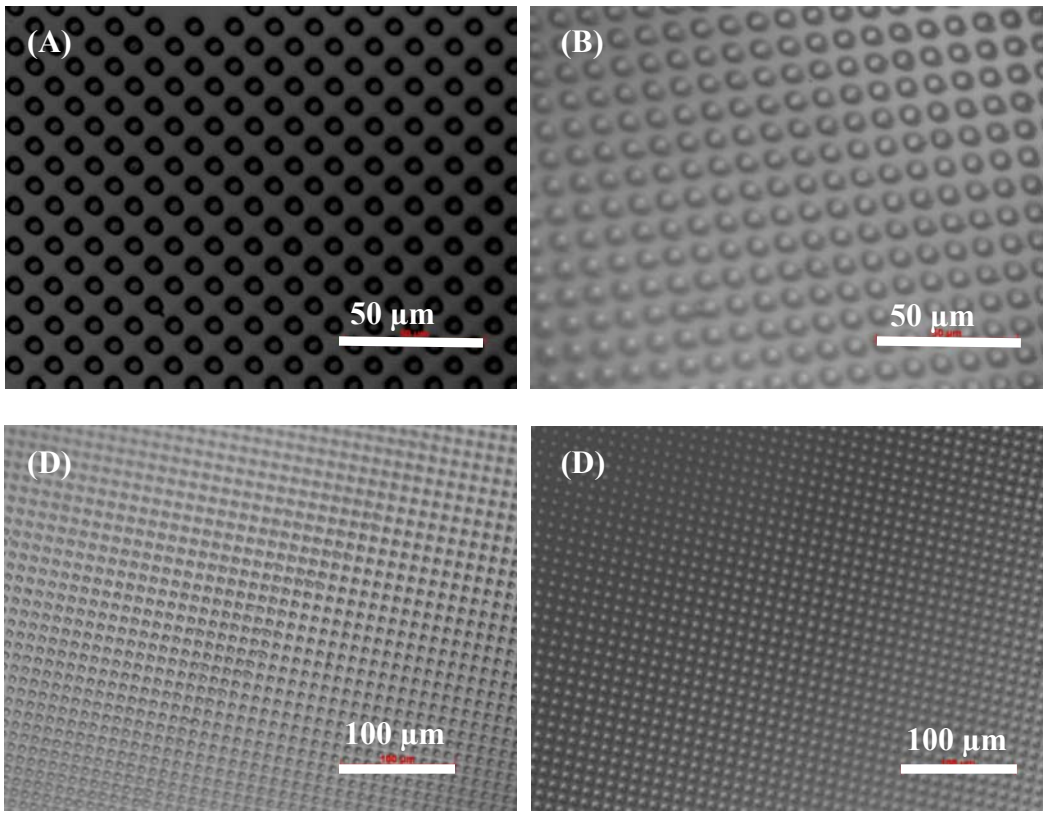

Figure 2-19. SEM micrographs of a silicon master template and replicas made from p(VF_2/EVEBr) cured with TAIC/DMPA; (A) silicon master template; (B) p(71:29 VF_2/EVEBr) with 10:5; (C) p(48:52 VF_2/EVEBr) with 5:5; (D) p(71:29 VF_2/EVEBr) with 10:10.

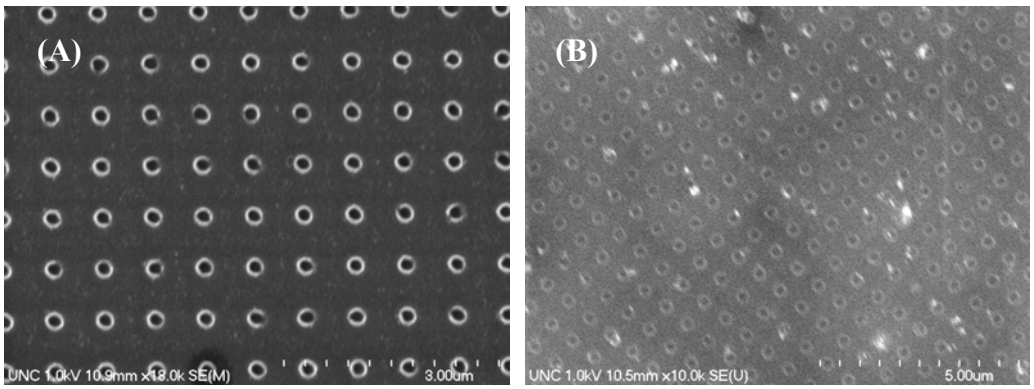

Figure 2-20. SEM images of (A) silicone master template; and (B) p(55:45 VF_2/EVEBr) cured with 25:5 wt-% of TAIC/ DMPA.

2.4 Conclusions: Elastomer Curing. In summary, a novel synthetic approach to the fabrication of fluorinated elastomers that is cost effective, environmentally friendly, and decreases manufacturing steps was presented. Fluorinated elastomers are commonly prepared via free radical emulsion polymerization, which result in aqueous waste and energy intensive drying steps. Using $scCO_2$ as a continuous phase for the polymerization of fluorinated monomers, the process avoids harmful aqueous waste and is a dry, environmentally friendly process. The dry nature of CO_2 enables reactive functional monomers to be used that one cannot use in aqueous based processes. In some cases the cure chemistry could be carried out as a solvent-less process. Easily processable materials that could be cured into elastomeric solids were achieved by synthesizing functional, low molecular weight oligomers with high fluorine content. Minimal solvent was used in some cases to facilitate homogenous mixing of curing components. A systematic study varying initiator, monomer feed ratios, percent solids, initiator concentration and pressure was conducted for the polymerization of new fluorinated oligomers for elastomer applications. Additionally, investigations of different initiators and co-reagents for the

cure chemistry and the effect on mechanical properties and surface free energy were studied. New fluoroelastomers have been prepared from a liquid or semi-solid precursor synthesized in supercritical carbon dioxide. These new fluorooligomer precursors were then cured into elastomers via a photochemically crosslinking process. Traditional reactions to fabricate fluorinated elastomers involve several co-regents for optimum crosslinking and to react with unwanted byproducts. A facile process using minimal reagents necessary to convert liquid precursors into new, solid fluoroelastomers has been demonstrated. Additionally, our synthesis decreases manufacturing costs by avoiding energy intensive drying steps that aqueous processes incur. A promising new route for the fabrication of fluorinated elastomers has been illustrated. By varying composition and cure chemistry one is able to tune the mechanical and surface properties to realize unique applications. The liquid cure mixtures were found to easily wet etched silicon surfaces for pattern replication. Upon curing the mixture an exact replica of the surface is produced, enabling increased utility for specific application including patterned proton exchange membranes for fuel cells, soft, solvent-resistant microfluidic devices, and enabling novel drug delivery platforms with the fabrication and replication of micron- and nanometer sized objects.

1. Woods, H. M.; Nouvel, C.; Licence, P.; Irvine, D. J.; Howdle, S. M., Dispersion polymerization of methyl methacrylate in supercritical carbon dioxide: An investigation into stabilizer anchor group. *Macromolecules* **2005,** 38, (8), 3271-3282.

2. Christian, P.; Giles, M. R.; Griffiths, R. M. T.; Irvine, D. J.; Major, R. C.; Howdle, S. M., Free radical polymerization of methyl methacrylate in supercritical carbon dioxide using a pseudo-graft stabilizer: Effect of monomer, initiator, and stabilizer concentrations. *Macromolecules* **2000,** 33, (25), 9222-9227.

3. Christian, P.; Howdle, S. M.; Irvine, D. J., Dispersion polymerization of methyl methacrylate in supercritical carbon dioxide with a monofunctional pseudo-graft stabilizer. *Macromolecules* **2000,** 33, (2), 237-239.

4. Giles, M. R.; Hay, J. N.; Howdle, S. M.; Winder, R. J., Macromonomer surfactants for the polymerisation of methyl methacrylate in supercritical CO2. *Polymer* **2000,** 41, (18), 6715-6721.

5. Giles, M. R.; O'Connor, S. J.; Hay, J. N.; Winder, R. J.; Howdle, S. M., Novel graft stabilizers for the free radical polymerization of methyl methacrylate in supercritical carbon dioxide. *Macromolecules* **2000,** 33, (6), 1996-1999.

6. Canelas, D. A.; Betts, D. E.; DeSimone, J. M., Dispersion polymerization of styrene in supercritical carbon dioxide: Importance of effective surfactants. *Macromolecules* **1996,** 29, (8), 2818-2821.

7. Canelas, D. A.; DeSimone, J. M., Dispersion polymerizations of styrene in carbon dioxide stabilized with poly(styrene-b-dimethylsiloxane). *Macromolecules* **1997,** 30, (19), 5673-5682.

8. Romack, T. J.; Maury, E. E.; Desimone, J. M., Precipitation Polymerization of Acrylic-Acid in Supercritical Carbon-Dioxide. *Macromolecules* **1995,** 28, (4), 912-915.

9. Liu, T.; Desimone, J. M.; Roberts, G. W., Continuous precipitation polymerization of acrylic acid in swercritical carbon dioxide: The polymerization rate and the polymer molecular weight. *Journal of Polymer Science Part a-Polymer Chemistry* **2005,** 43, (12), 2546-2555.

10. Liu, T.; Garner, P.; DeSimone, J. M.; Roberts, G. W.; Bothun, G. D., Particle formation in precipitation polymerization: Continuous precipitation polymerization of acrylic acid in supercritical carbon dioxide. *Macromolecules* **2006,** 39, (19), 6489-6494.

11. Desimone, J. M.; Guan, Z.; Elsbernd, C. S., Synthesis of Fluoropolymers in Supercritical Carbon-Dioxide. *Science* **1992,** 257, (5072), 945-947.

12. Romack, T. J.; Kipp, B. E.; Desimone, J. M., Polymerization of Tetrafluoroethylene in a Hybrid Carbon-Dioxide Aqueous-Medium. *Macromolecules* **1995,** 28, (24), 8432-8434.

13. Romack, T. J.; Desimone, J. M.; Treat, T. A., Synthesis of Tetrafluoroethylene-Based, Nonaqueous Fluoropolymers in Supercritical Carbon-Dioxide. *Macromolecules* **1995,** 28, (24), 8429-8431.

14. Romack, T. J.; Desimone, J. M.; Treat, T. A., Synthesis of Teatrafluoroethylene-Based, Nonaqueous Fluoropolymers in Supercritical Carbon-Dioxide. *Macromolecules* **1995,** 28, (24), 8429-8431.

15. Michel, U.; Resnick, P.; Kipp, B.; DeSimone, J. M., Copolymerization of tetrafluoroethylene and 2,2-bis(trifluoromethyl)-4,5-difluoro-1,3-dioxole in Supercritical carbon dioxide. *Macromolecules* **2003,** 36, (19), 7107-7113.

16. Wood, C. D.; Michel, U.; Rolland, J. P.; DeSimone, J. A., New fluoropolymer materials. *Journal of Fluorine Chemistry* **2004,** 125, (11), 1671-1676.

17. Saraf, M. K.; Gerard, S.; Wojcinski, L. M.; Charpentier, P. A.; DeSimone, J. M.; Roberts, G. W., Continuous precipitation polymerization of vinylidene fluoride in supercritical carbon dioxide: Formation of polymers with bimodal molecular weight distributions. *Macromolecules* **2002,** 35, (21), 7976-7985.

18. Ahmed, T. S.; DeSimone, J. M.; Roberts, G. W., Continuous precipitation polymerization of vinylidene fluoride in supercritical carbon dioxide: modeling the molecular weight distribution. *Chemical Engineering Science* **2004,** 59, (22-23), 5139-5144.

19. Charpentier, P. A.; DeSimone, J. M.; Roberts, G. W., Continuous precipitation polymerization of vinylidene fluoride in supercritical carbon dioxide: Modeling the rate of polymerization. *Industrial & Engineering Chemistry Research* **2000,** 39, (12), 4588-4596.

20. Tai, H.; Wang, W. X.; Howdle, S. M., Dispersion polymerization of vinylidene fluoride in supercritical carbon dioxide using a fluorinated graft maleic anhydride copolymer stabilizer. *Macromolecules* **2005,** 38, (5), 1542-1545.

21. Tai, H. Y.; Wang, W. X.; Martin, R.; Liu, J.; Lester, E.; Licence, P.; Woods, H. M.; Howdle, S. M., Polymerization of vinylidene fluoride in supercritical carbon dioxide: Effects of poly(dimethylsiloxane) macromonomer on molecular weight and morphology of poly(vinylidene fluoride). *Macromolecules* **2005,** 38, (2), 355-363.

22. Romack, T. J.; Combes, J. R.; Desimone, J. M., Free-Radical Telomerization of Tetrafluoroethylene in Supercritical Carbon-Dioxide. *Macromolecules* **1995,** 28, (5), 1724-1726.

23. Ahmed, T. S.; DeSimone, J. M.; Roberts, G. W., Copolymerization of vinylidene fluoride with hexafluoropropylene in supercritical carbon dioxide. *Macromolecules* **2006,** 39, (1), 15-18.

24. Ahmed, T. S.; DeSimone, J. M.; Roberts, G. W., Continuous copolymerization of vinylidene fluoride with hexafluoropropylene in Supercritical carbon dioxide: Low hexafluoropropylene content semicrystalline copolymers. *Macromolecules* **2007,** 40, (26), 9322-9331.

25. Charpentier, P. A.; DeSimone, J. M.; Roberts, G. W., Continuous polymerizations in supercritical carbon dioxide. *Clean Solvents* **2002,** 819, 113-135.

26. Bunyard, W. C.; Romack, T. J.; DeSimone, J. M., Perfluoropolyether synthesis in liquid carbon dioxide by hexafluoropropylene photooxidation. *Macromolecules* **1999,** 32, (24), 8224-8226.

27. Forsythe, J. S. H., D. J. T.; Logothetis, A. L.; Seguchi, T.; Whittaker, A. K., NMR Study of the Radiation-Induced Cross-Linking of Poly(tetrafluoroethylene-co-perfluoromethyl vinyl ether). *Macromolecules* **1997,** 30, 8101-8108.

28. Forsythe, J. S. H., D. J. T., The Radiation Chemistry of Fluoropolymers. *Progress in Polymer Science* **2000,** 25, 101-136.

29. Zhoa, C. K. Z., R. M.; Pan, H.Q.; Jin, X. S.; Qu, Y. L.; Wu, C. J.; Jiang, X. K., *Journal of Organic Chemistry* **1982,** 47, 2009-2013.

30. Bunyard, W. C.; Kadla, J. F.; DeSimone, J. M., Viscosity effects on the thermal decomposition of bis(perfluoro-2-N-propoxypropionyl) peroxide in dense carbon dioxide and fluorinated solvents. *Journal of the American Chemical Society* **2001,** 123, (30), 7199-7206.

31. Haiting Zheng, W. B. K. H. R. B. C. P., Facile room temperature RAFT polymerization via redox initiation. *Journal of Polymer Science Part A: Polymer Chemistry* **2008,** 46, (7), 2575-2580.

32. *Polymer Handbook*. 4th ed.; John Wiley: New York, 1999; p II/2-69.

33. Xu, W. Z.; Li, X.; Charpentier, P. A., In situ ATR-FT-IR study of the thermal decomposition of diethyl peroxydicarbonate in supercritical carbon dioxide. *Polymer* **2007,** 48, (5), 1219-1228.

34. Ameduri, B.; Bauduin, G.; Boutevin, B.; Kostov, G.; Petrova, P., Synthesis and polymerization of fluorinated monomers bearing a reactive lateral group. 9. Bulk copolymerization of vinylidene fluoride with 4,5,5-trifluoro-4-ene pentyl acetate. *Macromolecules* **1999,** 32, (14), 4544-4550.

35. Duc, M.; Ameduri, B.; Boutevin, B.; Kharroubi, M.; Sage, J. M., Telomerization of vinylidene fluoride with methanol. Elucidation of the reaction process and mechanism by a structural analysis of the telomers. *Macromolecular Chemistry and Physics* **1998,** 199, (7), 1271-1289.

36. Ameduri, B.; Boutevin, B.; Kostov, G., Synthesis and copolymerization of vinylidene fluoride (VDF) with trifluorovinyl monomers, 11 - Telomers of VDF with 1-chloro-1,2-dibromotrifluoroethane as precursors of bromine-containing copolymers. *Macromolecular Chemistry and Physics* **2002,** 203, (12), 1763-1771.

37. Pianca, C. M. E. B., G. Esposto, S. Radice, *Journal of Fluorine Chemistry* **1999,** 95, 71-84.

38. Guiot, J.; Ameduri, B.; Boutevin, B., Radical homopolymerization of vinylidene fluoride initiated by tert-butyl peroxypivalate. Investigation of the microstructure by F-19 and H-1 NMR spectroscopies and mechanisms. *Macromolecules* **2002,** 35, (23), 8694-8707.

39. Forsythe, J. S.; Hill, D. J. T.; Logothetis, A. L.; Seguchi, T.; Whittaker, A. K., NMR Study of the Radiation-Induced Cross-Linking of Poly(tetrafluoroethylene-co-perfluoromethyl vinyl ether). *Macromolecules* **1997,** 30, (26), 8101-8108.

40. Lalevee, J.; Allonas, X.; Jradi, S.; Fouassier, J. P., Role of the medium on the reactivity of cleavable photoinitiators in photopolymerization reactions. *Macromolecules* **2006,** 39, (5), 1872-1879.

CHAPTER 3

PERFLUOROPOLYETHER MATERIALS AND THEIR UTILITY

3.0 Introduction.

3.1 Liquid Perfluoropolyether Precursors and Their Utility. Perfluoropolyethers (PFPEs) are a class of polymers which exhibit an impressive range of properties for applications in extreme environments. Exceptionally high chemical and thermal stabilities derived from the strong C-F and C-O bonds in the polymer backbone. As high-performance lubricants for aerospace and industrial applications, pump and heat transfer fluids, as well as additives for surface modification, PFPE materials possess physical and chemical properties over a wide range in temperatures.[1-8] Similar to functional oligomers discussed in Chapter 2, PFPEs are liquid at room temperature. Their aliphatic structure and ether linkages result in a totally amorphous morphology. High thermal stability, excellent chemical inertness, and low surface tension summarize their intriguing properties. Perfluoropolyethers are typically synthesized through anionic ring opening polymerizations of hexafluoro propylene oxide. Less conventional synthetic routes include the photooxidation of fluoroolefins as with tetrafluoroethylene (TFE) and hexafluoropropylene (HFP), or through Lewis acid-catalyzed ring opening polymerization of 2,2,3,3-tetrafluorooxetane followed by direct fluorination under UV light.[4] Lagow and coworkers also achieved the PFPE synthesis by direct fluorination of hydrogenated polyethers.[9] Bunyard and coworkers described the photooxidation of HFP in carbon dioxide[10] as an environmentally friendly alternative to organic and fluorinated solvent systems. They exploit the benefits of utilizing an environmentally friendly and tunable continuous phase. Functionalization of PFPE can be accomplished using a number of different chemistries.[11, 12] A common PFPE, ZDOL, contains alcohol end groups that can postfunctionalized with 2-isocyanatoethylmethacrylate in the presence of

catalyst to afford a methacrylate-terminated PFPE. With a functionality of four, this liquid material can be crosslinking into a solid elastomer network with the addition of an initiator and stimulus (heat or UV irradiation, depending on the initiator). Cured PFPE materials may not result in the most chemically or mechanically robust properties attributed to more traditional flouroelastomers, they do however bring unique attributes that advancing industries in nano- and biotechnology are exploiting.

3.2 Novel PFPE Applications: in Microfluidic Device Fabrication and Soft Lithographic Applications in Pattern and Particle Replication, PRINT Technology. Recent progress has established PFPE-like materials as leading benchmark materials for solvent resistant, soft microfluidic devices (Figure 3-1). Such lab-on-a-chip devices enable combinatorial chemistry and screening reactions, separations, in-situ analyses and rapid synthesis of radio labeled 19F contrast agents for PET imaging[7, 8] using nanoliters of reagents. Rapid drug screening in microfludics, novel routes to DNA and peptide synthesis, and a wide scope of new combinatorial organic reactions, previously unavailable in PDMS microfluidic devices[13-17] are realized in a PFPE-based microfluidic device and maintains the cost effectiveness compared to hard devices made from glass or silicon. Devices fabricated from photocurable PFPEs[7, 8] were first reported by Rolland and coworkers. The devices are composed of replicated, patterned layers obtained by using master templates and imprint lithography (Figure 3-2). The uncanny wetting properties of uncured PFPE realizes unsurpassed precision in replicating patterns on size scales on the order of nanometers.[6-8, 18] Whitesides and coworkers have pioneered efforts in soft and imprint lithography using poly(dimethylsiloxane) (PDMS) based materials.[13-17, 19-22] Rolland and coworkers have shown that even the benchmark PDMS materials could not replicate intricate patterns

with the utmost fidelity.[23] Poly(dimethyl siloxane) based liquids are also incapable of wetting features as clearly as PFPE- type liquids.

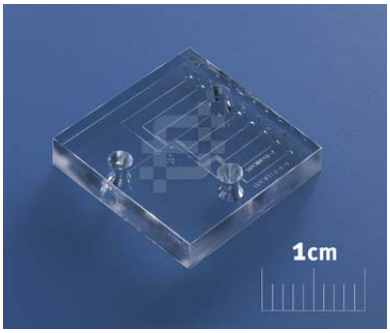

Figure 3-1. Image of a soft microfluidic device.

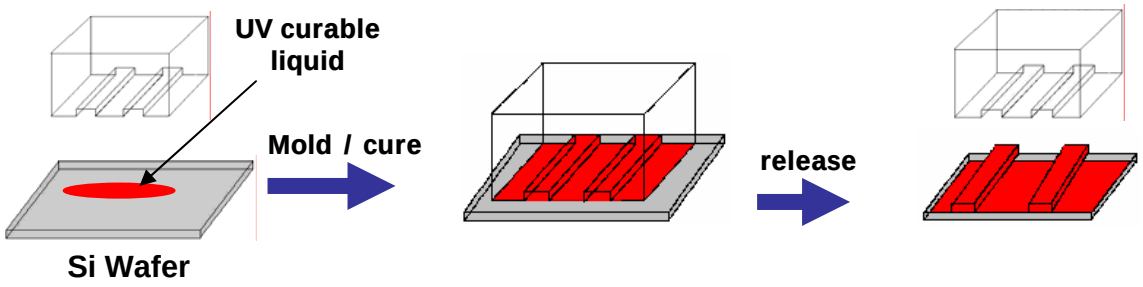

Figure 3-2. Illustration of pattern replication using traditional imprint lithography.

As illustrated in Figure 3-2, a PFPE mold comes into contact with a curable liquid on a substrate (here a Si wafer). Using in this case UV radiation, the curable liquid is crosslinked into a solid network. Subsequent to curing, the PFPE is released, leaving a patterned replica of the PFPE mold. PFPE maintains flexibility and conformal contact with a remarkably low surface energy which facilitates unprecedented release from substrates. They also have excellent feature integrity. Imprint lithography traditionally replicated patterns and features and with a stamping-like technique leaves the land area between the features containing the stamped material, as illustrated in Figure 3-2. Rolland and coworkers exploited the non-wetting and facile release

properties by bringing a PFPE mold into contact with another PFPE, flat surface. When a monomer solution becomes sandwiched between a mold and a flat surface, the formation of discrete features is realized as the excess curable liquid is pushed out. Building on this work, an emerging technology developed, referring to Particle Replication In Non-Wetting Templates (PRINT).[18]

3.3 The Microelectronics Industry Meets Personal Health Care. It is evident that research originating from the microelectronics industry is becoming a benchmark for bio- and nanotechnology. The precision fabrication technology of the microelectronics industry is translating the field of bioengineering and nanotechnology and fundamentally altering the landscape of medicine. Methodology and fabrication processes in nanoparticle synthesis and templating[13, 24-30] are being expanded and utilizing procedures typically used to make microchips. It has thus become increasingly apparent that imprint and soft lithography are tools that the life sciences are exploiting for pattern replication,[6] templating of biomaterials,[16, 28, 30-34] and for synthesizing drug delivery vectors.[35-37] Only until recently has the fabrication of organic, shape-specific, monodisperse nanoparticles for therapeutics and drug delivery vectors been realized through imprint lithography using non-wetting templates.[35] Rolland et al. reported the first particle fabrication strategy demonstrating rigorous control over size, shape, composition, surface decoration, and deformability.[18] This versatile "top-down" method to fabricate discrete particles using traditional lithographic processes opens up new possibilities for fundamental and applications driven research, previously unattainable.

3.3.1 Fabrication of Discrete, Shape-Specific, Monodisperse Polymer Nanoparticles Using PRINT. Bio- and nanotechnology is becoming an ever growing and exciting research field with billions of dollars being invested in hopes of developing state-of-the-art therapeutics, contrast agents, delivery vectors, devices, coatings, smart particles, and other biomedical applications for overall improvement in personalized health care. Emerging bio- and nanotechnology are adapting methodology of the microelectronic industry to create novel drug delivery platforms opening up unlimited opportunities in areas such as disease fighting, improved health sustainability, and finding cures. Particle Replication In Non-wetting Templates, PRINT, enables the fabrication of discrete, shape-specific, monodisperse drug delivery vectors. PRINT exploits the wetting properties of functionalized PFPE to completely wet the surface of silica master templates to create an elastomeric mold of the inverse pattern. This mold is used to create nano- and microparticles by filling each cavity of the mold and avoiding an interconnecting layer, a so called flash layer, to produce discrete, shape-specific particles. Compositions already investigated are PEG-based systems, PLGA, poly(pyrrole), triacrylate and diacrylate systems and variations thereof. Various fabrication methodologies have been established and investigated for ease, speed, and composition dependency. Different shapes were studied in cylinders, trapazoids, conical, arrows, and bars for initial investigation and since have been broadened to include more biologically relevant shapes and sizes.

3.3.2 Drug Delivery and Nanotechnology Platforms: Shape and Size Matter. Bio- and nanotechnology are quickly realizing that size and shape holds vast

significance and at times consequence in biological mechanisms and processes[6, 37-47] These nanofabricated tools (e.g., precisely defined particles) hold significant promise to provide insight into the fundamentals of cellular and biological processes as they can yield essential insights into the design of effective vectors for use in nanomedicine. Systems to date have the ability to fabricate either ill-defined particles or systems where there is little control to systematically vary the key variables of size, shape, deformability and surface chemistry until PRINT. The effect of these variables on biological systems has largely been unexplored, mostly due to the fact that no methodology has been developed coming even close to the breadth that the PRINT process offers. No other fabrication process is as unique as the PRINT technology.

3.3.3 PRINT Micro- and Nanoparticles: Implication in Cancer Research. Therapies to treat diseases such as cancer have yet to realize facile, 100 % effective treatment regiments that circumvent undesired side effects. Additional challenges that anti-cancer therapeutics face is increasing drug tolerances developed by patients, non-specific cell killing, and general toxicities. On top of that, each individual cancer and their stages often require a unique approach to therapy and has unmet needs for effective treatment agents or cocktails thereof. The holy grail of a therapeutic drug delivery vehicle may comprise many unknown variables, variables that have been undiscovered and unexplored due in part to the limited fabrication procedures present to date. There are however a few characteristics known to affect outcomes within biological mechanisms and processes. Size and shape of a drug carrier have tremendous implications.[45, 47] An ideal size range (below 500 nm) will allow drug carrier circulate for longest time periods

compared to micron sized particles. The careful investigation of a monodisperse (in size and shape) carrier has a tremendous impact on particle performance. Monodispersity is a key property to enable optimal non-specific targeting and incur the highest efficiency of therapeutic index.

One aspect of an ideal approach utilizes a drug carrier which is non-toxic, is not recognized as foreign to the body and carries the drug to a target area, i.e, a tumor, and does not release its cargo before being internalized by the tumor cell. In order to accomplish one of those characteristics of a delivery vehicle, free drug has to be encapsulated into the delivery vector such as a polymer matrix. This matrix should be readily soluble within a cell, but tightly shielding the drug until internalization to decrease or eliminate toxicity issues. As such crosslinks of the matrix could be composed of labile groups, reactive only under specific conditions such as a reducing environment, enabling an activated release. The rest of the matrix, the raw polymer, is ideally soluble in aqueous media, such that without the crosslinks the particle would not retain its shape and dissolve.

Petros and coworkers reported encapsulation of doxorubicin into a degradable disulfide matrix.[35] Upon internalization of the vector in a cell, doxorubicin is released in response to the reducing environment. This study illustrated HeLa cell killing in vitro by release of the doxorubicin without the addition of any external reducing agent. Petros and coworkers emphasize that the fabrication of nano- and microparticles offer distinct advantages over other delivery vectors currently in use such as liposomes, dendrimers, viruses, conjugated, and micelles.[35] The drug delivery vector discussed by Petros and coworkers afford low cargo loading and a more sophisticated matrix is warranted.

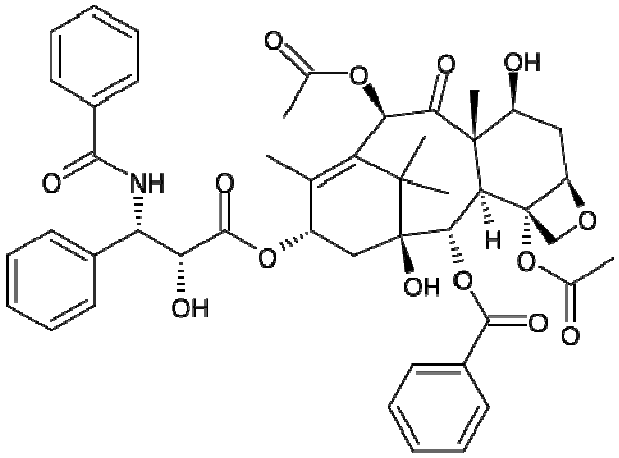

Figure 3-3. Chemical structure of paclitaxel.

3.4 Biomaterials: Leading Forefront of Disease Treatment, Recognition, Sensing, and Marking. Synthetic, polymer nanoparticles used as drug delivery vectors have overcome some challenges faced with circulation and retention in a human body.[48-63] The innate behavior to clear unidentifiable, foreign, matrices from the body using different clearing mechanisms remains challenging for delivery vectors to overcome. PEGylation has introduced nanoparticles to longer circulation times, but even with today's best efforts, no particle recipe has been comparable to circulation times of red blood cell (120 days). If synthetic particles can never overcome certain barriers of clearance mechanisms of the body, what alternatives are left? Proteins circulate in a human for over weeks and months. Allowing for long circulation and effective targeting are the next steps in nanomedicine and curing cancer.

If certain proteins are not recognized as foreign objects and retain the ability for long circulation, rapid clearance through uptake in the liver or kidneys or by macrophages is circumvented. This is especially needed for anticancer drugs, such as doxorubicin or paclitaxel, which often create undesired side effects. The side effects are in part as a result to early clearance and non-specific cell uptake. Random cells taking up anti-cancer agents are arrested, leading to cell death to otherwise healthy cells. Peripheral neuropathy is another such serious side effect of chemotherapy. Peripheral neuropathy describes damage to the peripheral nervous system and originates partially from the toxicity levels of anti-cancer agents not reaching tumerous tissue, thus being internalized by healthy tissue. Some people may experience temporary numbness, tingling, and pricking sensations (paresthesia), sensitivity to touch, or muscle weakness. Others may suffer more extreme symptoms, including burning pain (especially at night), muscle wasting, paralysis, or organ or gland dysfunction. People may become unable to digest food easily, maintain safe levels of blood pressure, and sweat normally.

Part of what is so challenging and eludes current sophisticated treatment regimens, is that cancer cells have, for the most part, the makeup of a healthy cell, with differences for the most part being exceedingly more rapid growth and cell division and have are decorated with significantly more markers and receptors on their cell surface. Most cell receptors are identical on cancerous cells compared to healthy tissue. The hope is that since cancerous cells have the amplification of receptors, that targeting particle platforms would be directed to the cancer cells, and not healthy tissue. This approach relies on the partitioning of particles to extent toward cancer cells thus creating a exceedingly more effective and efficient therapeutic. Current drug delivery platforms also

rely on the EPR effect (Enhanced Permeability and Retention) of cancer cells with their leaky vasculature.

3.4.1 Abraxane™: Overcoming Toxicity Hurdles. As eluded to, peripheral neuropathy significantly declines a cancer patient's quality of like. Most anti-cancer agents have some levels of peripheral neuropathy associated with treatment, and paclitaxel is no exception.[64, 65] Paclitaxel (Firgure 3-3), an antineoplastic agent, has a unique action by inhibiting microtubule network reorganization which is essential for cell division and has proven to be a benchmark drug for the treatment of metastatic breast cancer.[66, 67] A Solvent-based delivery of paclitaxel was established through a formulation called Cremaphor EL, which is Castrol oil and ethanol. The solvent-based delivery system of paclitaxel is referred to as Taxol®.[68, 69] Due to extremely high toxicity levels, the maximum tolerated dose is relatively low and subsequently treatment regiments that typically take three hours per dose are prolonged for effectiveness. Premedication with steroids or antihistamines for hypersensitivity reactions caused by these solvents were required. Recently, Abraxis Bioscience discovered a formulation containing 10 % by weight paclitaxel that was much less toxic and mitigated the use of Cremaphor EL as a delivery method. Abraxane™ is a nanoparticle platform composed of paclitaxel bound to albumin, the most abundant protein in our circulation.[66-74]

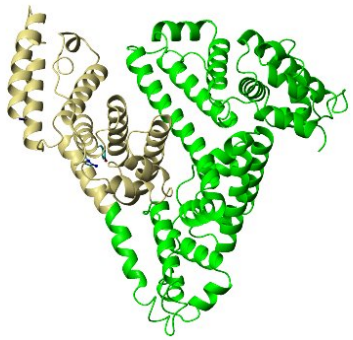

Figure 3-4. Cartoon of the Structure of Albumin.

3.4.1.1 Background: Abraxane. The albumin-bound paclitaxel was approved by the FDA in January of 2005. It comes as a lyophilized power and is reconstituted into saline just prior to injection, which is infused over a shortened infusion time 30 minutes. Abraxane is formulated using a proprietary coascervation method to bind paclitaxel to albumin in a non-covalent mechanism and produces spherical particles ranging from 50 to 150 nm in diameter upon reconstitution. It is hypothesized that once albumin-bound paclitaxel is in circulation, the particles bind to albumin's natural receptor, gp60, on vascular endothelial cells, just as normal albumin would.[75-79] The gp60 receptor is like many other overproliferated receptors on cancerous cell. The activated receptor interacts with cavelein-1 protein leading to caveolae. The caveolae transports its cargo then to the tumor interstisum. For optimal effectiveness, the cytotoxic agent still needs to cross the tumor cell membrane. Many tumors have evolved a biological process allowing for maximum extraction of albumin-rich nutrients. As such, tumors secrete a special protein, SPARC, referring to secreted protein acidic and rich in cysteine, into the tumor interstsum. The SPARC acts as a receptor to find and bind to albumin. As a result of SPARC's rich affinity to albumin, it attracts and binds to albumin-bound paclitaxel,

concentrating it at the tumor cell surface. The cytotoxic agent is released and diffuses into the tumor bed through the leaky vasculature and EPR effect, reaching the nucleus and halting cell division.

This approach exploits albumin's properties and receptors and leverages the SPARC interaction for cell death of tumor cells, and while the gp60 receptor is overprolifferated on tumor cells' surfaces, this mechanism is arguably not well understood. It should be noted that the lungs and heart have a substantial amount of gp60 receptors present.[75-78] Clinical trials have proven that Abraxane is not found in these areas in a substantial concentration.[66, 72-74, 80] Regardless, albumin-bound paclitaxel has pushed the frontiers of nanomedicine in the treatment of cancer. There are, however, opportunities present for optimization, improvement, and further exploitation of albumin's properties and the body's natural mechanisms of particle uptake.

Due to the fact that Abraxane is not one covalent entity, the bound mixture has a finite stability. It is said that albumin contains a hydrophobic pocket, where paclitaxel may likely reside. However, the hydrogen bonds and van der Waals forces over time become over ridden by other driving forces and paclitaxel becomes disassociated from albumin. Once reconstituted, Abraxane is stable for a few hours at room temperature in aqueous continuous phases. It forms spheres with diameters ranging from 50 to 150 nm. Albumin typically readily dissolves in aqueous systems. In the case of Abraxane, the albumin fraction remains associated with paclitaxel at first. After a few hours, the albumin-solvent interaction surpasses the albumin-paclitaxel association and forces the paclitaxel to become disassociated from the albumin. The disassociation effect is catalyzed at higher temperatures. It is possible that this dissociation occurs partially in

circulation, before particles can reach gp60 receptors on vascular endothelial cell, creating the cytotoxic drug premature release and affecting unwanted toxicity issues responsible for undesired side effects of chemotherapy, such as peripheral neuropathy. Free paclitaxel will readily permeate cell membranes and thus needs to be protected before arriving at tumor cells.[81, 82] Stability investigations were of great interest to see if the PRINT technology could enhance properties and increase efficacy for treating cancer using Abraxane.

3.4.1.2 Characterization

3.4.1.2.1 Materials. Abraxane (Abraxis BioScience, Inc. and AstraZeneca) was obtained from the UNC Hospital pharmacy and handled with extreme caution. Sodium chloride was used to create a 0.9 weight percent solution in water to produce saline. Ultra pure (17 MΩ), deionized water was used throughout.

3.4.1.2.2 SEM. Scanning electron microscopy (SEM) (Hitachi model S-4700) was used to analyze dry and reconstituted Abraxane. Samples were placed on a glass slide and were coated with 1.5 nm of Pd/Au alloy using a Cressington 108 auto sputter coater (Cressington Scientific Instruments Ltd.). The Pd/Au coated glass slide was then adhered to the sample holder using double-sided adhesive tape, and placed inside the vacuum chamber of the SEM and observed under low vacuum (10^{-3} Torr). SEM analysis of dry and reconstituted Abraxane illustrates the non-uniformity of this product (Figure 3-5). Dispersity in size and shape of this product are evident as shown in the SEM micrographs (Figure 3-6).

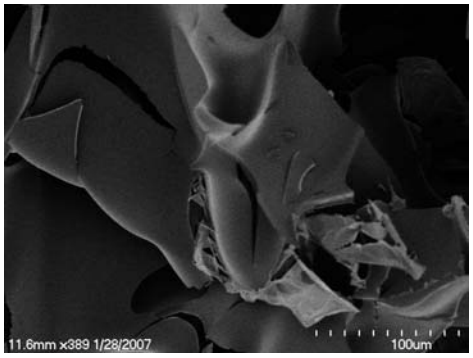

Figure 3-5. SEM of Abraxane as received.

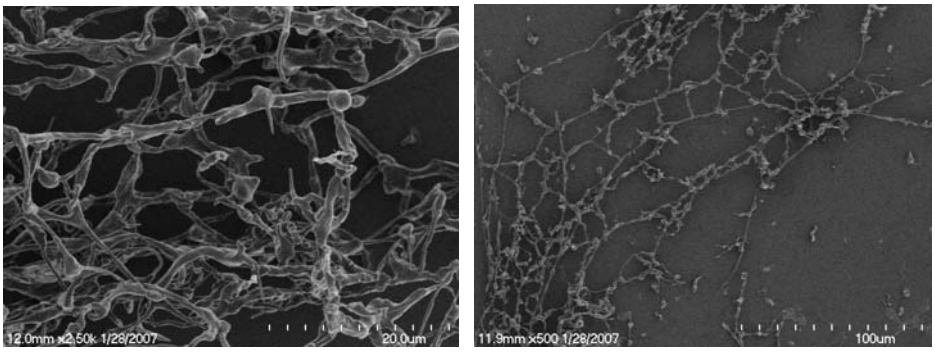

Figure 3-6. SEM micrographs of Abraxane reconstituted to 50 mg/mL in water. (Image taken one hour after preparation).

3.4.1.2.3 DLS. Dynamic scattering studies were performed using a 90Plus Particle Analyzer (Brookhaven Instruments) with 30 mW laser source. Data collection was performed at a detection angle of 90^{o} and typical sample volume of 2 mL. The experiment temperatures were controlled by the heating system integrated inside the 90Plus. The scattering data of the samples was analyzed by Cumulant analysis to obtain polydispersity, and by COTIN and NNLS methods to obtain size and distribution. Samples of DLS experiments were dissolved in distilled water or saline (equal to 0.9 wt% NaCl in water) solutions at concentrations from 0.01 to 1 mg/mL. To minimize dust interference and to obtain accurate measurements, all solutions were freshly prepared.

Five milligrams of Abraxane was dissolved in 100 mL saline solution to obtain a concentration of 0.05 mg/mL. Two millilitres of the Abraxane solution was placed inside a cubic light scattering cell. DLS experiments were initially performed at 25 ^{o}C. The solvent refractive index was set to water. The dust cut off ratio was 80%. The experiment duration time extended one minute. Each sample was measured five times.

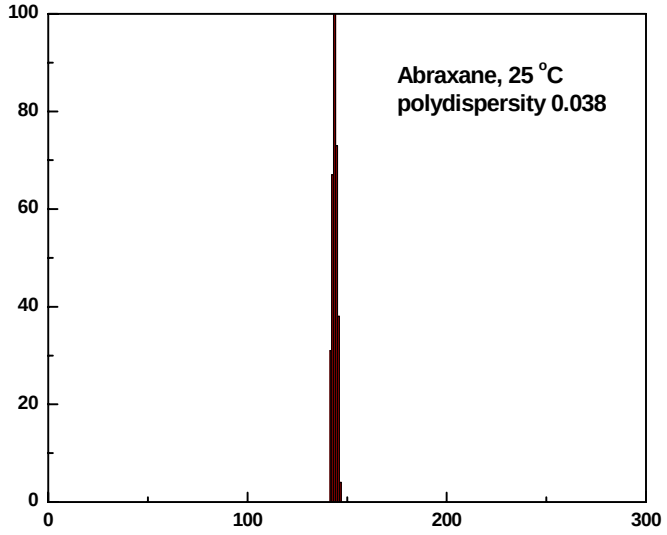

Figure 3-7. Dynamic light scattering analysis of Abraxane solution at room temperature.

Figure 3-7 illustrates that upon reconstitution, Abraxane forms particles consisting of a size just below 150 nm. Though it is not extremely broad, some polydispersity exists in the sample, in the range of 0.2.

A fresh solution at the same concentration as above was prepared to investigate the size and dispersion of reconstituted Abraxane at physiological temperature. Two millilitres of Abraxane solution was placed inside a cubic light scattering cell. The temperature controller of the DLS was programmed for 37 ^{o}C. Once the cuvette reached equilibrium at 37 ^{o}C, the DLS experiment was conducted. The solvent refractive index was set as water and dust cut off ratio was 80%. The experiment duration time lasted one minute and each sample was measured five times.

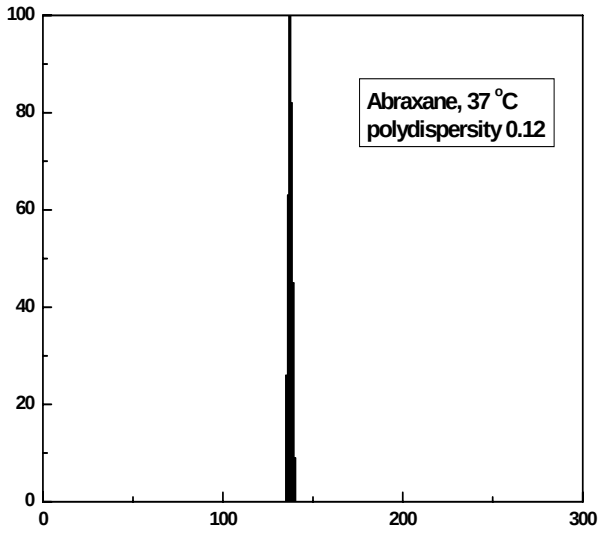

Figure 3-8. Dynatic light scattering analysis of Abraxane solution at physiological temperature.

The size and dispersity of reconstituted Abraxane at physiological temperatures is shown in Figure 3-8. It is apparent that the stability of Abraxane particles is present at least initially at higher temperatures. The stability of reconstituted Abraxane was monitored over time using DLS analysis and investigated the effect of temperature and solvent over time. Studies investigating reconstitution of Abraxane is water versus saline showed little difference in stability. Ions is saline may promote the disassociation of Abraxane particles compared to water, but clear effects are more pronounced looking at temperature, as one might expect. It is clearly stated in the directions that once a dose is reconstituted, one has a limited amount of time for administration. This is likely due to disassociation of the paclitaxel from the albumin as solvent interactions override any binding forces that may keep paclitaxel temporarily bound to albumin. As one might expect, this stability decreases sooner at higher temperatures. At physiological temperatures, reconstituted Abraxane remains stable for three hours before complete

dissolution. One can clearly see in Figure 3-12 and Figure 3-13 that the size versus time and the polydispersity versus time show dramatic change at or after three hours. The infusion time for a patient, though significantly reduced from previous products, is still 30 minutes. This impacts potential side effects and whether with circulation time all of the drug can arrive at the tumor bed before disassociation. Additionally, reconstituted Abraxane particles range from 50 to 150 nm is diameter. The disassociation of the smaller particles may likely be different compared to the larger spheres due to the surface area of the particle exposed to solvent. Though Abraxane has overcome major challenges in delivering paclitaxel and has improved toxicity levels, decreased undesired side effects in peripheral neuropathy, shortened infusion length times, and identified a targeting strategy by exploiting the properties and characteristics of albumin and tumor mechanisms in obtaining nutrients, the benefits are capable of being extended with the fabrication of an Abraxane-like particle having shape and size specificity and monodisperseness.

3.4.2 Abraxane-PRINT Efforts.

3.4.2.1 Fabrication. Commercially available Abraxane was purchased from the University of North Carolina Hospital Pharmacy. Great caution was taken when handling Abraxane. For greater ease in handling the lyophilized powder was aliquoted into multiple, pre-weighed (tared) eppendorf tubes in a glove bag under positive nitrogen pressure. Aliquots were stored covered in a desiccator in the glove bag. Samples (eppendorfs) were taken out of the desiccator under positive nitrogen flow just prior to

use. Individual eppendorf samples were weighed and the amount of Abraxane contained was calculated by subtracting the eppendorf's tare weight. Each sample of lyophilized powder was reconstituted in water to make a 25 % by weight solution. This mixture was vortexed until all Abraxane was dissolved. An opaque, stable solution was obtained. This solution was used with the time frame indicated in the instructions prior to infusion and otherwise properly disguarded. This solution was then used to fabricate PRINT particles. Similar to fabricating PVP particles, a master template was first fabricated by selectively etching a pattern generated by photolithography into a silicon substrate to yield a densely packed micro- or nano-sized features on a two-dimensional array (Figure 3-9A). A fluorocarbon elastomeric mold was created by pouring a photochemically curable telechelic perfluoropolyether (PFPE)[18, 23] onto the patterned master templates and curing it while in contact with the master template to yield a patterned PFPE PRINT mold containing the corresponding 200 nm features as cavities (Figure 3-9B). Nanomolding of Abraxane was achieved by a lamination technique where the aqueous Abraxane solution was placed between the patterned PFPE mold and another film (counter sheet) having a higher surface energy (Figure 3-9C). In this particular case a polyethylene sheet was used as the counter sheet during the PRINT lamination process. The PFPE mold, aqueous protein solution and polyethylene sandwich structure was passed through a roller with an applied pressure of 50 psi, higher than what was used for PVP particles. The applied pressure was needed to help spontaneous filling of the cavities since aqueous solutions have a higher surface energy than most organics. As the mold passes under the roller the high energy film was peeled away leaving a filled mold of individual cavities containing

the aqueous protein solution without the formation of a flash layer between each filled cavity. The filled mold is subsequently frozen and lyophilized overnight

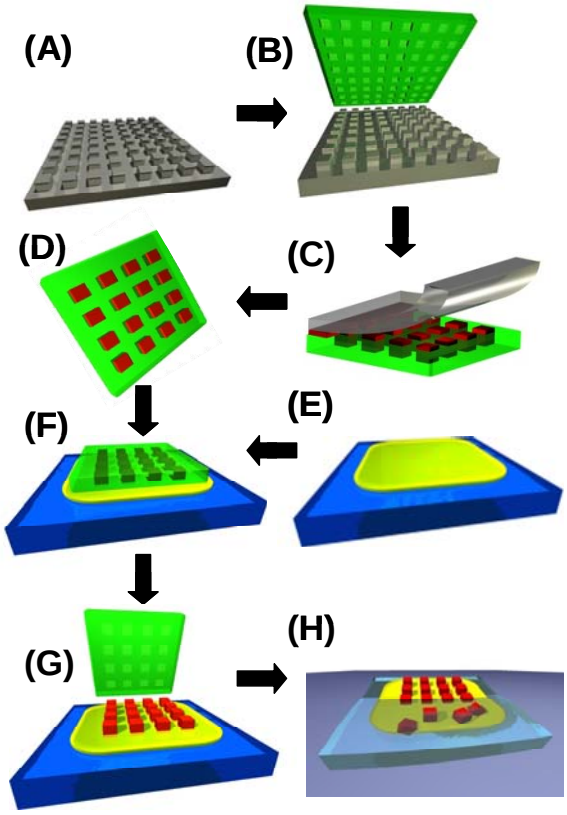

Figure 3-9. Illustration of PRINT process to make nanomolded Abraxane particles.

3.4.2.2 Characterization.

3.4.2.2.1 SEM. The size of nanomolded Abraxane PRINT nanoparticles was analyzed via scanning electron microscopy (Hitachi model S-4700). Particles were harvested onto PET or a glass slide and were coated with 1.5 nm of Pd/Au alloy using a Cressington 108 auto sputter coater (Cressington Scientific Instruments Ltd.). The Pd/Au coated PET was then adhered to the sample holder using double-sided adhesive tape, and placed inside the vacuum chamber of the SEM and observed under low vacuum (10^{-3} Torr).

Figures 3-10 and 3-11 illustrate SEM micrographs of nanomolded Abraxane PRINT particles. The left SEM micrograph of Figure 3-10 shows 200 nm (diameter) x 200 nm cylinders harvested wet onto a poly(ethylene terethalate) sheet. The right image of Figure 3-10 reflects particles of the same size harvested using a glass slide, gentle mechanical force and a drop of chloroform to lift particles from the PFPE mold. The two SEM micrographs of Figure 3-11 illustrate particles of 200 nm (diameter) x 600 nm cylinders harvested in the same fashion as the latter example. Uniform, monodisperse particles, of different aspect ratios composed of Abraxane was successfully fabricated.

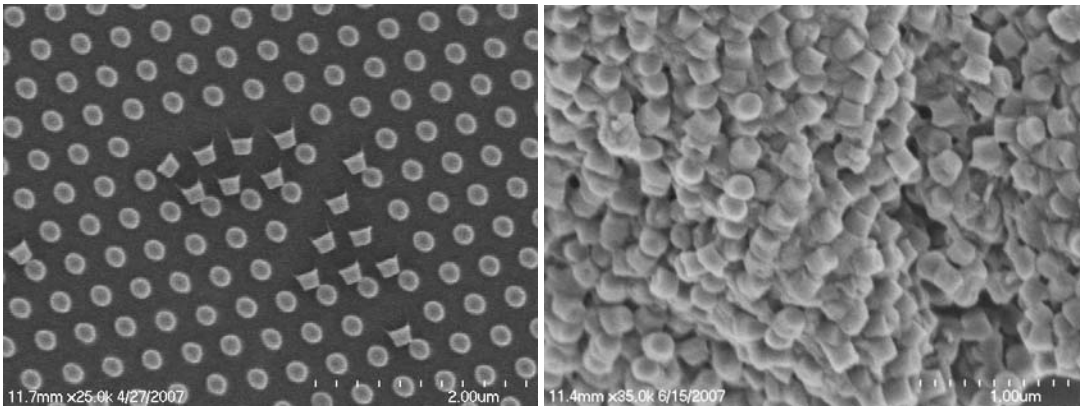

Figure 3-10. SEM micrographs of nanomolded Abraxane PRINT particles.

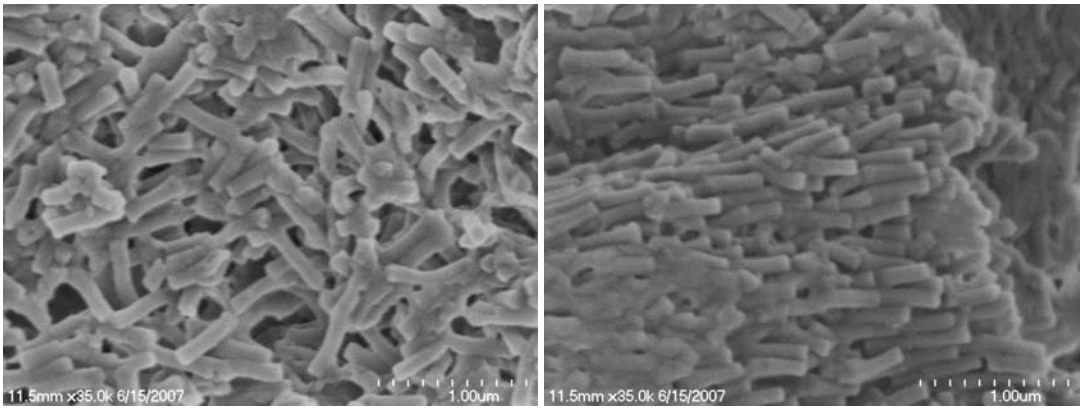

Figure 3-11. SEM micrographs of nanomolded Abraxane PRINT particles.

3.4.2.3 DLS. Solutions of Abraxane and nanomolded Abraxane PRINT particles of the same concentration were analyzed using DLS at physiological temperature. Investigating the size distribution and the polydispersity showed similar results. As expected, Abraxane's stability (mean size at 130 nm and low polydispersity) drastically dropped off after two hours. The size data suggests that after two hours the favorable dissolution characteristics of albumin into saline override the binding forces of paclitaxel in albumin clusters. The larger spheres start to dissolve as the strongest DLS size population is below 50 nm. The polydispersity data in conjunction illustrates that after two hours the disperisity value dramatically increases, suggesting multiple size populations, and thus lesser stability of the product.

Nanomolded Abraxane PRINT particles of 200 nm (diameter) x 200 nm cylinders show increased stability with respect to size and polydispersity, out to at least eight hours. One hypothesis to explain this phenomenon is that these particles are monodisperse in size and shape and thus have the same surface area exposed to solvent. The PRINT process also enables consistency in the ratio of paclitaxel to albumin. The fabrication technique may also improve the binding forces that hold paclitaxel bound to albumin together due to the high concentration utilized in the PRINT process. The proprietary coascervation process used to fabricate Abraxane particles is extremely dilute. It is possible that this creates only loosely bound paclitaxel to albumin (stable for two hours), relative to the binding farces created from the PRINT process.

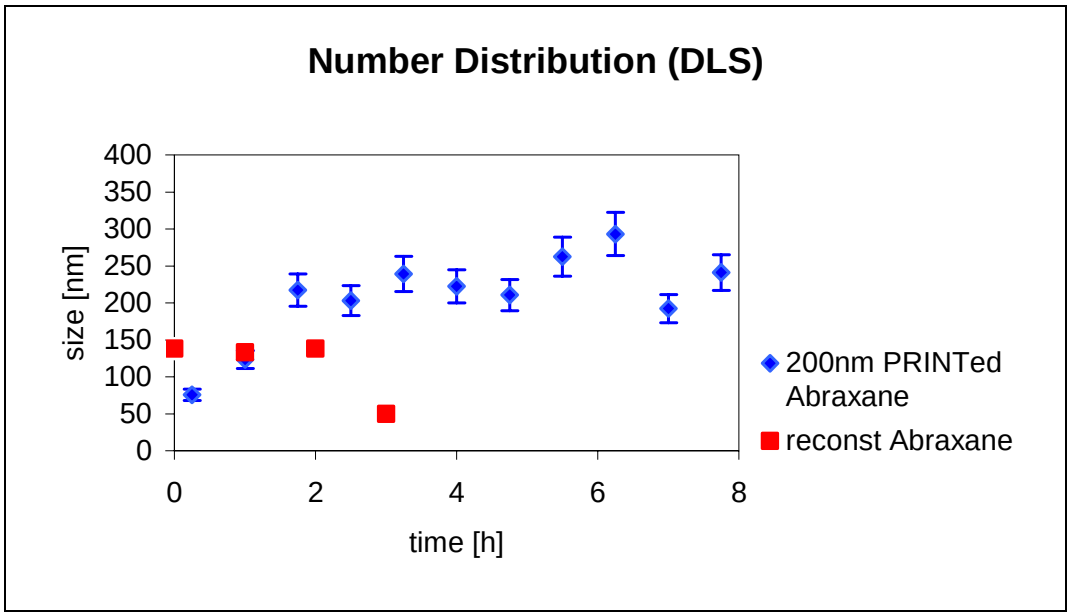

Figure 3-12. Size and stability of reconstituted Abraxane and PRINT particles.

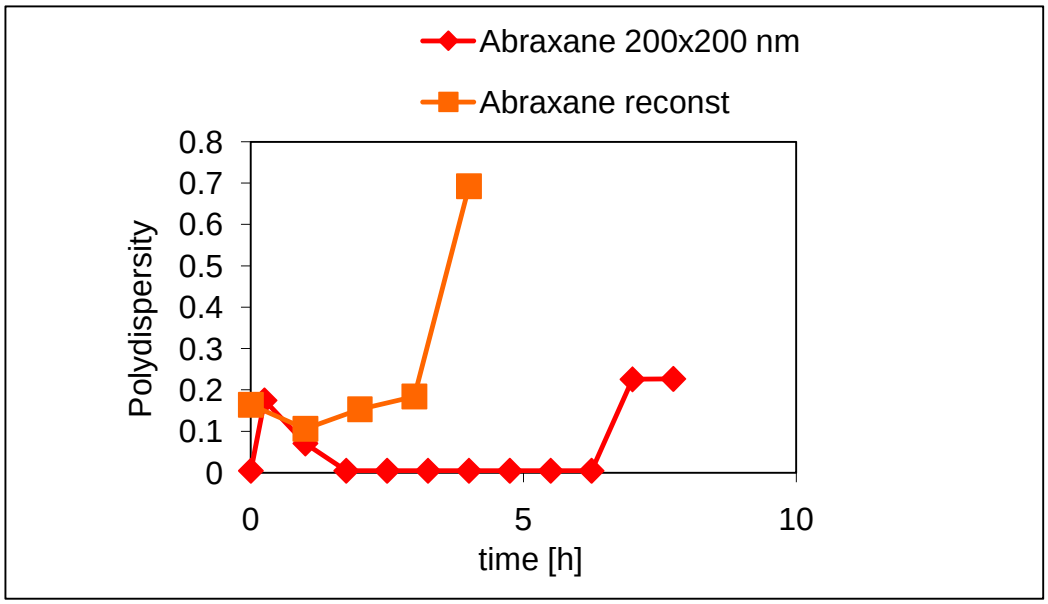

Figure 3-13. Polydispersity and stability of reconstituted abraxane and PRINT particles.

3.4.3 Summary and Future Efforts. Nanomolded Abraxane PRINT particles illustrate longer stability at physiological conditions which may increase the therapeutic efficacy and decrease undesired side effects. Initial cytotoxicity studies using 3T3 Fibroblast cell were conducted comparing free Abraxane, 200 nm (diameter) x 200 nm cylinders of nanomolded Abraxane, free albumin, nanomolded albumin, and free paclitael at the same relative concentration of paclitaxel. Initial results looked promising. The nanomolded Abraxane particles were killing more cells than Abraxane or paclitaxel alone at the same relative concentration. Unfortunately, negative controls in albumin particles showed some toxicity. After once repeating these experiments and obtaining similar results, efforts were halted to pursue protein PRINT particle fabrication and investigations thereof. Future directions of this work could include carefully repeating cell dosing experiments and monitor call viability. The cytotoxicity levels of nanomolded Abraxane PRINT particles in comparison to Abraxane should be investigated using a different cell line as well. Different size and shape particles should be investigated for nanomolded Abraxane and albumin. It is possible that harvesting methods need to be varied to overcome any introduced toxicity, not otherwise incurred by the particle matrix as with albumin. Ultimately, in vivo studies in healthy and in tumored mice are warranted. These studies would investigate the maximum tolerated dose of the therapeutic and compare Abraxane to nanomolded Abraxane. Within tumored mice studying the time line of tumor regression and present of relapse would be of tremendous value. As the PRINT technology develops particle sizes and shapes ideal for treatment of cancer, nanomolded Abraxane may show significant utility in the role to fight cancer and become the newest gold standard therapeutic.

1. Schiers, J., *Modern Fluoropolymers*. John Wiley & Sons, Ltd: New York, 1997; p 435-485.

2. Banks, R. E. S., B.E.; Tatlow, J. C., *Organofluorine Chemistry Principles and Commercial Applications*. Plenum Press: New York, 1994.

3. Ameduri, B.; Boutevin, B., Update on fluoroelastomers: from perfluoroelastomers to fluorosilicones and fluorophosphazenes. *Journal of Fluorine Chemistry* **2005,** 126, (2), 221-229.

4. Ameduri, B.; Boutevin, B.; Kostov, G., Fluoroelastomers: synthesis, properties and applications. *Progress in Polymer Science* **2001,** 26, (1), 105-187.

5. Liu, B.; Rolland, J. P.; DeSimone, J. M.; Bard, A. J., Fabrication of ultramicroelectrodes using a "Teflon-like" coating material. *Analytical Chemistry* **2005,** 77, (9), 3013-3017.

6. Maynor, B. W.; Larue, I.; Hu, Z.; Rolland, J. P.; Pandya, A.; Fu, Q.; Liu, J.; Spontak, R. J.; Sheiko, S. S.; Samulski, R. J.; Samulski, E. T.; DeSimone, J. M., Supramolecular nanomimetics: Replication of micelles, viruses, and other naturally occurring nanoscale objects. *Small* **2007,** 3, (5), 845-849.

7. Rolland, J. P.; Van Dam, R. M.; Schorzman, D. A.; Quake, S. R.; DeSimone, J. M., Solvent-resistant photocurable "liquid teflon" for microfluidic device fabrication. *Journal of the American Chemical Society* **2004,** 126, (8), 2322-2323.

8. Wood, C. D.; Michel, U.; Rolland, J. P.; DeSimone, J. A., New fluoropolymer materials. *Journal of Fluorine Chemistry* **2004,** 125, (11), 1671-1676.

9. Persico, D. F. G., G. E.; Lagow, R. J, *Journal of American Chemical Society* **1985,** 107, (1197-203).

10. Bunyard, W. C.; Romack, T. J.; DeSimone, J. M., Perfluoropolyether synthesis in liquid carbon dioxide by hexafluoropropylene photooxidation. *Macromolecules* **1999,** 32, (24), 8224-8226.

11. Scheirs, J.; Camino, G.; Costa, L.; Tonelli, C.; Turri, S.; Scicchitano, M., Photooxidation of functionalized perfluorinated polyethers - II. *Polymer Degradation and Stability* **1998,** 62, (2), 327-336.

12. Scheirs, J.; Camino, G.; Costa, L.; Tonelli, C.; Turri, S.; Scicchitano, M., Photooxidation of functionalized perfluorinated polyethers .1. *Polymer Degradation and Stability* **1997,** 56, (2), 239-253.

13. Gates, B. D.; Xu, Q.; Stewart, M.; Ryan, D.; Willson, C. G.; Whitesides, G. M., New Approaches to Nanofabrication: Molding, Printing, and Other Techniques. *Chem. Rev.* **2005,** 105, (4), 1171-1196.

14. McDonald, J. C.; Duffy, D. C.; Anderson, J. R.; Chiu, D. T.; Wu, H. K.; Schueller, O. J. A.; Whitesides, G. M., Fabrication of microfluidic systems in poly(dimethylsiloxane). *Electrophoresis* **2000,** 21, (1), 27-40.

15. McDonald, J. C.; Whitesides, G. M., Poly(dimethylsiloxane) as a material for fabricating microfluidic devices. *Accounts of Chemical Research* **2002,** 35, (7), 491-499.

16. Sia, S. K.; Whitesides, G. M., Microfluidic devices fabricated in poly(dimethylsiloxane) for biological studies. *Electrophoresis* **2003,** 24, (21), 3563-3576.

17. Wu, H. K.; Odom, T. W.; Chiu, D. T.; Whitesides, G. M., Fabrication of complex three-dimensional microchannel systems in PDMS. *Journal of the American Chemical Society* **2003,** 125, (2), 554-559.

18. Rolland, J. P.; Maynor, B. W.; Euliss, L. E.; Exner, A. E.; Denison, G. M.; DeSimone, J. M., Direct fabrication and harvesting of monodisperse, shape-specific nanobiomaterials. *Journal of the American Chemical Society* **2005,** 127, (28), 10096-10100.

19. Deng, T.; Wu, H. K.; Brittain, S. T.; Whitesides, G. M., Prototyping of masks, masters, and stamps/molds for soft lithography using an office printer and photographic reduction. *Analytical Chemistry* **2000,** 72, (14), 3176-3180.

20. Jackman, R. J.; Brittain, S. T.; Adams, A.; Wu, H. K.; Prentiss, M. G.; Whitesides, S.; Whitesides, G. M., Three-dimensional metallic microstructures fabricated by soft lithography and microelectrodeposition. *Langmuir* **1999,** 15, (3), 826-836.

21. Xia, Y. N.; Whitesides, G. M., Soft lithography. *Angewandte Chemie-International Edition* **1998,** 37, (5), 551-575.

22. Zhao, X. M.; Xia, Y. N.; Whitesides, G. M., Soft lithographic methods for nano-fabrication. *Journal of Materials Chemistry* **1997,** 7, (7), 1069-1074.

23. Rolland, J. P.; Hagberg, E. C.; Denison, G. M.; Carter, K. R.; De Simone, J. M., High-resolution soft lithography: Enabling materials for nanotechnologies. *Angewandte Chemie-International Edition* **2004,** 43, (43), 5796-5799.

24. Liying Wang, M. H. L., Jeremy Barton, Laura Hughes, and Teri Odom, Shape-Control of Protein Crystals in Patterned Microwells. *Journal of American Chemical Society* **2008**.

25. Heyries, K. A.; Marquette, C. A.; Blum, L. J., Straightforward protein immobilization on Sylgard 184 PDMS microarray surface. *Langmuir* **2007,** 23, (8), 4523-4527.

26. Wang, C.; Zhang, Y., A microsphere coupled micropatterning method for cytokine detection. *Sensors and Actuators B-Chemical* **2006,** 120, (1), 125-129.

27. Wang, Y. J.; Caruso, F., Nanoporous protein particles through templating mesoporous silica spheres. *Advanced Materials* **2006,** 18, (6), 795-+.

28. Zhang, Y., Micropatterning of proteins on nanospheres. *Colloids and Surfaces B-Biointerfaces* **2006,** 48, (1), 95-100.

29. Mahmud, G. K. J. M. B., Yuriy Chegel, Stoyan K. Smoukov, and Bartosz A. Grzybowski, Wet-Stamped Precipitant Gradients Control the Growth of Protein Microcrystals in an Array of Nanoliter Wells. *Journal of American Chemical Society* **2008**.

30. Li, J. R.; Henry, G. C.; Garno, J. C., Fabrication of nanopatterned films of bovine serum albumin and staphylococcal protein A using latex particle lithography. *Analyst* **2006,** 131, (2), 244-250.

31. Kane, R. S.; Takayama, S.; Ostuni, E.; Ingber, D. E.; Whitesides, G. M., Patterning proteins and cells using soft lithography. *Biomaterials* **1999,** 20, (23-24), 2363-2376.

32. Mayer, M.; Yang, J.; Gitlin, I.; Gracias, D. H.; Whitesides, G. M., Micropatterned agarose gels for stamping arrays of proteins and gradients of proteins. *Proteomics* **2004,** 4, (8), 2366-2376.

33. Weibel, D. B.; DiLuzio, W. R.; Whitesides, G. M., Microfabrication meets microbiology. *Nature Reviews Microbiology* **2007,** 5, (3), 209-218.

34. Whitesides, G. M.; Ostuni, E.; Takayama, S.; Jiang, X. Y.; Ingber, D. E., Soft lithography in biology and biochemistry. *Annual Review of Biomedical Engineering* **2001,** 3, 335-373.

35. Petros, R. A.; Ropp, P. A.; DeSimone, J. M., Reductively Labile PRINT Particles for the Delivery of Doxorubicin to HeLa Cells. *J. Am. Chem. Soc.* **2008**.

36. Olson, D. A.; Gratton, S. E. A.; DeSimone, J. M.; Sheares, V. V., Amorphous linear aliphatic polyesters for the facile preparation of tunable rapidly degrading elastomeric devices and delivery vectors. *Journal of the American Chemical Society* **2006,** 128, (41), 13625-13633.

37. Gratton, S. E. A.; Pohlhaus, P. D.; Lee, J.; Guo, I.; Cho, M. J.; DeSimone, J. M., Nanofabricated particles for engineered drug therapies: A preliminary Biodistribution study of PRINT (TM) nanoparticles. *Journal of Controlled Release* **2007,** 121, (1-2), 10-18.

38. Discher, B. M.; Won, Y. Y.; Ege, D. S.; Lee, J. C. M.; Bates, F. S.; Discher, D. E.; Hammer, D. A., Polymersomes: Tough vesicles made from diblock copolymers. *Science* **1999,** 284, (5417), 1143-1146.

39. Discher, D. E., Polymer vesicles of PEO-PLA and related for controlled release. *Abstracts of Papers of the American Chemical Society* **2003,** 225, U679-U679.

40. Discher, D. E.; Ahmed, F., Polymersomes. *Annual Review of Biomedical Engineering* **2006,** 8, 323-341.

41. Discher, D. E.; Eisenberg, A., Polymer vesicles. *Science* **2002,** 297, (5583), 967-973.

42. Euliss, L. E.; DuPont, J. A.; Gratton, S.; DeSimone, J., Imparting size, shape, and composition control of materials for nanomedicine. *Chemical Society Reviews* **2006,** 35, (11), 1095-1104.

43. Geng, Y.; Dalhaimer, P.; Cai, S. S.; Tsai, R.; Tewari, M.; Minko, T.; Discher, D. E., Shape effects of filaments versus spherical particles in flow and drug delivery. *Nature Nanotechnology* **2007,** 2, (4), 249-255.

44. Zauner, W.; Farrow, N. A.; Haines, A. M. R., In vitro uptake of polystyrene microspheres: effect of particle size, cell line and cell density. *Journal of Controlled Release* **2001,** 71, (1), 39-51.

45. Champion, J. A.; Katare, Y. K.; Mitragotri, S., Particle shape: A new design parameter for micro- and nanoscale drug delivery carriers. *Journal of Controlled Release* **2007,** 121, (1-2), 3-9.

46. Champion, J. A.; Mitragotri, S., Role of target geometry in phagocytosis. *Proceedings of the National Academy of Sciences of the United States of America* **2006,** 103, (13), 4930-4934.

47. Rejman, J.; Oberle, V.; Zuhorn, I. S.; Hoekstra, D., Size-dependent internalization of particles via the pathways of clathrin-and caveolae-mediated endocytosis. *Biochemical Journal* **2004,** 377, 159-169.

48. Chen, J.; Tian, B.; Yin, X.; Zhang, Y.; Hu, D.; Hu, Z.; Liu, M. Z.; Pan, Y. F.; Zhao, J. F.; Li, H.; Hou, C.; Wang, J. W.; Zhang, Y. D., Preparation, characterization and transfection efficiency of cationic PEGylated PLA nanoparticles as gene delivery systems. *Journal of Biotechnology* **2007,** 130, (2), 107-113.

49. Craparo, E. F.; Cavallaro, G.; Bondi, M. L.; Mandracchia, D.; Giammona, G., PEGylated nanoparticles based on a polyaspartamide. Preparation, physico-chemical characterization, and intracellular uptake. *Biomacromolecules* **2006,** 7, (11), 3083-3092.

50. des Rieux, A.; Fievez, V.; Momtaz, M.; Detrembleur, C.; Alonso-Sande, M.; Van Gelder, J.; Cauvin, A.; Schneider, Y. J.; Preat, V., Helodermin-loaded nanoparticles: Characterization and transport across an in vitro model of the follicle-associated epithelium. *Journal of Controlled Release* **2007,** 118, (3), 294-302.

51. Hayes, M. E.; Drummond, D. C.; Kirpotin, D. B.; Zheng, W. W.; Noble, C. O.; Park, J. W.; Marks, J. D.; Benz, C. C.; Hong, K., Genospheres: self-assembling nucleic acid-lipid nanoparticles suitable for targeted gene delivery. *Gene Therapy* **2006,** 13, (7), 646-651.

52. Hong, R.; Fischer, N. O.; Emrick, T.; Rotello, V. M., Surface PEGylation and ligand exchange chemistry of FePt nanoparticles for biological applications. *Chemistry of Materials* **2005,** 17, (18), 4617-4621.

53. Kaul, G.; Amiji, M., Cellular interactions and in vitro DNA transfection studies with poly(ethylene glycol)-modified gelatin nanoparticles. *Journal of Pharmaceutical Sciences* **2005,** 94, (1), 184-198.

54. Kaul, G.; Amiji, M., Long-circulating poly(ethylene glycol)-modified gelatin nanoparticles for intracellular delivery. *Pharmaceutical Research* **2002,** 19, (7), 1061-1067.

55. Owens, D. E.; Peppas, N. A., Opsonization, biodistribution, and pharmacokinetics of polymeric nanoparticles. *International Journal of Pharmaceutics* **2006,** 307, (1), 93-102.

56. Peracchia, M. T.; Vauthier, C.; Desmaele, D.; Gulik, A.; Dedieu, J. C.; Demoy, M.; d'Angelo, J.; Couvreur, P., Pegylated nanoparticles from a novel methoxypolyethylene glycol cyanoacrylate hexadecyl cyanoacrylate amphiphilic copolymer. *Pharmaceutical Research* **1998,** 15, (4), 550-556.

57. Rehor, A.; Schmoekel, H.; Tirelli, N.; Hubbell, J. A., Functionalization of polysulfide nanoparticles and their performance as circulating carriers. *Biomaterials* **2008,** 29, (12), 1958-1966.

58. Suh, J.; Choy, K. L.; Lai, S. K.; Suk, J. S.; Tang, B. C.; Prabhu, S.; Hanes, J., PEGylation of nanoparticles improves their cytoplasmic transport. *International Journal of Nanomedicine* **2007,** 2, (4), 735-741.

59. Sun, X. K.; Rossin, R.; Turner, J. L.; Becker, M. L.; Joralemon, M. J.; Welch, M. J.; Wooley, K. L., An assessment of the effects of shell cross-linked nanoparticle size,

core composition, and surface PEGylation on in vivo biodistribution. *Biomacromolecules* **2005,** 6, (5), 2541-2554.

60. Yoncheva, K.; Lizarraga, E.; Irache, J. M., Pegylated nanoparticles based on poly(methyl vinyl ether-co-maleic anhydride): preparation and evaluation of their bioadhesive properties. *European Journal of Pharmaceutical Sciences* **2005,** 24, (5), 411-419.

61. Zahr, A. S.; de Villiers, M.; Pishko, M. V., Encapsulation of drug nanoparticles in self-assembled macromolecular nanoshells. *Langmuir* **2005,** 21, (1), 403-410.

62. Zhang, Y. Q.; Chen, J. J.; Zhang, Y. D.; Pan, Y. F.; Zhao, J. F.; Ren, L. F.; Liao, M. M.; Hu, Z. Y.; Kong, L.; Wang, J. W., A novel PEGylation of chitosan nanoparticles for gene delivery. *Biotechnology and Applied Biochemistry* **2007,** 46, 197-204.

63. Zillies, J. C.; Zwiorek, K.; Winter, G.; Coester, C., Method for quantifying the PEGylation of gelatin nanoparticle drug carrier systems using asymmetrical flow field-flow fractionation and refractive index detection. *Analytical Chemistry* **2007,** 79, (12), 4574-4580.

64. Scripture, C. D. F., W. D.; Sparreboom, A., Peripheral Neuropathy Induced by Paclitaxel: Recent Insights and Future Perspectives. *Current Neuropharmacology* **2006,** 4, 165-172.

65. Mielke, S. S., Alex; Mross, Klaus, Peripheral neuropathy: A persisting challenge in paclitaxel-based regimes. *European Journal of Cancer* **2006,** 42, 24-30.

66. Desai, N.; Campbell, K. J.; Ellerhorst, J.; Ibrahim, N.; Soon-Shiong, P., Preclinical and clinical pharmacokinetics and safety of ABI-007, a novel, cremophor-free, protein-engineered nanotransporter of paclitaxel. *Breast Cancer Research and Treatment* **2002,** 76, S131-S131.

67. Desai, N.; Trieu, V.; Hwang, L.; Wu, R.; Hawkins, M.; Soon-Shiong, P.; Gradishar, W., HER2 and SPARC status in tumors play an important role in the relative effectiveness of nanoparticle albumin-bound (nab) paclitaxel versus polysorbate-based docetaxel. *Breast Cancer Research and Treatment* **2007,** 106, S88-S88.

68. Desai, N.; Trieu, V.; Yao, Z. W.; Louie, L.; Ci, S.; Yang, A.; Tao, C. L.; De, T.; Beals, B.; Dykes, D.; Noker, P.; Yao, R.; Labao, E.; Hawkins, M.; Soon-Shiong, P., Increased antitumor activity, intratumor paclitaxel concentrations, and endothelial cell transport of Cremophor-free, albumin-bound paclitaxel, ABI-007, compared with Cremophor-based paclitaxel. *Clinical Cancer Research* **2006,** 12, (4), 1317-1324.

69. Ng, S. S. W.; Sparreboom, A.; Shaked, Y.; Lee, C.; Man, S.; Desai, N.; Soon-Shiong, P.; Figg, W. D.; Kerbel, R. S., Influence of formulation vehicle on metronomic

taxane chemotherapy: Albumin-bound versus cremophor EL-based paclitaxel. *Clinical Cancer Research* **2006,** 12, (14), 4331-4338.

70. Desai, N.; Trieu, V.; Hawkins, M.; Soon-Shiong, R., Improved effectiveness of nab-paclitaxel versus clocetaxel in various xenografts as a function of HER2 and SPARC status. *Ejc Supplements* **2006,** 4, (12), 153-154.

71. Desai, N.; Trieu, V.; Yang, A.; De, T.; Cordia, J.; Yim, Z.; Ci, S.; Louie, L.; Beals, B.; Hawkins, M., Enhanced antitumor activity and safety of albumin-bound nab-docetaxel versus polysorbate 80-based docetaxel. *Ejc Supplements* **2006,** 4, (12), 49-49.

72. Gradishar, W. J.; Tjulandin, S.; Davidson, N.; Shaw, H.; Desai, N.; Bhar, P.; Hawkins, M.; O'Shaughnessy, J., Phase III trial of nanoparticle albumin-bound paclitaxel compared with polyethylated castor oil-based paclitaxel in women with breast cancer. *Journal of Clinical Oncology* **2005,** 23, (31), 7794-7803.

73. Ibrahim, N. K.; Desai, N.; Legha, S.; Soon-Shiong, P.; Theriault, R. L.; Rivera, E.; Esmaeli, B.; Ring, S. E.; Bedikian, A.; Hortobagyi, G. N.; Ellerhorst, J. A., Phase I and pharmacokinetic study of ABI-007, a cremophor-free, protein-stabilized, nanoparticle formulation of paclitaxel. *Clinical Cancer Research* **2002,** 8, (5), 1038-1044.

74. Nyman, D. W.; Campbell, K. J.; Hersh, E.; Long, K.; Richardson, K.; Trieu, V.; Desai, N.; Hawkins, M. J.; Von Hoff, D. D., Phase I and pharmacokinetics trial of ABI-007, a novel nanoparticle formulation of paclitaxel in patients with advanced nonhematologic malignancies. *Journal of Clinical Oncology* **2005,** 23, (31), 7785-7793.

75. Durr, E.; Yu, J.; Krasinska, K. M.; Carver, L. A.; Yates, J. R.; Testa, J. E.; Oh, P.; Schnitzer, J. E., Direct proteomic mapping of the lung microvascular endothelial cell surface in vivo and in cell culture. *Nat Biotech* **2004,** 22, (8), 985-992.

76. Schnitzer, J. E., gp60 is an albumin-binding glycoprotein expressed by continuous endothelium involved in albumin transcytosis. *Am J Physiol Heart Circ Physiol* **1992,** 262, (1), H246-254.

77. Schnitzer, J. E., Caveolae: from basic trafficking mechanisms to targeting transcytosis for tissue-specific drug and gene delivery in vivo. *Advanced Drug Delivery Reviews* **2001,** 49, (3), 265-280.

78. Schnitzer, J. E.; Oh, P., Albondin-mediated capillary permeability to albumin. Differential role of receptors in endothelial transcytosis and endocytosis of native and modified albumins. *J. Biol. Chem.* **1994,** 269, (8), 6072-6082.

79. Schnitzer, J. E.; Oh, P., Antibodies to SPARC inhibit albumin binding to SPARC, gp60, and microvascular endothelium. *Am J Physiol Heart Circ Physiol* **1992,** 263, (6), H1872-1879.

80. Sparreboom, A.; Scripture, C. D.; Trieu, V.; Williams, P. J.; De, T. P.; Yang, A.; Beals, B.; Figg, W. D.; Hawkins, M.; Desai, N., Comparative preclinical and clinical pharmacokinetics of a cremophor-free, nanoparticle albumin-bound paclitaxel (ABI-007) and paclitaxel formulated in cremophor (Taxol). *Clinical Cancer Research* **2005,** 11, (11), 4136-4143.

81. Hren, M.; Zel, J.; Baebler, S.; Nemec, M.; Ravnikar, M.; Schara, M., Estimating the plasma membrane permeability of Taxus x media cells with the spin probe TEMPOL by EPR. *Plant Science* **2005,** 168, (2), 535-540.

82. Balasubramanian, S. V.; Straubinger, R. M., Taxol-Lipid Interactions: Taxol-Dependent Effects on the Physical Properties of Model Membranes. *Biochemistry* **1994,** 33, (30), 8941-8947.

CHAPTER 4

NANOMOLDING SHAPE- AND SIZE-SPECIFIC PROTEIN PARTICLES USING THE PRINT TECHNOLOGY

4.0 Introduction.

4.1 PRINT Technology Enabling Nano-Fabrication of Shape-Specific, Monodisperse Protein Particles. Protein particles are at the forefront of a surge in research and development for enhanced therapeutics and are being utilized as powerful drug delivery vectors, to overcome solubility concerns, or being realized as the key therapeutic in often invasive treatment regiments. Handling and storage protocols of these sensitive materials have proven to be challenging at times due to the susceptible nature of these liable biologics. Storage needs are pertinent in this field and much effort has been dedicated to investigations of the variables and parameters that effect biological efficacy such as temperature, moisture, formulation, particle fabrication method, and composition. A need for a facile, robust technique to store and handle therapeutic proteins remains unmet. Recent drive for attaining discrete control over particle shape, size, dispersity, and surface interaction for drug delivery has proven essential particularly in targeted cancer research. Additionally, these methods are not robust and slight variation of any parameter in the fabrication process greatly affects the stability and overall outcome of the desired product.[1-4] The PRINT™ technology (Particle Replication In Non-Wetting Templates) offers a broad platform for the facile fabrication, handling, and storage of protein particles that remain un-aggregated until just prior to use. This versatile methodology lends itself to easy scale-up and avoids any loss of monomer or degradation of the protein. No surfactants, stabilizing agents, co-solvents, or co-monomers are necessary for the protein particle delivery vector. The PRINT process enables a gentle, facile route to non-disperse particles of 100 percent protein as small as 200 nm cylinders.

Rolland et al reported in 2004 the exploitation of the excellent solvent resistance and inherent release properties of perfluoropolyether (PFPE) elastomers as a molding material for soft lithography. When molding onto a non-wetting surface the fabrication of individual particles is realized, in contrast to traditional soft lithography techniques that typically create embossed films having a residual or flash layer interconnecting the features. PRINT uses the non-wetting characteristic of PFPE-based elastomers to generate high-resolution micro- and nano-meter sized objects that are free of the interconnecting flash layer, creating arrays of discrete particles or features. The fabrication of "smart particles" with independent control over size, shape, composition, cargo encapsulation, surface functionality, and biodistribution[5] have been achieved using the PRINT technology. PRINT is capable of generating shape-specific, mono-disperse nanoparticles composed of a variety of materials including synthetic polymers, hydrogels, and active pharmaceutical ingredients.[6, 7] The gentle nature of this process allows for particle fabrication of even delicate biologics such as proteins. In this chapter the first account of unique protein particle fabrication of discrete size and shape. These protein particles and mono-disperse and non-aggregated. The fabrication process is conducted with high fidelity and precision. The physical and functional characterization of the fabricated protein particles were conducted using SEM, ELISA, DSC, FTIR, and fluorescence. The work is reported using albumin as a model protein and shows preliminary work for numerous other proteins including insulin, hemoglobin, transferrin, interferon-beta, trypsin, horseradish peroxidase, and IgG polyclonal antibody.

4.2 Importance and Implication of Proteins in Disease Fighting, Biomarkers, and Targeting Ligands. As discussed to in section 3.4, proteins encompass bio- and nanotechnologies, which are ever-growing and interrelated research fields with billions of dollars being invested in the development and improvement of state-of-the-art therapeutics,[8] delivery vectors, imaging agents,[9, 10] biosensors,[11, 12] devices, coatings, and other biomedical applications.[13] Biomolecules and protein particles are leading this surge in research and development of enhanced therapeutics. They are being utilized as powerful targeting ligands, drug delivery vectors, and as the key therapeutic in invasive treatment regiments. Handling and storage protocols of these sensitive materials have proven to be challenging at times due to the susceptible nature of these labile biologics. Storage demands are pertinent in this field and much effort has been dedicated to investigating the effects of numerous parameters such as temperature, humidity, composition, and fabrication method in order to retain the protein's native state and biological function. Much attention has been dedicated to attaining and investigating effects of judicious control over particle shape, size, dispersity, and surface interaction for targeted drug delivery and has emerged as essential, particularly in cancer research.[14-21] However, current state-of-the-art methods for developing mono-disperse, discrete size and shape particles comprised of proteins have not been successful or are not robust and slight variations in parameters of the fabrication process can greatly affect the stability and overall outcome of the desired product. Hence, until now the need for a facile, robust technique to store and handle therapeutic proteins has remained unmet.

4.3 How Protein Particles are Typically Prepared. Protein particles are often made through complicated processes which include wet-milling, spray-freeze-drying,[1, 4, 22-27] micro-emulsion,[28] micro-encapsulation,[2, 29-34] or super critical fluid[29, 35, 36] methods. These procedures result in highly disperse particle sizes in the tens of microns are strictly spherical, and tend to aggregate. Protein particles are typically stored as a lyophilized powder. Studies are increasingly showing the size, shape, and dispersity have a tremendous impact on biological processes.[15] Most manufacturing processes are also dependent on very strict parameters and precise control of conditions, some of which strongly influence the product outcome and often induce stresses leading to denaturation. Size, morphology, and stability of these proteins have tremendous implication on the outcome and efficacy of various bio-pharmaceutical applications.

Proteins require their native structure not to be significantly disrupted in order to be biologically active, thus maintaining their conformation is crucial in developing protein pharmaceuticals.[25] However, due to the inherent frailty of these biomaterials a variety of intra- and intermolecular chemical reactions are capable of irreversibly perturbing their native structure and thus rendering them biologically inactive. The approach to particle fabrication composed of proteins requires a gentle process which will not disrupt the protein's activity, affecting its potential use in biopharmaceuticals.

Recently, techniques used by the microelectronics industry to fabricate patterns on the micro- and nano-scale have been adopted by the life sciences for patterning,[37-39] particle fabrication,[40] and crystallization[41, 42] of a wide range of biologically-relevant materials.[43] However, a significant improvement in the methodologies used in this field is required because proteins are extremely sensitive compounds that are easily denatured or

degraded. Engineered protein particle fabrication with control over shape and size that preserves biofunctionality has not been realized to date.

4.4 Nanomolding Proteins.

4.4.1 Fabrication Methodology and Variables. The fabrication of protein PRINT particles is achieved similarly to nanomolded Abraxane, as discussed in Chapter 3. Due to the sensitive nature of proteins and biologics, extreme care must be taken in fabricating shape- and size specific, monodisperse micro- and nanoparticles. External stimuli such as heat and UV irradiation often affect biomaterials detrimentally and alter their integrity, functionality, and bioavailability. Additional concerns within the fabrication methodology include concentration-dependant denaturation and choice of continuous phase with proteins in solution. Variables of the fabrication process investigated included protein concentration, solvent/buffer choice for protein reconstitution prior to nanomolding, speed of laminator stage, material of counter sheet, pressure of roller and thus counter sheet, and harvesting methods. Best results were obtained in most cases when 25 weight percent protein in water was nanomolded at relatively low stage speed, 50 psi applied pressure, using poly(ethylene terethalate) as a counter sheet, and utilizing a harvesting film or excipient to extract particles from the mold. Directly harvesting with water or buffer also collects protein particles from the mold (Figure 4-1).

4.4.2 Protein Choice for Investigation. Albumin was chosen as the model protein due to the extensive citing in literature including its use as a delivery vector,[43-45]

exploitation of its receptor (gp60),[46] and protein conjugate systems.[47-49] Additional biomaterials were investigated for their clinical importance and to gage the breadth and gentleness of the PRINT process with therapeutic proteins and enzymes. Insulin, tranferrin, hemoglobin, IFN-beta, trypsin, HRP, and IgG differ greatly in molecular weight, crystallinity, and solubility in water. Insulin was chosen for its importance in the treatment of diabetes and the potential enhancement of a pulmonary drug delivery system. Much work has been dedicated to better delivery systems and methods of insulin for treatment of diabetes.[50-54] Interferon-beta possesses anti-inflammatory properties and has been shown to improve the integrity of the blood-brain barrier in multiple sclerosis (MS) patients. Commercial interferon-beta-based drugs are typically sold in two formulations, a lyophilized powder requiring reconstitution and a pre-mixed liquid syringe kit, which is administered via an intramuscular injection. Hemoglobin is an important oxygen carrier in the body and plays a crucial role in iron-deficiency anemia and sickle-cell disease. Transferrin has recently made an impact as a targeting ligand and is implicated in the transport of iron.

Enzymes as a whole perform an all-encompassing function in the development and maintenance of the human body and are being utilized for disease treatment and prevention. Trypsin is a serine protease enzyme found in the digestive system and is used in biotechnological processes with implications in the treatment of cystic fibrosis. However, when its break-down of other proteins runs unchecked, it can lead to pancreatic and cellular diseases. Horseradish peroxidase has been shown to improve marking neurons and to amplify biotechnical analyses in the field of neuron biology. Many others are finding opportunities in treatments for cardiovascular disease (Natrecor, GPIIB

receptor, protein G receptor), HIV (Interferon, Somatostatin, T20, T1249, IL-2), inflammation (TNF-α, IL1-RA), Alzheimer's disease (antisense, laminin), Crohn's disease, and cancer (interferons, monoclonal antibodies).

4.4.3 Methods.

4.4.3.1 Materials. Fluorocur™ and untreated PET sheets were purchased from Liquidia Technologies. An ELISA starter kit and standard sandwich ELISA kits for human albumin, hemoglobin, and transferrin was purchased from Bethyl Laboratories. A sandwich ELISA kit for human insulin was purchased from CalBiotech. Human albumin, hemoglobin, transferrin, insulin, and recombinant rat interferon-β were purchased from Sigma Aldrich as lyophilized powders. Trypsin, horseradish peroxidase, N-benzoyl- L-arginine-nitroanalide, hydrogen peroxide, pyrogallol, and D(+)-trehalose was purchased from Sigma Aldrich and used as received. Ultrapure 17 mega Ohm water was filtered through a 0.22 μm Millipore PES membrane. PBS (1x) was used for harvesting and various characterizations. Rhodamine B was purchased from Acros Organics and used as received. With a target sequence of N.N.G.A.U.U.A.U.G.U.C.C.G.G.U.U.A.U.G.U.A and an antisense sequence of 5'-P.U.A.C.A.U.A.A.C.C.G.G.A.C.A.U.A.A.U.C.U.U, siRNA was purchased from DHARMACON as a 2.0 μmol lyophilized powder. Standard laboratory practices when handling RNA including decontamination were conducted. Poly(vinyl pyrrolidone), avg MW 58000 g/mol, was purchased from Acros Organics and dissolved in water to create a 10 % by weight solution, used as a harvesting film.

4.4.3.2 Fabrication of Protein PRINT™ Particles. The preparation of patterned Fluorocur has been described elsewhere. Briefly, inside an enclosed UV chamber 20 mL of Fluorocure with 0.1 % of 2,2-diethoxyacetophenone was cast onto an eight inch patterned master (feature sizes ranging between master template cavity sizes of 200 nm and 5 μm). After complete spreading of the Fluorocur, the UV chamber was purged with nitrogen for five minutes and subsequently irradiated (λ=365 nm, power < 20 mW/cm^2) to cure the Fluorocur resin with ongoing purge for three minutes. The fluorinated elastomer was then gently peeled from the silicon master. The elastomer was then placed on a stage. A sandwich structure of the PFPE mold, aqueous protein solution and a high energy counter sheet, in this case a polyethylene film, was slowly moved through a roller. As the mold passed through the roller, the high energy counter sheet was peeled away from the sandwich structure, leaving the mold filled with no interconnecting flash layer. Pressure was applied to the roller, typically 50 psi. The aqueous protein solution was 25 wt % in ultrapure water, unless stated otherwise. In the case of insulin, a 4 wt % aqueous solution was prepared and added to the sandwich structure for nano-molding. In the case of IFN-beta, a 10 wt % aqueous solution was prepared. Filled molds were frozen and lyophilized. Particles were harvested directly using a glass slide with minimal pressure and a drop of a non-solvent, typically chloroform or with PBS for further analysis. Particles were harvested in an array onto medical grade poly(cyanoacrylate) or an excipient film (poly(vinyl pyrrolidone). In this case, a drop of the harvesting solution is placed onto a substrate, usually a glass slide or in the case of ELISA in the bottom of a well in a 96-well polystyrene plate. The filled mold is rolled onto the drop. Once dry, the elastomer is peeled from the substrate, and particles adhere to the substrate.

4.4.3.3 SEM. The size of PRINT nanoparticles was analyzed via scanning electron microscopy (Hitachi model S-4700). Particles were harvested onto PET and a thin film of 10 wt % Povidone in water and were coated with 1.5 nm of Pd/Au alloy using a Cressington 108 auto sputter coater (Cressington Scientific Instruments Ltd.). The Pd/Au coated PET was then adhered to the sample holder using double-sided adhesive tape, and placed inside the vacuum chamber of the SEM and observed under low vacuum (10^{-3} Torr).

4.4.3.4 ATR-FTIR. ATR-FTIR analysis was performed with a Tensor 27 FTIR instrument (Bruker) using a Hyperion microscope fitted with an ATR objective with a Ge crystal as the internal reflectance element (IRE) and a MCT detector. OPUS software was employed for data processing. FTIR spectroscopy was used to investigate the presence of functional groups and the amide I region (1500 to 1700 wavenumbers) and establish qualitative secondary structure information of free lyophilized albumin and lyophilized albumin PRINT particles.

4.4.3.5 CD. Protein solutions were prepared at a final concentration of 0.1 mg/mL in 16.7 MΩ deionized water. PRINT protein samples were nano-molded, lyophilized in the mold, harvested directly into water, and lyophilized again. Five micron cube PRINT particles were fabricated for CD analysis. Data was collected on an Applied Photophysics Pistar-180 Circular Dichroism, at 25 C, with a 1 mm path length cell, a 15-nm/min scan rate and a 2 nm bandwidth. Spectra were an average of 25 scans from 185 to 260 nm. A

spectrum of water was collected and subtracted from the protein samples. Protein samples were run in triplicate.

4.4.3.6 BCA. Standard BCA protocol was followed in order to determine protein sample concentrations. Bovine albumin (BSA) standards were always prepared fresh for each assay. All samples were analyzed with n=3. After addition of reagents to a 96 well plate, standard or enhanced assays were conducted for the respective BSA working concentration ranges. Incubation for 30 min at 37 °C for the standard protocol and 30 min at 60 °C for the enhanced assay was conducted. After cooling to room temperature absorption of the plate was analyzed at 562 nm. Average OD values for the BSA standards were plotted versus concentration. A linear trend line was fit to the data. The equation of the trend line was used to solve for the concentrations of the unknown protein solutions.

4.4.3.7 Fluorescence Microscopy. Relative fluorescence intensity of the tryptophan residue in albumin was measured as a function of concentration in PBS at an excitation wavelength of 280 nm and an emission wavelength of 348 nm in a black plate. Concentrations of the free and PRINT protein solutions were analyzed prior to fluorescence measurements using a BCA assay. Black 96-well plates were used in a plate reader. 50 uL solution was added to each well. Each sample was measured at least in triplicate.

4.4.3.8 ELISA. Standard sandwich ELISA assays were conducted unless otherwise stated. A typical sandwich ELISA protocol was followed to accommodate a 96 well-plate. Detection antibodies were polyclonal and HRP conjugates. Kit standards were added in the concentration range that was recommended and diluted as suggested with sample diluents provided in the ELISA starter kit. Free and PRINT protein samples were diluted such that four concentrations being investigated were in the linear range. The HRP conjugate dilutions were twice as concentrated as the starting recommendation, but well within the working range i.e. if the recommended dilution was 1:100,000, the actual dilution used was 1:50,000. In the case of insulin, a coated plate with capture antibody was used as received. Substrate solution was added just prior to use and allowed to warm to room temperature. Once adequate color was observed, 2M H_2SO_4 was added as stopping solution. Absorbance was measured with a SpectraMax M5 plate reader (Molecular Devices) at 450 nm.

4.4.3.9 Enzymatic Activity Assay. Standard protocols were followed at room temperature to measure the enzymatic activity of trypsin and HRP, respectively. In the case of HRP, the substrates used were hydrogen peroxide and pyrogallol, and absorbance was measured at 450nm every 20 seconds for five minutes. HRP concentrations ranged from 2.5 ug/mL to 0.63 ug/mL in PBS. In the case of trypsin, the catalytic hydrolysis of N-benzoyl- L-arginine-nitroanalide was monitored in phosphate buffer. Trypsin concentrations ranged from 1 mg/mL to 0.25 mg/mL in PBS. The absorbance was measured at 380 nm every 20 seconds for five minutes. Enzyme concentrations were chosen such that after five minutes the OD at the respective wavelength was close to 1.

Measurements were taken of solutions in a quartz cuvette using a UV-vis spectrophotometer. Substrate solution was mixed by inversion and used as the reference. Enzyme solution was added to the cuvette and inverted five times before starting a kinetic analysis of absorbance. In the case of trypsin, enzyme solutions were prepared just prior to characterization and kept on ice.

4.4.4 Results.

4.4.4.1 Albumin.

4.4.4.1.1 Fabrication of Nanomolded Albumin PRINT Particles. A master template was first fabricated by selectively etching a pattern generated by photolithography into a silicon substrate to yield a densely packed micro- or nano-sized features on a two-dimensional array (Figure 3-9A). A fluorocarbon elastomeric mold was created by pouring a photochemically curable telechelic perfluoropolyether (PFPE) onto the patterned master templates and curing it while in contact with the master template to yield a patterned PFPE PRINT mold containing the corresponding different features as cavities (Figure 3-9B). Molds from masters including 200x200 nm cylinder, 2x2x4 μm square post, 3x3x3 μm cubes, 5x5x5 μm cubes, 10 μm boomerangs, and 3 μm hex nuts were fabricated for use in protein PRINT™ particle production. Nano-molding of protein particles was achieved by a lamination technique where an aqueous protein solution, typically 25 wt % protein in water, was placed between the patterned PFPE mold and another film (counter sheet) having a higher surface energy (Figure 3-9C). In this particular case a polyethylene sheet was used as the counter sheet during the PRINT lamination process. The PFPE mold, aqueous protein solution and polyethylene sandwich

structure was passed through a roller with an applied pressure of 50 psi. As the mold passes under the roller the high energy film was peeled away leaving a filled mold of individual cavities containing the aqueous protein solution without the formation of a flash layer between each filled cavity. The filled mold is subsequently frozen and lyophilized overnight to remove the majority of the water (Figure 3-9D). Protein particles were harvested directly by gently moving a drop of a polar non-solvent such as chloroform across the mold. Harvesting the protein particles in the form of a two dimensional array on a film, such as medical adhesive grade poly(cyano acrylate) or on an excipient film such as Povidone™ (poly(vinyl pyrollidinone)), was achieved by first casting a uniform thin film of the harvesting layer onto a glass slide using a Meyer Rod (Figure 3-9E). Then the patterned PFPE mold containing the protein particles was run through a roller, pattern side down, onto the liquid harvesting film (Figure 3-9F). Once the harvesting film was dried (in the case of using a Povidone harvesting film) or polymerized (if using the cyano acrylate harvesting film), the filled patterned mold was peeled away from the harvesting film to yield a two-dimensional array of protein particles (Figure 3-9G). During this harvesting step, the protein particles were transferred from the patterned PFPE mold onto the harvesting film in an essentially quantitative manner. By dissolving the harvesting film, individual protein particles could be collected (Figure 3-9H).

Albumin PRINT particles were fabricated in a similar method as to nanomolded Abraxane PRINT particles. Lyophilized human albumin was purchased from Sigma Aldrich and used as received. Albumin was added to filtered, 18 MΩ water to create a 25 weight % solution. In the case of albumin with cargo, dye or siRNA was added before the

addition of water. A PFPE mold was made from pouring and curing onto an etched silicon wafer and used in a sandwich structure with a 25 % by weight of albumin in water and a high energy counter sheet, again in this case PET. More concentrated solutions are capable of creating albumin PRINT particles including 30 and 35 % by weight in water. The sandwich structure was passed under a roller with an applied pressure of 50 psi. As the structure passed under the roller the PET sheet is peels away, leaving discrete cavities of the PFPE mold filled with a concentrated albumin solution. Some of the water may be driven off in the molding process. The filled mold is frozen and lyophilized to ensure total removal of water. This last step is also conducted for quality control, as most protein particle fabrication processes include a lyophilization step. Additionally, I felt that lyophilizing the PRINT protein particles would give a more direct comparison to lyophilized free protein as received.

A number of studies were explored with albumin. Harvesting methods were examined. Harvesting onto thin film adhesives resulted extremely feasible. Sipper harvesting with a non-solvent was considered. The choice of solvent utilized for sipper harvesting was scrutinized as it should not dissolve the particles, but also not denature the labile protein. Chloroform resulted in discrete, free flowing particles as indicated by SEM analysis. However, upon reconstitution in water the entire product did not seem to redissolve potentially indicating irreversible denaturation had occurred. Exhaustive drying may not have occurred, leaving a thin layer of chloroform around the albumin particles. This would create challenges for water to have clear access to the albumin for dissolution. It has been noted that cold ethanol is used to precipitate albumin from whole serum without denaturing albumin. Future investigations to use cold ethanol with sipper

harvesting methods could lead to free flowing, discrete protein particles, which can be fully reconstituted, would be of interest.

Cargo encapsulation was investigated by adding siRNA to the aqueous albumin solution prior to nanomolding. Since the compound was received in as a lyophilized powder, an aliquot was reconstituted in water. Due to cost, little antisense was used. Loading amount was close to 0.5 %. Visual conformation of cargo encapsulation was indicated by the magenta color (as a result of the antisense) of the molding solution and after harvesting, of the particles. Particles were harvested on a thin layer of medical grade adhesive. Dissolution of albumin particles was also monitored by adding a water-soluble dye, rhodamine B, to the composition. This mixture was nanomolded and particles were harvested onto Povidone, a water soluble adhesive film previously described. For this study particles of 5 μm cubes were fabricated, such that the dissolution study could be easily monitored using fluorescence microscopy.

4.4.4.1.2 SEM and Fluorescent Microscopy. Scanning electron microscopy was used to analyze the size and shape of all protein particles. Figures 4-1 through 4-6 illustrates albumin particles of different size, shape, and harvesting methods. These micrographs confirm the consistent nature of the PRINT process enabling facile fabrication of uniform, shape-specific, monodisperse particles composed of any protein.

Figure 4-1 illustrates albumin nano- and microparticles harvested on thin film adhesives and Figure 4-2 contains micrographs of directly harvested albumin particles of 200 nm cylinders using chloroform. Figure 4-3 and 4-4 illustrate SEM micrographs 200 nm cylinder particles of albumin with 0.5 % siRNA and gadolinium oxide loading, respectively. Discrete, uniform size and shape specific nanomolded albumin particles were fabricated as illustrated in the SEM micrographs. Particle sizes around or below 200 nm are thought to be of a therapeutic size range. The breadth of the PRINT process within fabricating different sizes was investigated by attempting the fabrication of larger sized cubes, up to 5 micron as illustrated in Figure 4-5.

Five micron particles were fabricated composed of albumin and a small weight fraction of rhodamineB, a non-covalently linked, water soluble dye. This size allows for facile analysis and monitoring using optical microscopy. The dye allows for additional increased image quality by using fluorescence microscopy in the red channel. Dissolution of the fabricated PRINT particles was investigated. The effect of the PRINT process on the protein's state can qualitatively be studied with dissolution. Denaturation often results in aggregated or polymerized protein that remains insoluble in water. Five micron particles composed of albumin and dye were harvested on Povidone. Figure 4-6 illustrates optical and fluorescent images of five micron particles before, during, and after

addition of water to monitor dissolution. The last two images clearly show dissolved particles as the dye is evenly distributed across the sample and no structures or features of partially dissolved protein particles are observed.

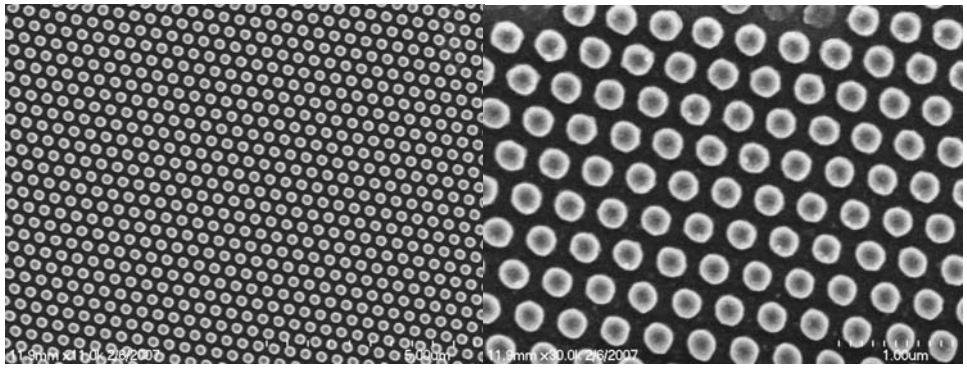

Figure 4-1. SEM micrographs of albumin nanoparticles harvested on medical grade adhesive.

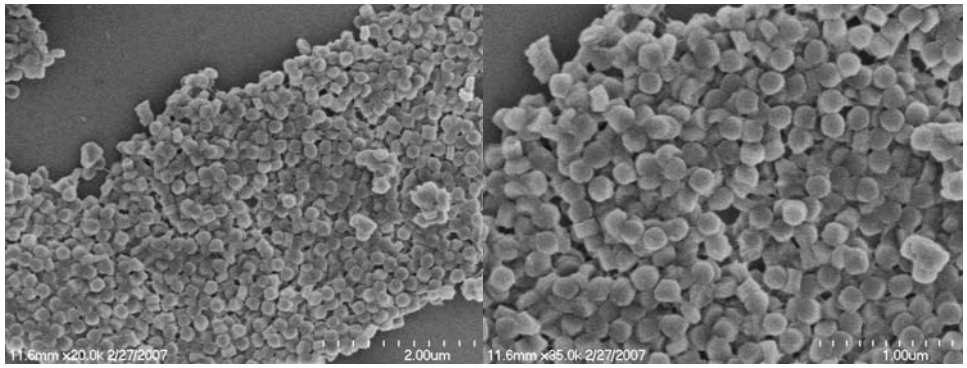

Figure 4-2. SEM micrograph of albumin nanoparticles harvested directly using chloroform.

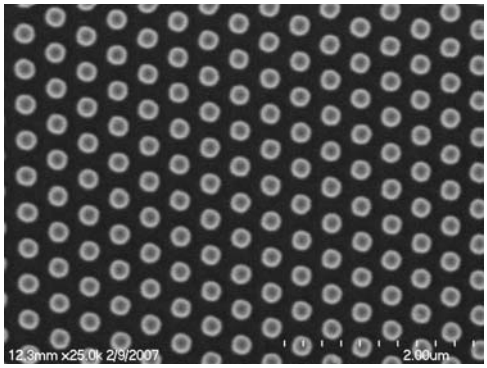

Figure 4-3. SEM micrograph of albumin nanoparticles with siRNA harvested on adhesive.

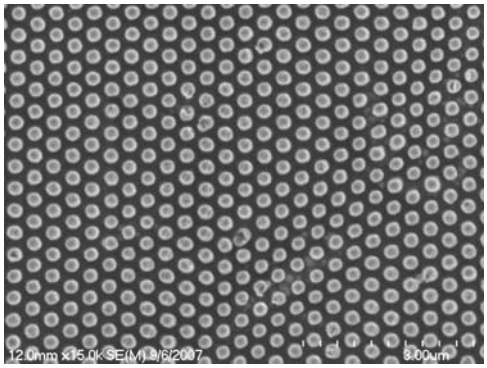

Figure 4-4. SEM micrographs of 200 nm (diameter) x 200 nm cylinders composed of nanomolded albumin loaded with ethylene glycol coated gadolinium oxide.

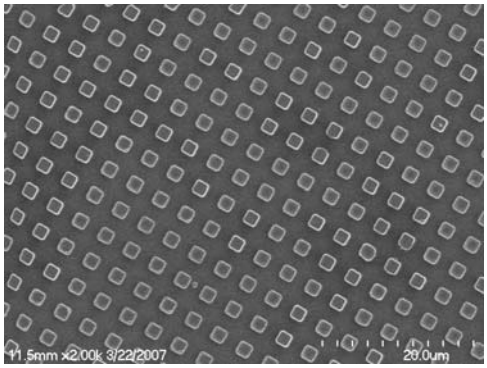

Figure 4-5. SEM micrograph of 2 x 2 x 2 micron^3 sized albumin particles harvested on medical grade adhesive.

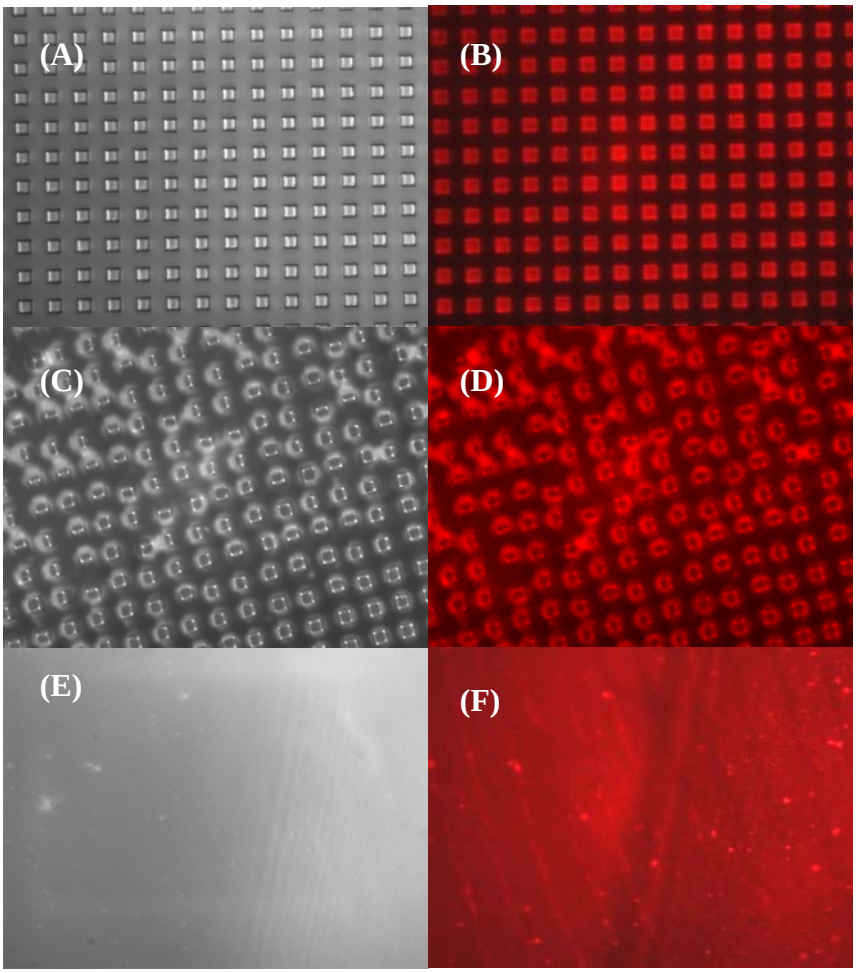

Figure 4-6. DIC and fluorescent images of 5 x 5 x 5 micron^3 particles harvested on Povidone and composed of albumin and rhodamineB before (A,B), during (C,D), and after (E,F) dissolution of particles.

In order to determine the effects that the PRINT process had on the proteins, several biophysical methods were exploited to gain a better understanding of possible structural affects had on the proteins during the course of the fabrication, harvesting and storage processes. The methods used were ATR-FTIR, differential scanning calorimetry, fluorescence microscopy, and circular dichroism, all of which are used to determine the details regarding the secondary structure of proteins.

4.4.4.1.3 BCA Protein Assay. In order to determine protein concentration of free and harvested PRINT particles in solution, BCA protein assays were conducted. The protein assay combines the well-known reduction of Cu^{2+} to Cu^{1+} by protein in an alkaline medium with the highly sensitive and selective colorimetric detection of the cuprous cation (Cu^{1+}) by bicinchoninic acid. The first step is the chelation of copper with protein in an alkaline environment to form a blue colored complex. In this reaction, known as the biuret reaction, peptides containing three or more amino acid residues form a colored chelate complex with cupric ions in an alkaline environment containing sodium potassium tartrate. This became known as the biuret reaction because a similar complex forms with the organic compound biuret (NH_2-CO-NH-CO-NH_2) and the cupric ion. Biuret, a product of excess urea and heat, reacts with copper to form a light blue tetradentate complex.

Standard protocol was followed. Bovine serum albumin was used as standards and all samples were used in triplicate. Optical density was measured at 562 nm in order to quantify concentration of the Cu complex relative to concentration. At least five different concentrations of bovine albumin standards were used to create a standard

calibration curve. The calibration curve was used to obtain concentration values of unknown samples. Fresh standards were utilized for every assay.

4.4.4.1.4 Fluorescence Microscopy Assay. Fluorescence intensity was measured for free albumin and PRINT albumin at various concentrations in PBS. The concentration values of a series of serial dilutions for both free and PRINT albumin were obtained from a BCA assay. All samples were added to wells in a 96-well black plate in triplicate. Fluorescence intensity was measure at excitation wavelength of 280 nm and an emission wavelength of 348 nm. Intensity values for both free and PRINT albumin were each plotted with respect to concentration (see Figure 4-7). Free and PRINT proteins at the same concentration showed similar fluorescence intensity suggesting the microenvironment of the respective tryptophan residues are not significantly different.

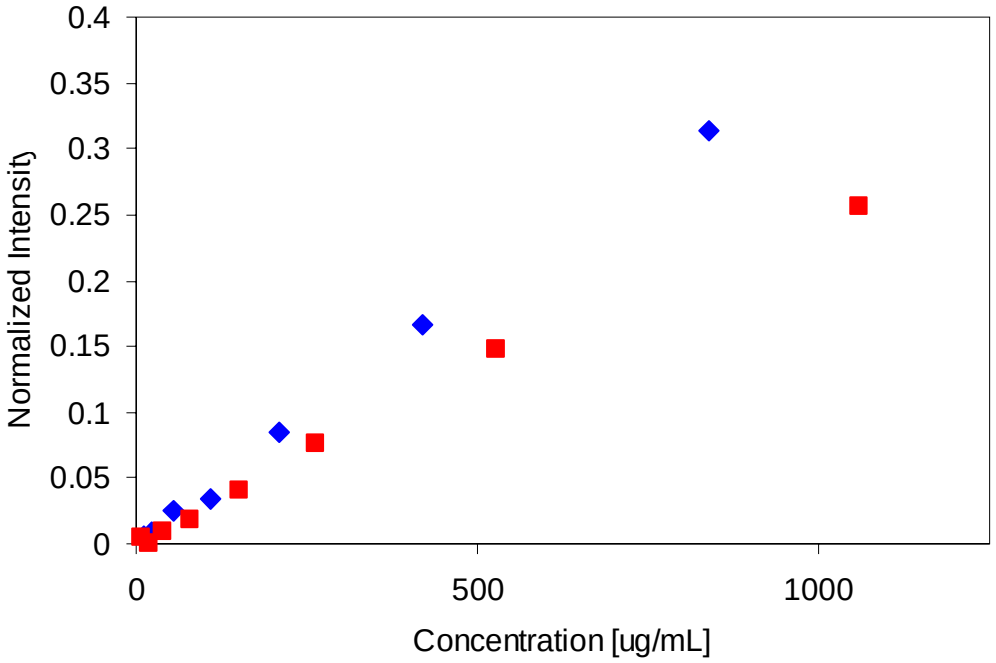

Figure 4-7. Relative fluorescence intensity of the tryptophan residue of free albumin compared to PRINT albumin in PBS. Fluorescence intensity of PRINT albumin is represented as red squares (■) and the free insulin as blue diamonds **(♦).**

4.4.4.1.5 ATR-FTIR. The chemical composition and qualitative secondary structure analysis of lyophilized, free protein and the respective protein PRINT particles were analyzed using FTIR. Protein PRINT particles of 5x5x5 μm square features were harvested directly using slight mechanical force and a glass slide and water. The harvested particle solution was frozen and subsequently lyophilized. Lyophilized proteins were analyzed by placing a small quantity of protein on a glass slide and placing the ATR tip into the protein. Figure 4-8 illustrates the absorbance of the amide I region of the free protein compared to the protein PRINT particles. (The good overlap signifies similar or identical secondary structure. This qualitative measure is a good indication that the PRINT process does not irreversibly denature the protein and that the secondary structure remains intact.) More of a conclusion than stating data, maybe better in discussion or in tying in all three methods used here. The overlapping spectra is indicative of similar or identical secondary structure of lyophilized free albumin and lyophilized albumin post PRINT process and thus the gentleness of PRINT leaving the protein unaltered and unaffected.

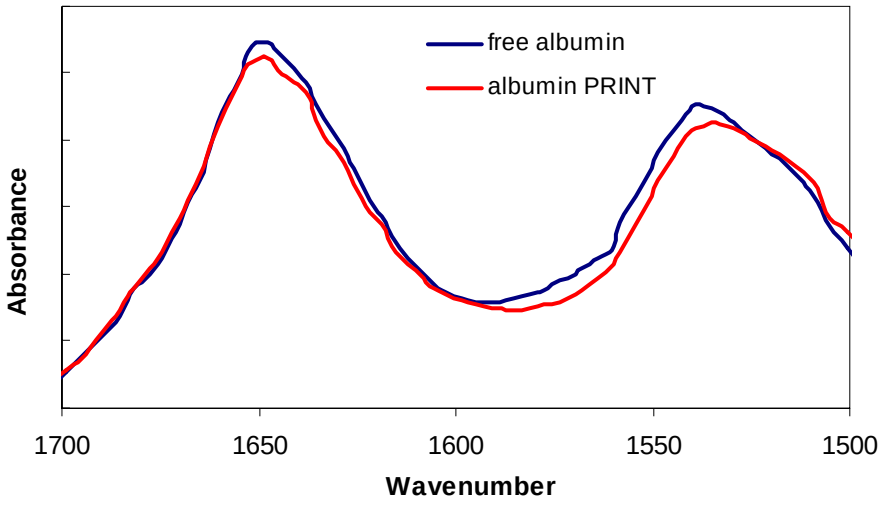

Figure 4-8. Absorbance of free and PRINT albumin in the amide I region using FTIR. Lyophilized protein samples were analyzed from 1700 to 1500 wavenumbers. Free albumin analysis is represented by a solid blue curve (—) and PRINT albumin analysis is represented by a solid red curve (—).

4.4.4.1.6 CD. Circular dichroism was measured in order to investigate the secondary structure of free albumin and PRINT albumin. Figure 4-9 clearly illustrates that free albumin and PRINT albumin have very similar secondary structure, as noted by the close overlap of the curves. As indicated in Figure 4-9 and in literature[55] albumin's structure consists of mostly α–helical structure.

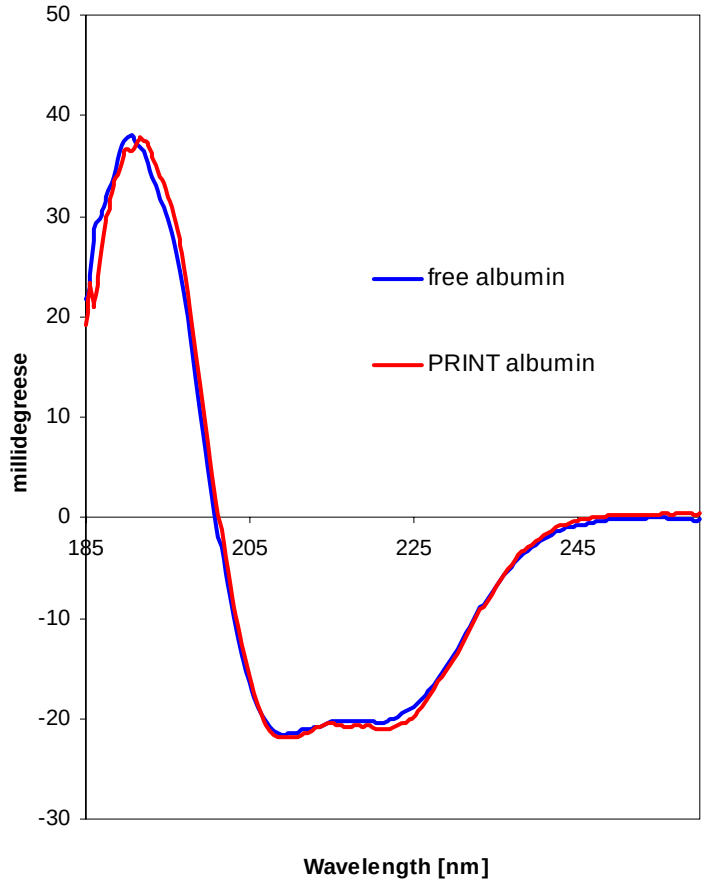

Figure 4-9. CD spectra of free and PRINT albumin. Protein was prepared in water solutions to approximately 0.1 ug/ml (or an OD of approx 1). Measurements were taken over a range of wavelengths (185- 260 nm) at a frequency of every 0.5 nm. Temperature was maintained at 25.0 ˚C throughout the experiment. Free albumin analysis is represented by a solid blue curve (—) and PRINT albumin analysis is represented by a solid red curve (—).

4.4.4.1.7 ELISA. In order to determine biological functionality of protein PRINT particles, standard sandwich ELISA analysis was conducted on free albumin and nanomolded albumin PRINT particles. Albumin PRINT particles used for ELISA were nano-molded into 200 x 200 nm cylinders cavities. Protein solutions were in the suggested working range (5-500 ng/mL) in sample/conjugate diluent. Negative controls included blank well (diluent only) and denatured free protein and denatured protein PRINT particles. Denatured samples for both free and PRINT albumin turned milky white and partially polymerized. Results, illustrated in Figure 4-10, reflect functionality retained for both free albumin as well as for nanomolded albumin PRINT particles. Results further indicate that the sequence/structure recognition of free albumin and albumin PRINT particles were indistinguishable.

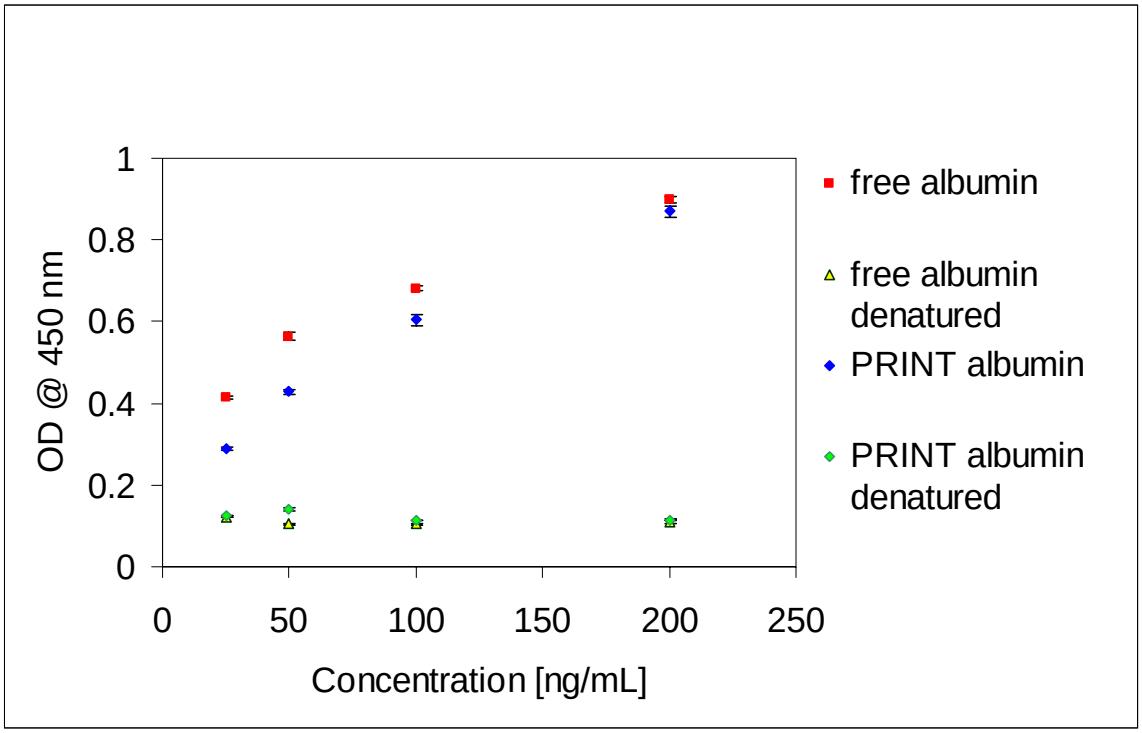

Figure 4-10. ELISA analysis of biological integrity of protein following preparation of PRINT particles. Free and PRINT particles in PBS were diluted to various concentrations in the optimal detection range for human serum albumin. Proteins were heat treated to denature protein as a negative control. Free proteins are denoted as blue diamonds (♦), and denatured as yellow triangles (▲). PRINT proteins are denoted as red squares (■) and denatured protein as green circles (●).

4.4.5 Insulin, Transferrin, Hemoglobin.

4.4.5.1 PRINT Particle Fabrication. Transferrin and hemoglobin were nanomolded similar to albumin as discussed in section 4.2.3 using a 25 weight percent solution of protein in water. Insulin is highly crystalline as illustrated in Figure 4-11 and thus has poor solubility in water relative to the other proteins investigated in this Chapter. Less than one weight percent of insulin was soluble in water. Various buffer systems and acedic acid solutions were attempted in efforts to obtain a more concentrated solution of insulin to nanomold. One buffer system in particular, HEPES, allowed for a ten weight percent solution to be obtained. Nanomolding insulin from a HEPES solution proved to introduce challenges caused by the buffer. Crystallization of the salt and possible interaction with insulin resulted in non-uniform particle fabrication as observed by SEM (not shown). It was established that nanomolding a simple solution containing protein and water only would circumvent introducing additional challenges into these systems. A four weight percent solution of insulin in water was made. Complete dissolution of insulin into water was not achieved. However with vortexing just prior to nanomolding, a uniformly distributed heterogeneous solution was obtained.

The four weight percent solution was nanomolded three times in a row using the same PFPE mold for complete filled. A forth pass through the roller was conducted using a new PET counter sheet as a polishing step. Due to insulin's crystallinity and poor solubility in water at high concentrations, crystallites of insulin were visually observed to crash out of solution near the nip before nanomolding, leaving some insulin on top of the mold instead of solely residing in the mold cavities. The polishing step removed any such insulin from the mold surface.

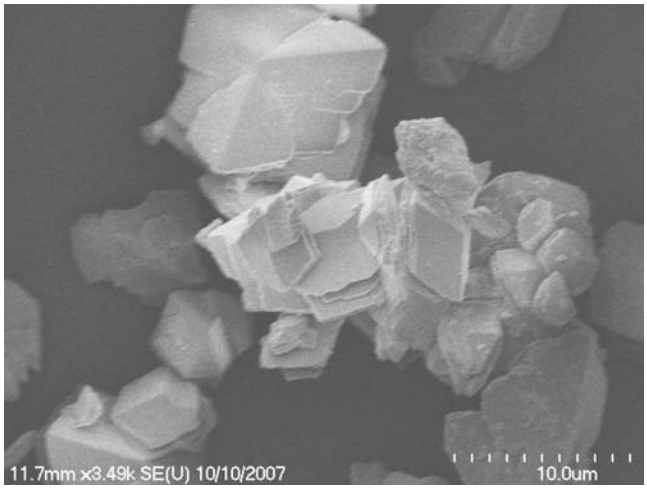

Figure 4-11. SEM micrograph of lyophilized insulin as received.

4.4.5.2 SEM, Optical Microscopy, and Confocal Microscopy. Nanomolded insulin, transferring and hemoglobin PRINT particles were analyzed using SEM and in some cases optical or confocal microscopy. Figures 4-12 and 4-13 illustrate insulin PRINT particles of different size and shape. Figure 4-13 especially highlights the versatility of the PRINT technology in fabricating precise micron sized particles of various shapes, potentially useful for pulmonary delivery of insulin. Optical microscopy was also used to analyze and monitor discrete particle fabrication by harvesting particles onto medical grade adhesive and subsequently dissolving the harvesting film to observe free flowing particles. Figure 4-14 illustrates 2x2x1 micron cubes of nanomolded insulin before and after dissolution of the adhesive harvest film.

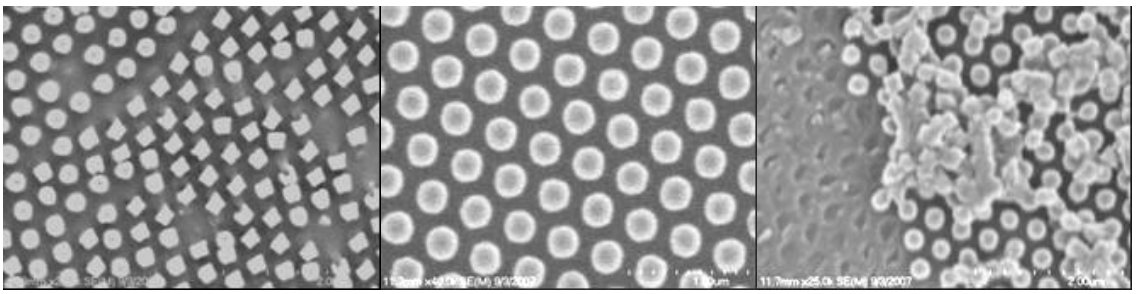

Figure 4-12. SEM micrographs of 200 nm (diameter) x 200 nm cylinders of nanomolded insulin particles harvested onto medical grade adhesive.

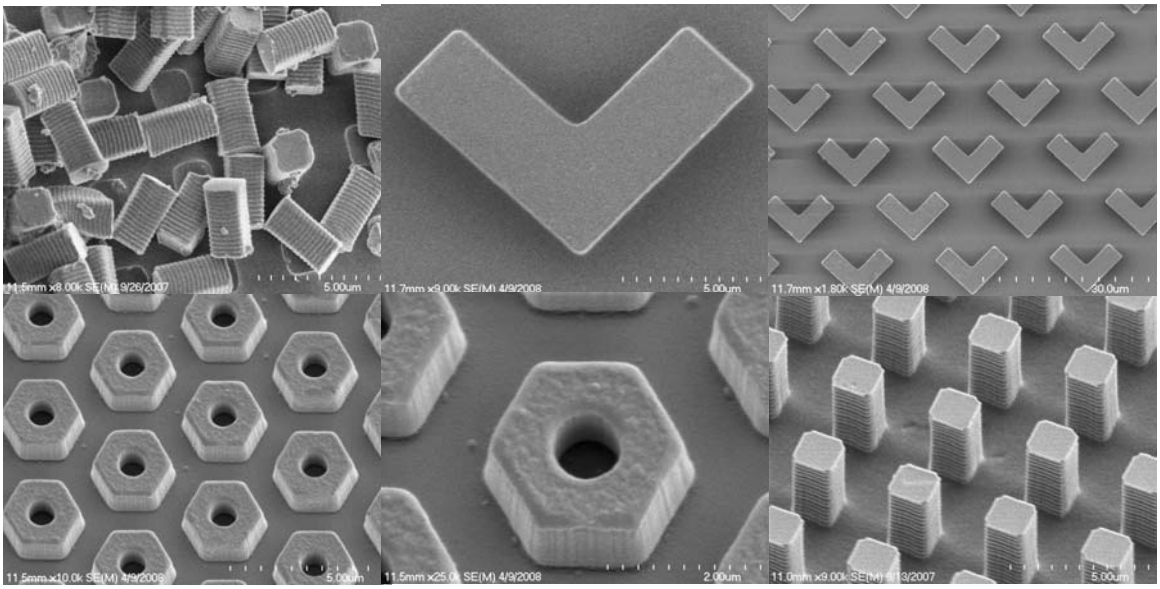

Figure 4-13. SEM micrographs of different shape and size PRINT particles composed of insulin; (A), (F) 2x2x4 µm Posts; (B), (C) 10 µm (length), 3 µm (width), 1 µm (height) boomerangs; (D), (E) 3 µm (side to side), 1 µm (diameter hole), 1 µm (height) hex nuts.

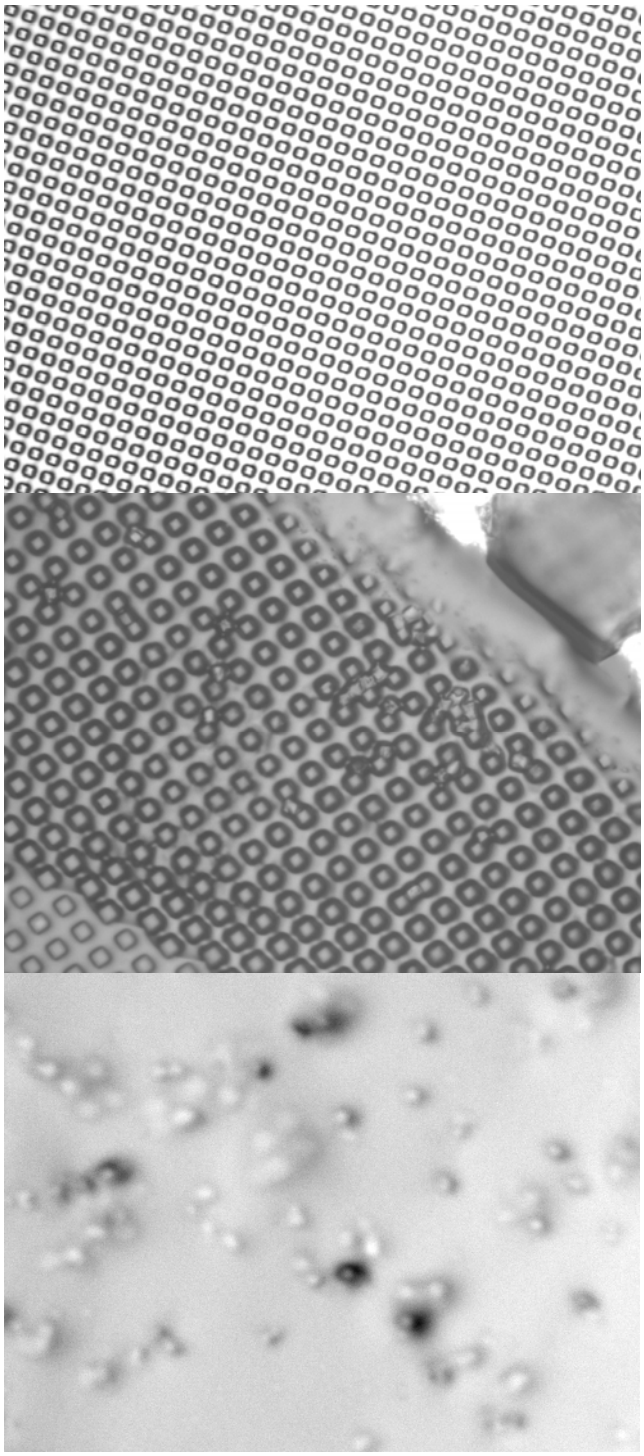

Figure 4-14. Optical microscopy images of 2 x 2 x 2 micron^3 cubes of insulin particles before and after dissolution of harvest film.

A SEM micrograph illustrating 200 nm (diameter) x 200 nm cylinders of nanomolded hemoglobin is shown in Figure 4-15. Hemoglobin has a unique property unlike any of the other proteins investigated herein in its auto-fluorescence. Micron sized particles of hemoglobin can therefore be analyzed using fluorescent microscopy. One facile method to investigate denaturation of a protein is monitoring its dissolution in water. One characteristic of a denatured protein is that it aggregates or polymerizes, resulting in an insoluble fraction or entire sample. The dissolution of hemoglobin PRINT particles was monitored at first using fluorescence microscopy, but later found that confocal microscopy resulted in better quality images, illustrated in Figure 4-16. Two micron cubes composed of hemoglobin were harvested onto Povidone. The upper right corner of the image shows where the particles were dissolved and illustrated even distribution of fluorescence over the section of the sample. The observed cracks in the upper portion of the sample were obtained after drying. The lower section of the image did not come into contact with water and thus reflects intact particles.

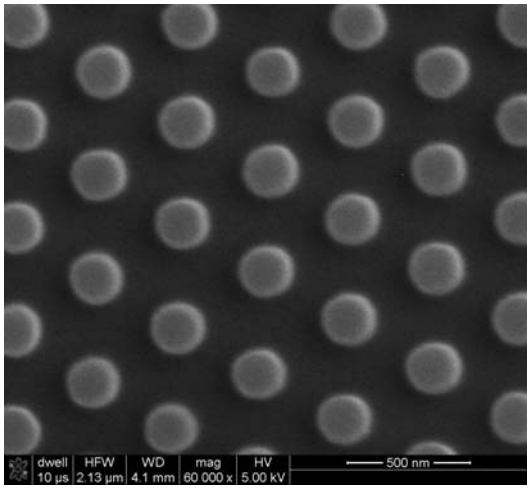

Figure 4-15. SEM micrograph of 200 nm (diameter) x 200 nm cylinders of nanomolded hemoglobin.

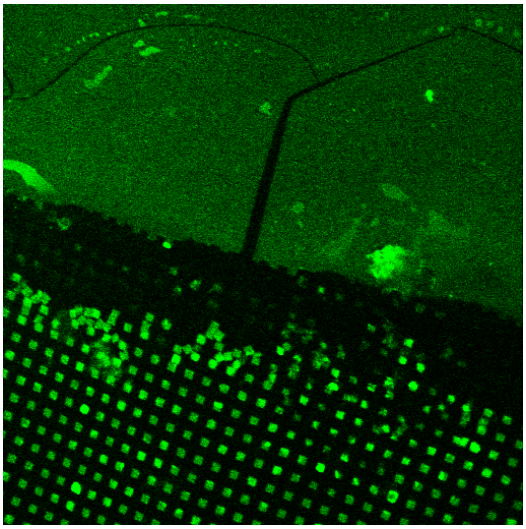

Figure 4-16. Confocal image of 2 x 2 x 2 μm^3 cubes of hemoglobin particles harvested on Povidone and top portion partially dissolved.

Nanomolded transferring was also investigated using SEM. Particles of 200 nm cylinders harvested directly using slight mechanical force and chloroform are illustrated in Figure 4-17. Similar particles were also harvested onto medical grade adhesive and are illustrated in Figure 4-18. Figure 4-18 also contains and SEM micrograph of five micron cubes composed of transferring harvested on medical grade adhesive.

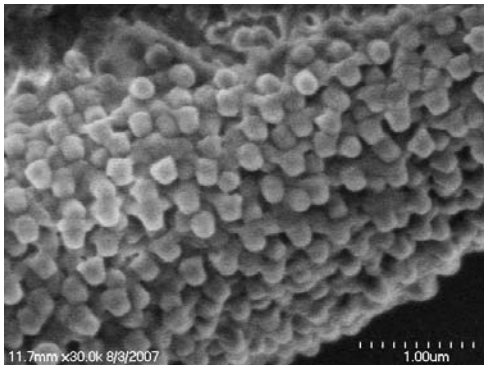

Figure 4-17. SEM micrograph of nanomolded transferrin particles of 200 nm (diameter) x 200 nm cylinders harvested directly using chloroform and slight mechanical force.

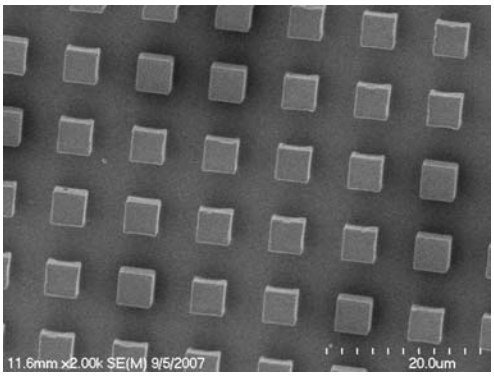

Figure 4-18. Nanomolded 5 x 5 x 5 micron^3 cubes composed of transferrin harvested on medical grade adhesive.

4.4.5.3 ELISA. Biological utility was analyzed for transferring, insulin, and hemoglobin using standard sandwich ELISA, similar to albumin. Free protein, protein PRINT, free denatured protein, and protein PRINT denatured samples were analyzed. In most cases denatured samples partially polymerized. Denatured insulin samples completely gelled and no solution sample was able to be added to wells. Results indicate that the sequence/structure recognition of free protein and protein PRINT particles were indistinguishable for insulin (Fig.4-19) and transferrin (Figure 4-21). Hemoglobin PRINT particles (Figure 4-20) showed less antibody binding at the same concentration compared to free hemoglobin, but still illustrated some binding.

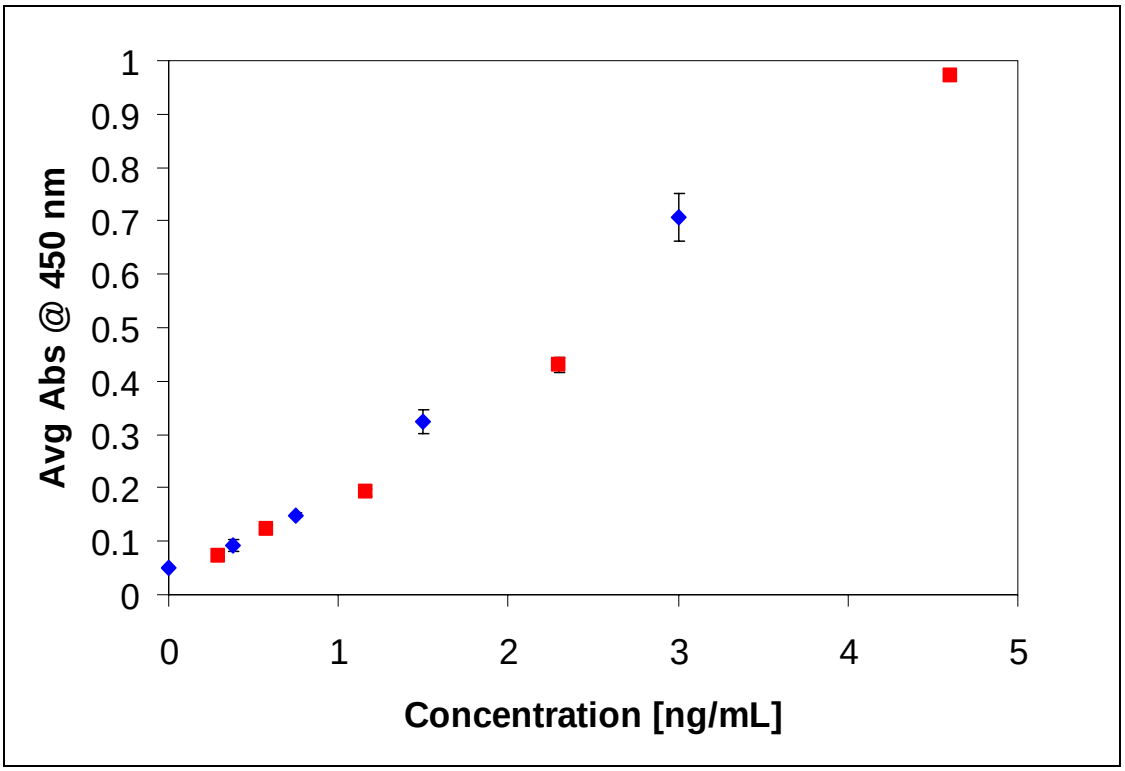

Figure 4-19. ELISA of free and PRINT insulin to investigate biological integrity of the protein. Free and PRINT insulin in PBS were diluted to several concentrations for the optimal detection. Absorbance values were found to increase as concentration of protein increased. Absorbance of PRINT insulin is represented as red squares (■) and the free insulin as blue diamonds **(♦).**

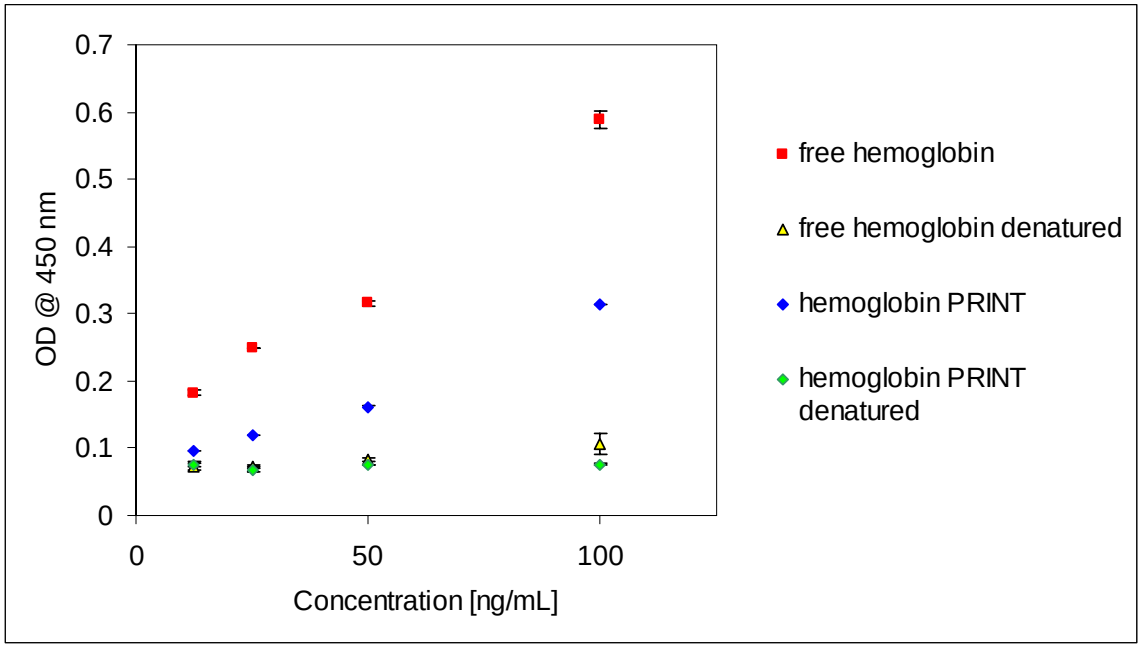

Figure 4-20. ELISA analysis of biological integrity of protein following preparation of PRINT particles. Free and PRINT particles in PBS were diluted to various concentrations in the optimal detection range for hemoglobin. Proteins were heat treated to denature protein as a negative control. Free proteins are denoted as blue diamonds (♦), and denatured as yellow triangles (▲). PRINT proteins are denoted as red squares (■) and denatured protein as green circles (●).

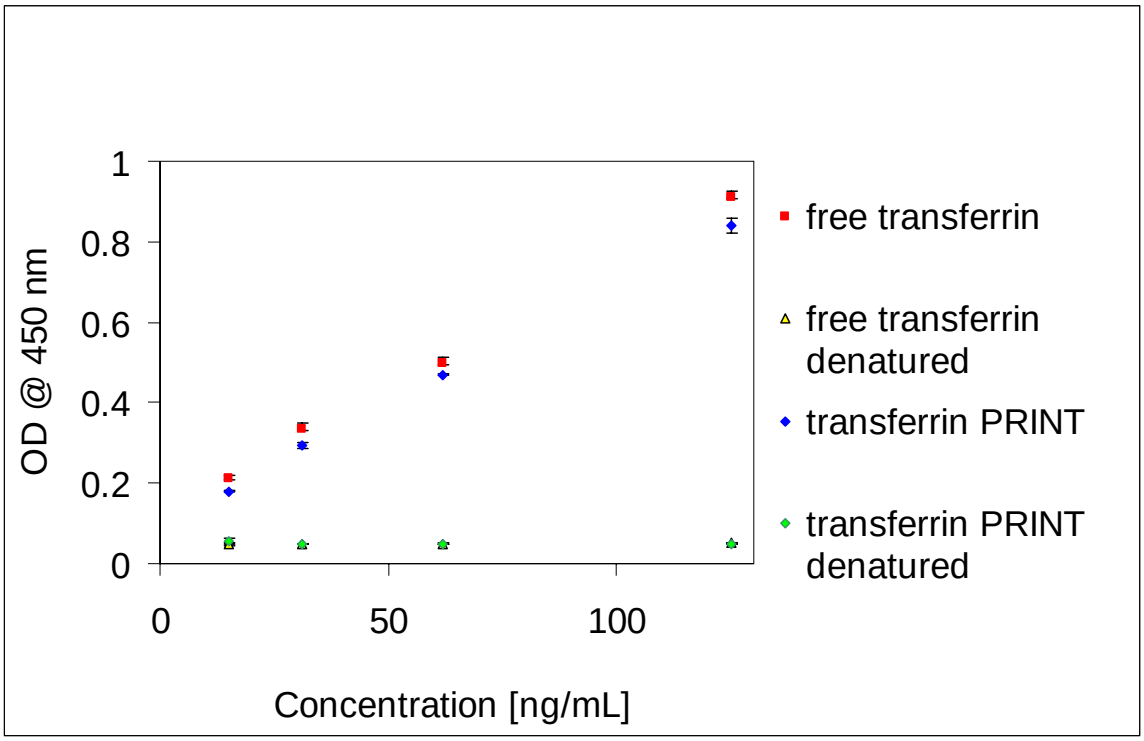

Figure 4-21. ELISA analysis of biological integrity of protein following preparation of PRINT particles. Free and PRINT particles in PBS were diluted to various concentrations in the optimal detection range for transferrin. Proteins were heat treated to denature protein as a negative control. Free proteins are denoted as blue diamonds (♦), and denatured as yellow triangles (▲). PRINT proteins are denoted as red squares (■) and denatured protein as green circles (●).

4.4.6 Interferon-beta.

4.4.6.1 PRINT Particle Fabrication. Similar to other proteins investigated herein, particles of interferon-beta were fabricated as described above. Due to high cost of material, a ten weight percent solution in water was used instead of 25 weight percent as with albumin, transferring, and hemoglobin to nanomold and fabricate protein PRINT particles using interferon-beta. In order to ensure complete filling of the cavities in the PFPE mold, the ten weight percent interferon-beta solution was nanomolded three times using the same mold.

The purchased interferon-beta product was received as a lyophilized powder, lyophilized from interferon-beta in buffer. Naturally, the lyophilized product contained buffer salts in the presence of interferon-beta. Since the nanomolding of interferon-beta was from a buffered mixture it was proven to be challenging to obtain enough PRINT particles for extensive physical characterization without making a vast amount of particles. When harvesting comparable amounts of particles that with other proteins (i.e, albumin) resulted in sufficient product for multiple characterizations, including ELISA and SEM, BCA analysis of nanomolded interferon-beta particles illustrated lower concentrations than the lower limit working range of five micrograms. Due to the high cost of the commercial product, characterizations were limited to SEM.

4.4.6.2 SEM. Figure 4-22 illustrates 200 nm (diameter) x 200 nm cylinders of nanomolded interferon-beta PRINT particles, harvested onto medical grade adhesive. A cell scraper was gently dragged across a section of the sample in attempts to lift particles from the harvest film and to illustrate discrete, monodisperse, shape- and size specific protein particles.

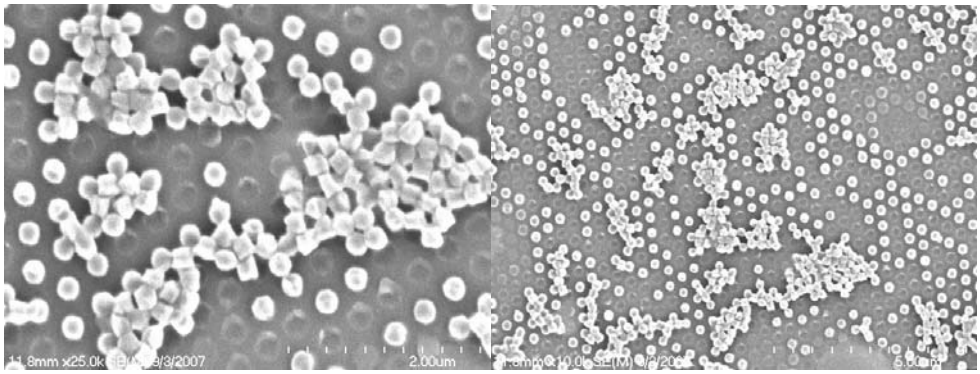

Figure 4-22. SEM micrograph of nanomolded interferon-beta particles harvested onto medical grade adhesive.

4.4.7 Horseradish Peroxide and Trypsin.

4.4.7.1 PRINT Particles Fabrication. Horseradish peroxidase and trypsin were used to fabricate nanomolded protein PRINT particles, similar to albumin. A 25 weight percent solution of the proteins in water was used for nanomolding as discussed previously. Horseradish peroxidase and trypsin are both enzymes and the utility and breadth of the PRINT process was challenged once again by investigating these biomaterials. The biophysical analysis of albumin and the functionality using ELISA for a number of protein PRINT samples illustrate that the PRINT process clearly does not significantly alter secondary structure and sequence allowing for antibody recognition and binding. By nanomolding two different enzymes, the activity is tested before and after the PRINT process.

4.4.7.2 SEM. SEM was used to analyze the fabrication enzyme PRINT particles, similar to the other proteins investigated in this chapter. Figure 4-23 illustrates SEM micrographs of different size and shape horseradish peroxidase particles harvested on medical grade adhesive. Nanomolded trypsin particles are illustrated in Figure 2-24.

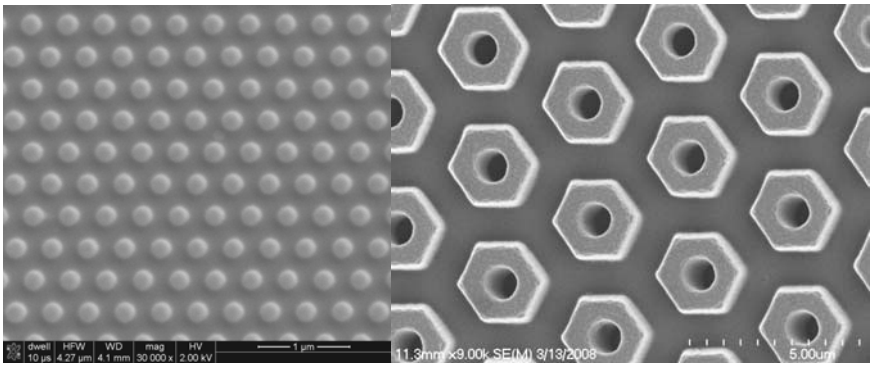

Figure 4-23. SEM micrographs of nanomolded 200 nm (diameter) x 200 nm cylinders and three micron hex nuts composed of horseradish peroxidase particles harvested onto medical grade adhesive.

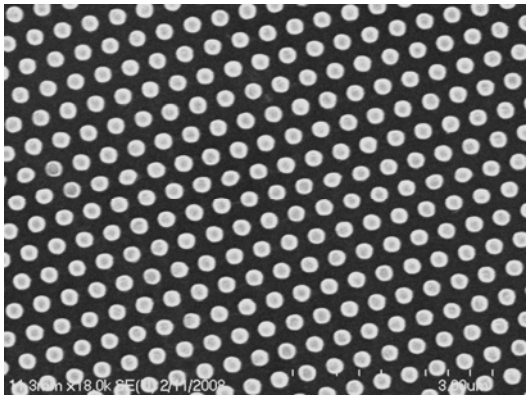

Figure 4-24. SEM micrograph of nanomolded 200 nm (diameter) 200 nm cylinders composed of trypsin harvested on medical grade adhesive.

4.4.7.3 Enzymatic Activity Assay. To better assess true biological functionality, two enzymes (i.e., trypsin and HRP) were fabricated into particles and then subjected to standard assays to determine their activity. Enzyme solutions were prepared at various concentrations in order to find a working range such that that enzymatic activity could be followed for five minutes at an optimal OD value. In the case of trypsin, free protein solutions were prepared immediately before analysis. HRP and trypsin PRINT particles were harvested directly into PBS prior to analysis. Results indicate that free enzyme and enzyme PRINT particles have similar activity for HRP (Fig. 4-25) and trypsin (Figure 4-26), respectfully. This illustrates enzymatic activity is maintained during the PRINT process, supporting the ELISA results for the other proteins.

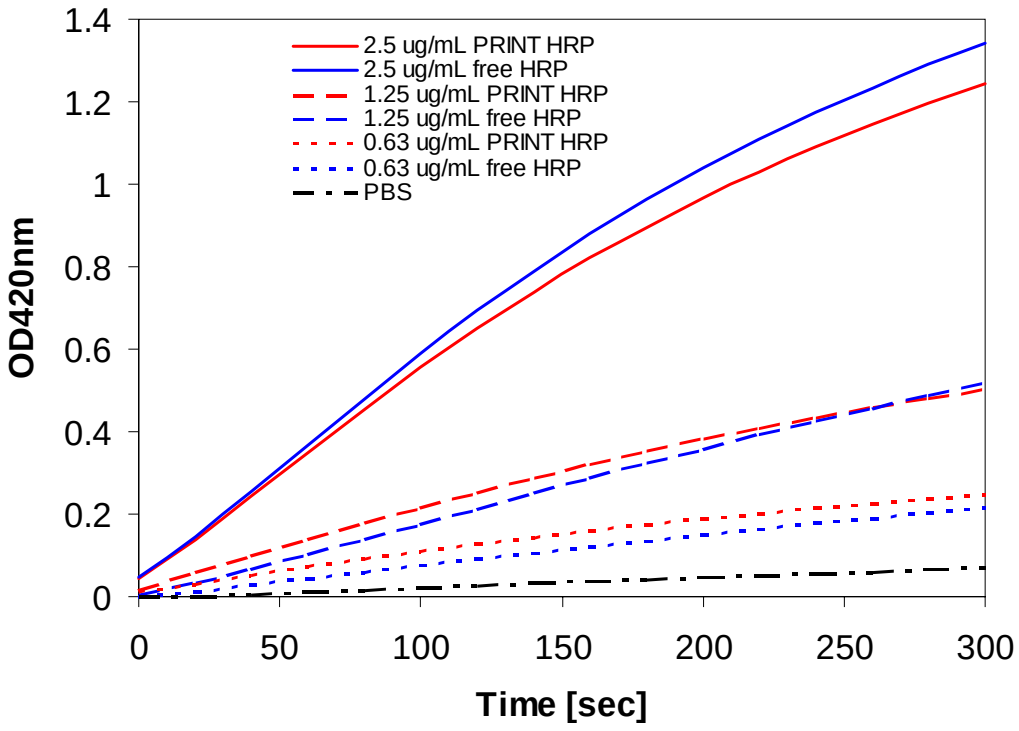

Figure 4-25. Enzymatic activity assay of free and PRINT horseradish peroxidase. Several concentrations of HRP were reacted with pyrogallol in the presence of hydrogen peroxide. The solution of free and PRINT HRP were prepared from lyophilized powder and resuspended in PBS. All reactions were measured at room temperature over the course of 5 min, measuring at 20 sec intervals at a wavelength of 450 nm. Concentrations are noted as follows: 2.5 ug/mL samples are represented with a solid line (——); 1.25 ug/mL samples are represented with a dashed line (-- -- --); 0.63 ug/mL samples are represented with a dotted line (- - -); PBS is represented as a dash and dotted line in black (-- - --). PRINT HRP samples are illustrated in red. Free HRP are illustrated in blue.

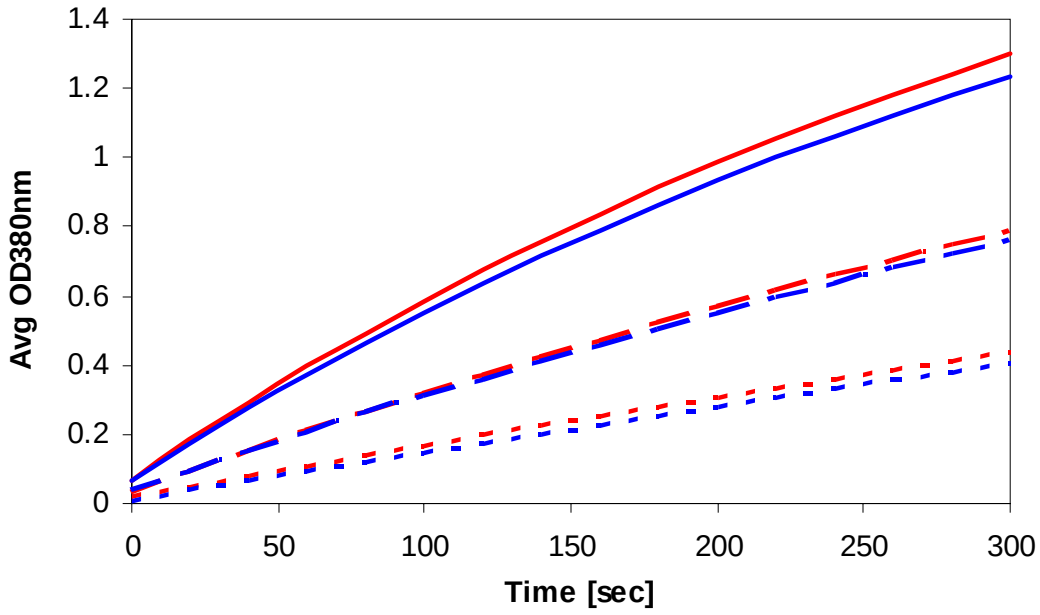

Figure 4-26. Enzymatic activity assay on trypsin, free and PRINT, at different concentrations. Several concentrations of trypsin were reacted with N-benzoyl- L-arginine-nitroanalide. The solution of free and PRINT trypsin were prepared from lyophilized powder and resuspended in PBS. All reactions were measured at room temperature over the course of 5 min, measuring at 20 sec intervals at a wavelength of 380 nm. Concentrations are noted as follows: 1 mg/mL samples are represented with a solid line (——); 0.5 mg/mL samples are represented with a dotted line (-- -- --); 0.25 mg/mL samples are represented with a dashed line (- - -). PRINT trypsin samples are illustrated in red. Free trypsin are illustrated in blue.

4.4.8 Discussion. Biomaterials have proven to be effective therapeutics and are at the forefront of diagnostics for a variety of diseases and illnesses. Many challenges in developing therapeutics lie in their fabrication process. The current fabrication process of micro- and nanoparticle-sized biomaterial is hampered by complicated manufacturing steps and requires expensive high pressure equipment. Yet in the end, product yield is low in part due to the production of particles highly disperse in size and due to the loss of biofunctionality or monomer. In current literature, the shape of biological therapeutics is currently limited to spherical particles with little control over their precise size. Therefore, the development of a particle fabrication process that can indefinitely expand and independently control variables that influence the characteristics of the nanoparticles, could have a profound impact on the development of therapeutics. With such a fabrication process and judicious control over monodisperse size, shape, cargo encapsulation, composition, and surface functionalization for directed vector delivery and stealthing capabilities, new opportunities would launch in personalized health care. By fabricating protein particles without perturbing structure, conformation, and functionality, such a drug delivery system is realized.

To establish finely tuned shape and size specific protein particles of different compositions with the ability to independently vary individual parameters without altering the outcome, the PRINT process is utilized for particle fabrication using a nano-molding technique with concentrated aqueous solutions of the respective proteins. The PRINT technology enables one to alter size, shape and protein formulation in an independent, straightforward manner without affecting the other parameters of the particle makeup, as described previously.[56] Using this specific method, the need for

introducing crosslinking, co-monomers, or stabilizing agents is circumvented, thus avoiding potentially arising toxicity issues.

The versatility of the PRINT platform enables the fabrication of particles composed of any chemical structure or composition ranging from organic, synthetic polymer delivery vehicles[5, 6, 57, 58] to naturally occurring biologics, such as proteins and hormones as previously introduced,[56] but also can include enzymes and antibodies. The PRINT process creates a flexible framework for exploring the effects that size and shape of biomaterials have on delivery mechanisms and methods as well as on actual disease processes progression. Nanoscale particles for the intravenous delivery of anticancer therapeutics can be fabricated with the same ease as micron sized insulin particles for pulmonary delivery. Through the versatility of the PRINT technology personalized medicine can be realized and further customized to each patient and each therapy application.

The importance of the biomaterials and their functionality is well established and influences the development of novel biological and biomedical technologies. All of the investigated proteins herein have biological significance, thus, careful analysis and characterization of these sensitive molecules was warranted. Further demonstration of the ability to fabricate functional protein particles by the PRINT method is realized herein. SEM micrographs of harvested protein PRINT particles confirm the uniformity of the size and shape of these particles, whether individual, discrete, and loose, or in an array. These images verify the ability of the PRINT process to replicate nano- and micron-sized features of a patterned wafer with the utmost fidelity to fabricate protein particles. Qualitative secondary structure analysis of albumin before and after the PRINT process

was conducted using fluorescence microscopy and FT-IR. Significant overlap of absorbance in the amide I regions provides positive structure information. The fluorescence of the tryptophan residue of PRINT albumin is less intense at higher concentrations relative to free albumin, but the results do not vary significantly, indicating that the microenvironment around the tryptophan residue is similar. The most compelling data is illustrated in Figure 4-10, using CD. Tremendous overlap between free albumin and PRINT albumin substantiates similar secondary structure of the protein. The analysis confirms predominant α-helix structure for both free and PRINT albumin. As expected, denaturing of both free and PRINT albumin causes structure lost, as illustrated in Figure 4-10.

ELISA analysis provides implications as to the biological integrity of the proteins as it relies upon protein-protein interactions to yield results. Complimentary to the biophysical analysis, this data indicates that the structure of the proteins is not greatly disturbed by the fabrication of particles. The ELISA investigation illustrates that antibody recognition and binding are minimally affected in the PRINT process, especially for albumin, transferrin, insulin (Figures 4-11, 4-22, and 4-20). Hemoglobin, found as a complex tetramer structure, shows less antibody binding after the PRINT process relative to its reconstituted, lyophilized free counterpart. This may largely be attributed to the complexity of the protein structure and the opportunity to disrupt the tertiary and quaternary structure of the protein.

Moreover, the most compelling results are demonstrated by the enzymatic activity assays for free trypsin and HRP and their respective PRINT particles. The kinetic profiles clearly illustrate that the enzymatic activity of both trypsin and horseradish peroxidase is

retained after the PRINT process. These findings lay the foundation for fundamental protein research and new applications in biomedical therapeutics and delivery systems.

In this study, the PRINT process was utilized for the facile fabrication of mono-disperse protein particles. The PFPE molds act as nano- and micron sized lyophilization chambers. The biological materials analyzed retain their structure and in most cases complete biological functionality. These protein PRINT particles offer new opportunities in enhanced therapeutics and drug delivery vectors. These particles are able to be stored for long periods of time while in the mold and are readily harvested in a variety of ways. Particles can be stored in arrays on medical adhesive or excipient films over large areas. Though the fabrication process may need to be optimized for ultra sensitive biomolecules with complex secondary structures, this study clearly illustrates the amenability of the PRINT process to proteins.

4.5 Future Work and Outlook. Complete bio-physical characterizations of the proteins investigated herein (aside from albumin) would be the next steps in this research effort. Specifically, circular dichroism and FT-IR analysis would provide (quantitative and qualitative) secondary structure characterization, respectfully. This data would be of interest for transferring, insulin, horseradish peroxidase, trypsin, but especially for hemoglobin with its complicated tertiary structures. To preserve structure, fabrication methodology might be varied for proteins like hemoglobin, which illustrated less effective antibody binding compared to the free protein. Furthermore, concentration variation may influence and reduce potential structural changes for such complex proteins.

Long term stability studies could be employed by varying the duration of time that the protein PRINT particles are kept in the mold or harvested in an array from weeks to months prior to characterization. Additionally, the process of how filled molds are frozen could be monitored in order to investigate the effects of speed and temperature of freezing on the bio-physical properties of the protein. Modifications to the protein particles such as light surface stitching or crosslinking of nanomolded protein particles could be conducted with degradable crosslinkers through free thiol moieties of the protein. By these means, protein particles would stay intact in circulation for delivery vehicles.

With respect to therapeutics, nanomolded protein PRINT particles may find applications in a variety of areas. For example, pulmonary delivery of insulin might be conducted by characterizing micron sized particles of different shape composed of insulin using an Andersen Cascade Impactor. The effect of shape can be studied in a straightforward, systematic manner by fabricating micromolded insulin particle of 10 μm boomerangs, 3 μm hex nuts, 5 μm cubes, and 2 μm (width) x 4 μm square posts with an aspect ratio of 2. In a similarly facile way, ideal size from pulmonary drug delivery can be conducted by fabricating micron sized cubes and cylinders of varying aspect ratio with dimensions ranging from one to five microns.

In vitro and *in vivo* studies with therapeutic proteins for example interferon-beta, insulin, enzymes, and even transferrin could be conducted. *In vitro* studies with nanomolded insulin particles could include markers to investigate triggering of (radiolabeled) glucose uptake. Cancer cell lines exposed to nanomolded interferon-beta particles could be monitored for tumor killing. Delivery of metals and imaging agents

using transferrin could be investigated to determine if protein carrier indeed can target and increase uptake. Cargo encapsulation of a therapeutic could be investigated using *in vitro* and *in vivo* studies. *In vitro* and *in vivo* studies could investigate size and shape relationships of protein particles with cell internalization and overall biodistribution. A comparison of synthetic polymer PRINT particles to nanomolded protein particle and their respective biodistribution would create a thorough platform for delivery vehicle compositions and a variety of their applications.

More fundamental studies could be conducted with nanomolded protein particles harvested in an array and investigate reactions with the protein, studying surface chemistry of bulk properties. These studies lend themselves especially well for exact development of kinetics and thermodynamics due in part to the finite mass and volume of harvested particles. Systematic variation of size and shape of nanomolded proteins will open new opportunities for fundamental research in biochemistry. Investigating nanomolded proteins in the mold or harvested in an array can allow for direct observation of the dynamics and structural changes of these biomaterials. This unique setting can help researchers study the molecular basis of disease and supply information for developing new pharmaceuticals.

These proposed studies barely scratch the surface of this new field when microelectronics meets biotechnology. This new, ever growing area of nano- and biotechnology is largely still unexplored and opens up tremendous opportunities.

1. Andya, J. D.; Maa, Y. F.; Costantino, H. R.; Nguyen, P. A.; Dasovich, N.; Sweeney, T. D.; Hsu, C. C.; Shire, S. J., The effect of formulation excipients on protein stability and aerosol performance of spray-dried powders of a recombinant humanized anti-IgE monoclonal antibody. *Pharmaceutical Research* **1999,** 16, (3), 350-358.

2. Carrasquillo, K. G.; Carro, J. C. A.; Alejandro, A.; Toro, D. D.; Griebenow, K., Reduction of structural perturbations in bovine serum albumin by non-aqueous microencapsulation. *Journal of Pharmacy and Pharmacology* **2001,** 53, (1), 115-120.

3. Costantino, H. R.; Griebenow, K.; Mishra, P.; Langer, R.; Klibanov, A., Fourier-Transform Infrared Spectroscopic Investigation of Protein Stability in the Lyophilized Form. *Biochimica Et Biophysica Acta-Protein Structure and Molecular Enzymology* **1995,** 1253, (1), 69-74.

4. Nguyen, X. C.; Herberger, J. D.; Burke, P. A., Protein powders for encapsulation: A comparison of spray-freeze drying and spray drying of darbepoetin alfa. *Pharmaceutical Research* **2004,** 21, (3), 507-514.

5. Gratton, S. E. A.; Pohlhaus, P. D.; Lee, J.; Guo, I.; Cho, M. J.; DeSimone, J. M., Nanofabricated particles for engineered drug therapies: A preliminary Biodistribution study of PRINT (TM) nanoparticles. *Journal of Controlled Release* **2007,** 121, (1-2), 10-18.

6. Rolland, J. P.; Maynor, B. W.; Euliss, L. E.; Exner, A. E.; Denison, G. M.; DeSimone, J. M., Direct fabrication and harvesting of monodisperse, shape-specific nanobiomaterials. *Journal of the American Chemical Society* **2005,** 127, (28), 10096-10100.

7. Gratton, S. E. A.; PohhauS, P. D.; Lee, J.; Guo, I.; Cho, M. J.; DeSimone, J. M., Nanofabricated particles for engineered drug therapies: A preliminary Biodistribution study of PRINT (TM) nanoparticles. *Journal of Controlled Release* **2007,** 121, (1-2), 10-18.

8. Bartus, R. T.; Tracy, M. A.; Emerich, D. F.; Zale, S. E., Sustained delivery of proteins for novel therapeutic products. *Science* **1998,** 281, (5380), 1161-1162.

9. McDonald, M. A.; Watkin, K. L., Small particulate gadolinium oxide and gadolinium oxide albumin microspheres as multimodal contrast and therapeutic agents. *Investigative Radiology* **2003,** 38, (6), 305-310.

10. Mcdonald, M. A.; Watkin, K. L., Acoustic properties of paramagnetic polymerized protein microspheres: A prototype multimodality contrast agent. *Radiology* **2002,** 225, 185-186.

11. Sexton, L. T.; Horne, L. P.; Martin, C. R., Developing synthetic conical nanopores for biosensing applications. *Molecular Biosystems* **2007,** 3, (10), 667-685.

12. Sexton, L. T.; Horne, L. P.; Sherrill, S. A.; Bishop, G. W.; Baker, L. A.; Martin, C. R., Resistive-pulse studies of proteins and protein/antibody complexes using a conical nanotube sensor. *Journal of the American Chemical Society* **2007,** 129, (43), 13144-13152.

13. Antonov, E. N.; Bagratashvili, V. N.; Whitaker, M. J.; Barry, J. J. A.; Shakesheff, K. M.; Konovalov, A. N.; Popov, V. K.; Howdle, S. M., Three-dimensional bioactive and biodegradable scaffolds fabricated by surface-selective laser sintering. *Advanced Materials* **2005,** 17, (3), 327-+.

14. Amsden, B. G.; Goosen, M. F. A., An examination of factors affecting the size, distribution and release characteristics of polymer microbeads made using electrostatics. *Journal of Controlled Release* **1997,** 43, (2-3), 183-196.

15. Chithrani, B. D.; Ghazani, A. A.; Chan, W. C. W., Determining the size and shape dependence of gold nanoparticle uptake into mammalian cells. *Nano Letters* **2006,** 6, (4), 662-668.

16. Cortez, C.; Tomaskovic-Crook, E.; Johnston, A. P. R.; Scott, A. M.; Nice, E. C.; Heath, J. K.; Caruso, F., Influence of size, surface, cell line, and kinetic properties on the specific binding of A33 antigen-targeted multilayered particles and capsules to colorectal cancer cells. *Acs Nano* **2007,** 1, (2), 93-102.

17. Discher, B. M.; Won, Y. Y.; Ege, D. S.; Lee, J. C. M.; Bates, F. S.; Discher, D. E.; Hammer, D. A., Polymersomes: Tough vesicles made from diblock copolymers. *Science* **1999,** 284, (5417), 1143-1146.

18. Discher, D. E., Polymer vesicles of PEO-PLA and related for controlled release. *Abstracts of Papers of the American Chemical Society* **2003,** 225, U679-U679.

19. Discher, D. E.; Ahmed, F., Polymersomes. *Annual Review of Biomedical Engineering* **2006,** 8, 323-341.

20. Discher, D. E.; Eisenberg, A., Polymer vesicles. *Science* **2002,** 297, (5583), 967-973.

21. Heath, J. R.; Davis, M. E., Nanotechnology and Cancer. *Annual Review of Medicine* **2008,** 59, (1), 251-265.

22. Carrasquillo, K. G.; Stanley, A. M.; Aponte-Carro, J. C.; De Jesus, P.; Costantino, H. R.; Bosques, C. J.; Griebenow, K., Non-aqueous encapsulation of excipient-stabilized spray-freeze dried BSA into poly(lactide-co-glycolide) microspheres results in release of native protein. *Journal of Controlled Release* **2001,** 76, (3), 199-208.

23. Costantino, H. R.; Firouzabadian, L.; Hogeland, K.; Wu, C. C.; Beganski, C.; Carrasquillo, K. G.; Cordova, M.; Griebenow, K.; Zale, S. E.; Tracy, M. A., Protein spray-freeze drying. Effect of atomization conditions on particle size and stability. *Pharmaceutical Research* **2000,** 17, (11), 1374-1383.

24. Costantino, H. R.; Firouzabadian, L.; Wu, C. C.; Carrasquillo, K. G.; Griebenow, K.; Zale, S. E.; Tracy, M. A., Protein spray freeze drying. 2. Effect of formulation variables on particle size and stability. *Journal of Pharmaceutical Sciences* **2002,** 91, (2), 388-395.

25. Forbes, R. T.; Barry, B. W.; Elkordy, A. A., Preparation and characterisation of spray-dried and crystallised trypsin: FT-Raman study to detect protein denaturation after thermal stress. *European Journal of Pharmaceutical Sciences* **2007,** 30, (3-4), 315-323.

26. Wang, Z. L.; Finlay, W. H.; Peppler, M. S.; Sweeney, L. G., Powder formation by atmospheric spray-freeze-drying. *Powder Technology* **2006,** 170, (1), 45-52.

27. Maa, Y. F.; Nguyen, P. A.; Sweeney, T.; Shire, S. J.; Hsu, C. C., Protein inhalation powders: Spray drying vs spray freeze drying. *Pharmaceutical Research* **1999,** 16, (2), 249-254.

28. Ma, D.; Li, M.; Patil, A. J.; Mann, S., Fabrication of protein/silica core-shell nanoparticles by microemulsion-based molecular wrapping. *Advanced Materials* **2004,** 16, (20), 1838-+.

29. Dos Santos, I. R.; Richard, J.; Pech, B.; Thies, C.; Benoit, J. P., Microencapsulation of protein particles within lipids using a novel supercritical fluid process. *International Journal of Pharmaceutics* **2002,** 242, (1-2), 69-78.

30. Fujibayashi, T.; Okubo, M., Preparation and thermodynamic stability of micron-sized, monodisperse composite polymer particles of disc-like shapes by seeded dispersion polymerization. *Langmuir* **2007,** 23, (15), 7958-7962.

31. Fu, K.; Griebenow, K.; Hsieh, L.; Klibanov, A. M.; Langer, R., FTIR characterization of the secondary structure of proteins encapsulated within PLGA microspheres'. *Journal of Controlled Release* **1999,** 58, (3), 357-366.

32. Johnson, O. L.; Jaworowicz, W.; Cleland, J. L.; Bailey, L.; Charnis, M.; Duenas, E.; Wu, C. C.; Shepard, D.; Magil, S.; Last, T.; Jones, A. J. S.; Putney, S. D., The stabilization and encapsulation of human growth hormone into biodegradable microspheres. *Pharmaceutical Research* **1997,** 14, (6), 730-735.

33. Polk, A.; Amsden, B.; Deyao, K.; Peng, T.; Goosen, M. F. A., Controlled-Release of Albumin from Chitosan-Alginate Microcapsules. *Journal of Pharmaceutical Sciences* **1994,** 83, (2), 178-185.

34. Polk, A. E.; Amsden, B.; Scarratt, D. J.; Gonzal, A.; Okhamafe, A. O.; Goosen, M. F. A., Oral Delivery in Aquaculture - Controlled-Release of Proteins from Chitosan-Alginate Microcapsules. *Aquacultural Engineering* **1994,** 13, (4), 311-323.

35. Moshashaee, S.; Bisrat, M.; Forbes, R. T.; Nyqvist, H.; York, P., Supercritical fluid processing of proteins I: Lysozyme precipitation from organic solution. *European Journal of Pharmaceutical Sciences* **2000,** 11, (3), 239-245.

36. Whitaker, M. J.; Hao, J. Y.; Davies, O. R.; Serhatkulu, G.; Stolnik-Trenkic, S.; Howdle, S. M.; Shakesheff, K. M., The production of protein-loaded microparticles by supercritical fluid enhanced mixing and spraying. *Journal of Controlled Release* **2005,** 101, (1-3), 85-92.

37. Li, J. R.; Henry, G. C.; Garno, J. C., Fabrication of nanopatterned films of bovine serum albumin and staphylococcal protein A using latex particle lithography. *Analyst* **2006,** 131, (2), 244-250.

38. Kimhi, O.; Bianco-Peled, H., Study of the interactions between protein-imprinted hydrogels and their templates. *Langmuir* **2007,** 23, (11), 6329-6335.

39. Heyries, K. A.; Marquette, C. A.; Blum, L. J., Straightforward protein immobilization on Sylgard 184 PDMS microarray surface. *Langmuir* **2007,** 23, (8), 4523-4527.

40. Wang, Y. J.; Caruso, F., Nanoporous protein particles through templating mesoporous silica spheres. *Advanced Materials* **2006,** 18, (6), 795-+.

41. Liying Wang, M. H. L., Jeremy Barton, Laura Hughes, and Teri Odom, Shape-Control of Protein Crystals in Patterned Microwells. *Journal of American Chemical Society* **2008**.

42. Mahmud, G. K. J. M. B., Yuriy Chegel, Stoyan K. Smoukov, and Bartosz A. Grzybowski, Wet-Stamped Precipitant Gradients Control the Growth of Protein Microcrystals in an Array of Nanoliter Wells. *Journal of American Chemical Society* **2008**.

43. Iemma, F.; Spizzirri, U. G.; Puoci, F.; Muzzalupo, R.; Trombino, S.; Picci, N., Radical crosslinked albumin microspheres as potential drug delivery systems: Preparation and in vitro studies. *Drug Delivery* **2005,** 12, (3), 179-184.

44. Langer, K.; Balthasar, S.; Vogel, V.; Dinauer, N.; von Briesen, H.; Schubert, D., Optimization of the preparation process for human serum albumin (HSA) nanoparticles. *International Journal of Pharmaceutics* **2003,** 257, (1-2), 169-180.

45. Sharma, R. I.; Pereira, M.; Schwarzbauer, J. E.; Moghe, P. V., Albumin-derived nanocarriers: Substrates for enhanced cell adhesive ligand display and cell motility. *Biomaterials* **2006,** 27, (19), 3589-3598.

46. Altundag, K.; Dede, D. S.; Purnak, T., Albumin-bound paclitaxel (ABI-007; Abraxane) in the management of basal-like breast carcinoma. *J Clin Pathol* **2007,** 60, (8), 958.

47. Zhang, L. K.; Hou, S. X.; Mao, S. J.; Wei, D. P.; Song, X. R.; Lu, Y., Uptake of folate-conjugated albumin nanoparticles to the SKOV3 cells. *International Journal of Pharmaceutics* **2004,** 287, (1-2), 155-162.

48. Takeoka, S.; Teramura, Y.; Ohkawa, H.; Ikeda, Y.; Tsuchida, E., Conjugation of von Willebrand factor-binding domain of platelet glycoprotein IB alpha to size-controlled albumin microspheres. *Biomacromolecules* **2000,** 1, (2), 290-295.

49. Takeoka, S.; Teramura, Y.; Okamura, Y.; Handa, M.; Ikeda, Y.; Tsuchida, E., Fibrinogen-conjugated albumin polymers and their interaction with platelets under flow conditions. *Biomacromolecules* **2001,** 2, (4), 1192-1197.

50. Benedict, C.; Dodt, C.; Hallschmid, M.; Lepiorz, M.; Fehm, H. L.; Born, J.; Kern, W., Immediate but not long-term intranasal administration of insulin raises blood pressure in human beings. *Metabolism-Clinical and Experimental* **2005,** 54, (10), 1356-1361.

51. Benedict, C.; Hallschmid, M.; Hatke, A.; Schultes, B.; Fehm, H. L.; Born, J.; Kern, W., Intranasal insulin improves memory in humans. *Psychoneuroendocrinology* **2004,** 29, (10), 1326-1334.

52. Benedict, C.; Hallschmid, M.; Schmitz, K.; Schultes, B.; Ratter, F.; Fehm, H. L.; Born, J.; Kern, W., Intranasal insulin improves memory in humans: Superiority of insulin aspart. *Neuropsychopharmacology* **2007,** 32, (1), 239-243.

53. Benedict, C.; Hallschmid, M.; Schultes, B.; Born, J.; Kern, W., Intranasal insulin to improve memory function in humans. *Neuroendocrinology* **2007,** 86, (2), 136-142.

54. Hallschmidt, M.; Benedict, C.; Born, J.; Kern, W., Targeting metabolic and cognitive pathway of the CNS by intranasal insulin administration. *Expert Opinion on Drug Delivery* **2007,** 4, (4), 319-322.

55. Stathopulos, P. B. S., G. A.; Hwang, Y-M.; Rumfeld, J. A. O.; Lepock, J. R.; Meiering, E. M., Sonication of proteins causes formation of aggregates that resemble amyloid. *Protein Science* **2004,** 13, 3017-3027.

56. Kelly, J. Y.; DeSimone, J. M., Shape-Specific, Monodisperse Nano-Molding of Protein Particles. *J. Am. Chem. Soc.* **2008,** 130, (16), 5438-5439.

57. Stephanie E. A. Gratton, P. D. P., J. Christopher Luft, Patricia A. Ropp, Victoria J. Madden, Mary Napier, Joseph M. DeSimone, The Effect of Particle Design on Cellular Internalization Pathways. *submitted* **2008**.

58. Petros, R. A.; Ropp, P. A.; DeSimone, J. M., Reductively Labile PRINT Particles for the Delivery of Doxorubicin to HeLa Cells. *J. Am. Chem. Soc.* **2008,** 130, (15), 5008-5009.